NOTE TO USERS

Synthesis and Characterization of Sulfonate and Phosphonate Functionalized Monolayer Protected Gold Clusters

By

Fiurasek Petr

A thesis submitted to McGill University in partial fulfillment of the requirements for the degree of

Master of Science

Department of Chemistry
McGill University
Montreal, Quebec
Canada, H3A 2K6

December 2003

Your file Votre référence
ISBN: 0-612-98633-0
Our file Notre référence
ISBN: 0-612-98633-0

Abstract

Gold clusters protected with self-assembled monolayers of sodium, 10-mercaptodecanesulfonate, $HS(CH_2)_{10}SO_3Na$, and 11-mercaptoundecanylphosphonic acid, $HS(CH_2)_{11}PO_3H_2$, were synthesized to provide negatively charged nanoparticles. The negatively charged end groups of the sulfonate- and phosphonate-monolayers protected clusters, SO_3-MPCs and PO_3-MPCs, allowed the particles to be water soluble in addition to be stable in air, and can be dried and redissolved without change. Modifications of experimental conditions, namely the thiol:gold ratio, gold concentration and the type of surfactant, yielded MPCs of 1.8-5.7 nm core diameters with a broad range of size dispersity, and solubilities. Transmission electron microscopy, proton nuclear magnetic resonance (^{1}H NMR), UV-Visible and infrared spectroscopies, thermogravimetric and zeta-potential analyses were consistent with nanoparticle formation. The chain conformation, dynamic behavior and ordering of SO_3-MPCs and PO_3-MPCs were further investigated by solid-state NMR. Despite the high surface curvature of the nanoparticles and the bulky end groups, medium length chains of SO_3-MPCs (C10) and PO_3-MPCs (C11) showed a high degree of organization and restricted mobility when compare to long chains of alkanethiolate MPCs (C18). The more extensive hydrogen bonding interactions between the phosphonic acid groups led to a reduced chain mobility and a higher thermal stability. The PO_3-MPCs exhibit a high order-disorder transition, partial decomposition and a very marked hysteresis in the chain recrystallization similar to MPCs stabilized by $HS(CH_2)_nCO_2H$. Solid-state ^{31}P-NMR allowed studies of the hydrogen-bonded self-assembled structure in the PO_3-MPCs as well as in the bulk phosphonic acid. The 1.8 nm-diameter SO_3-MPCs produced large aggregates in presence of poly(diallyldimethyl-ammonium chloride) (PDADMAC). However, the encapsulation of individual particles was favored when the same polyelectrolyte was adsorbed on the 3.1 nm-diameter PO_3-MPCs, which to date is the smallest reported coated particle size.

Résumé

Des clusters d'or recouverts de monocouches auto-assemblées avec 10-sulfonyldécanesulfonate de sodium, $HS(CH_2)_{10}SO_3Na$, et acide 11-sulfonylundécyl-phosphonique, $HS(CH_2)_{11}PO_3H_2$, ont été synthétisés pour fournir les nanoparticules négativement chargées. La protection des clusters par des monocouches de sulfonate (SO_3-MPCs) et de phosphonate (PO_3-MPCs) rend les particules solubles dans l'eau. En plus d'être stables à l'air, elles peuvent être séchées et redispersées sans former d'agrégats. La modification des conditions expérimentales, plus précisement, du ratio thiol:or, de la concentration en or et du type d'agent de surface a conduit à l'obtention de MPCs ayant des diamètres compris entre 1,8 et 5,7 nm ainsi que des dispersités de tailles et solubilités variées. Les résultats obtenus par microscopie électronique à transmission, resonance magnétique nucléaire du proton (RMN ^1H) en solution, spectroscopie UV-Visible et infrarouge, analyses thermogravimétriques et mesure de ξ-potentiels ont pu metre en évidence la formation des nanoparticules. Des études plus approfondies sur la conformation, l'ordre et le comportement dynamique des chaînes stabilisant les particules SO_3-MPCs et PO_3-MPCs ont été menées par RMN à l'état solide. En dépit de la courbure des nanoparticules et de l'encombrement stérique des groupes terminaux, les chaînes de longueur moyennes de SO_3-MPCs (C10) et de PO_3-MPCs (C11) ont demontrées un organisation très élevée avec une mobilité réduite comparativement à des MPCs stabilisés par de longs alcanethiols (C18). La mobilité réduite et la stabilité thermique plus élevée des PO_3-MPCs ont été attribuées à la presence de ponts hydrogène entre les groupes acides phosphoniques. Les PO_3-MPCs subissent une transition ordre-désordre à une température très élevée, une décomposition partielle et une hystérésis très marquée dans la recristallisation des chaînes semblable aux MPCs stabilisés par des $HS(CH_2)_nCO_2H$. RMN ^{31}P à l'état solide a permi d'étudier les structures résultant des ponts hydrogène dans les PO_3-MPCs et dans l'acide phosphonique pur. Les SO_3-MPCs avec diamètre de 1,8 nm ont formés de grands agrégats en présence du chlorure de poly(diallyldimethylammonium), (PDADMAC). Toutefois, l'encapsulage des particules

individuelles a été favorisée lorsque le même polyélectrolyte a été adsorbé sur les PO_3-MPCs avec un diamètre de 3,1 nm. Ce sont les plus petites particules recouvertes par un polyélectrolyte décrites à ce jour.

Acknowledgement

I would like acknowledge Professor Linda Reven for her guidance, encouragement and continued devotion to her work. I was happy to be enrolled in her group and proud to be her graduate student. I wish Linda and her husband all the best with their children, Blandine and Sadrac.

I was very fortunate to have worked with Shane, Victor, Andrew, Michael, Rashida and Elizabeth and thank them for the things they taught me.

I would like to express my thanks to people who train me on various instruments or showed me laboratory techniques that were necessary for my research. Fred Morin, for his help and guidance in solid-state NMR and proofreading chapter three. Nadim Saade for running samples on MS. Paul Xia who trained me on the solution NMR and Muriel Corbierre on DSC and TGA. Patrick Lim Soo for introducing me to dialysis, Valerie Gandubert for initializing me to TEM and to nanoparticles, and proofreading my French abstract, Andrew O'Donnell for solid-state NMR assistance and Arndsten group for giving me helpful organic laboratory suggestions.

Special thanks to Elizabeth Hulme, who worked with Dr. Reven and myself as a summer student on a project that consisted of coating gold nanoparticles with polyelectrolytes. All the coating of particles with polyelectrolytes and TEM pictures of the coated particles were carried out by Elizabeth.

I am pleased to acknowledge very helpful discussions with Professor Bruce Lennox, Professor Denis Gilson, Dr. Antonella Badia, and Professor Adi Eisenberg.

Access to the TEM equipment was provided by McGill facility for Electron Microscopy Research, where the assistance of Jeannie Mui, Professor Hojatollah Vali and Kelly Sears were greatly appreciated. The use of PAS-FTIR at University of Montreal is also acknowledged.

This work was supported by grants from the Fonds de recherche sur la nature et les technologies (FCAR), Natural Sciences and Engineering Research Council of Canada (NSERC) and McGill University.

Finally, I would like to give a lot of kisses, hugs and love to my precious mother, Mirka Fiuraskova, for her patience, courage, and her encouragement.

Dedicated to my Mother for
her accomplishments and her hard work

Table of Contents

Chapter 1

General Introduction

Chapter 2

Sulfonate-Monolayer Protective Clusters

Chapter 3

Phosphonate-Monolayer Protected Clusters

Chapter 4

Overview, Conclusions, and Future Work

Appendix

List of Tables

List of Figures

Chapter 1

General Introduction

1.1 SELF-ASSEMBLED MONOLAYERS (SAMs)

1.1.1 Chain structure

The study of the formation, and interfacial behavior of self-assembled structures has a long history and continues to be one of the more active areas of surface chemistry. In 1917, Langmuir reported the first systematic study[1] of molecules called amphiphilies (i.e., soaps and phospholipids), containing one hydrophobic and one hydrophilic part. The study was continued by Blodgett, who was able to transfer fatty acid monolayers from the water surface onto a solid substrate[2]. This method is now universally know as the Langmuir-Blodgett (L-B) technique.

Langmuir-Blodgett (L-B) and self-assembly techniques are the most common methods for forming ultrathin organic films. The first study of amphiphilic molecules by self-assembly technique was published by Bigelow et al[3], in 1946. Bigelow reported that well-oriented and nearly close packed monolayer film spontaneously forms when a substrate was immersed into a solution containing amphiphilic compounds. Many years later, findings by Nuzzo and Allara[4] on the formation of alkanethiolates on gold showed very promising advantages over the Langmuir-Blodgett technique and since then the volume of work published on self-assembled monolayers has increased immensely.

Self-assembled monolayers (SAMs) are polycrystalline films of long chain hydrocarbons that form a single molecular layer and well ordered chainlike or rodlike domains after they adsorbed onto a substrate.[5] The SAMs are composed generally of three parts: a head group that binds to the substrate, a tail or the end group that constitutes the outer shell of the surface, and a spacer that connects head and the tail group. The graphical representation of SAMs is shown in Figure 1.1.

The characteristics of the SAMs are a function of the overall interactions; bonding of the head group to the substrate, interchain van der Waals interactions of the spacers and interactions between the end group of the monolayer and its constituents. The

equilibrium of these interactions will determine the chain packing density and pattern. Early electron diffraction studies reported hexagonal (7×7) molecular pattern for $CH_3C_{21}Au$ SAM.[6] It was later reported that the structures of the n-alkanethiol monolayers are similar from 10-carbon to 22-carbon chains and that they all probably adopt the $(\sqrt{3}\times\sqrt{3})R30°$ pattern, which is a 30° rotation of the hexagonal (7×7) pattern.[7] Infrared (IR) studies and X-ray diffraction showed and confirmed that long chains of n-alkane thiols are tilted ~30° off of the surface normal and that all-trans hydrocarbon chains result in a chain packing density of 22 $Å^2$ per molecule.[8-9]

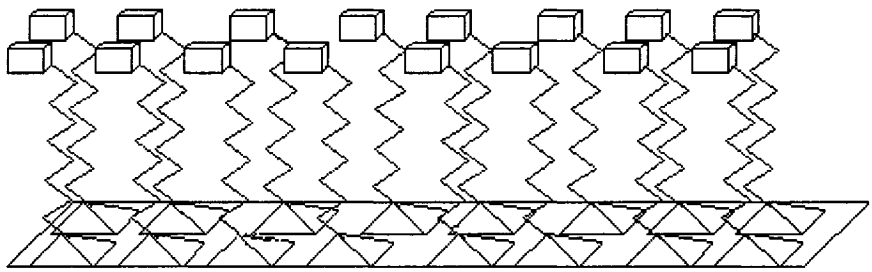

Figure 1.1 The graphical representation of molecular packing present in self-assembled monolayers (SAMs): bonding of the head group, , to the substrate, interchain ven der Waals interactions of the spacers and interaction between the end group, ,of the monolayer and the constituents.

1.1.2 Head group and the surface of SAMs

SAMs composed of thiol (S-H) head group and gold substrates have been extensively studied in the past[10]. Gold substrates were mainly studied because gold can be handled at ambient conditions since it does not have a stable oxide.[5] However, several other types of head group/substrate systems were investigated such as phosphonic acid groups adsorbed on ZrO_2 and TiO_2[11] and carboxylic acid groups on AgO and Al_2O_3[12-14]. The nature of the bond between the head group and the surface plays an important role on the chain packing density and the self-organization. Consequently, the bond energies associated with the type of bond can give an indication on the stability and the behavior of the highly organized monolayers. The bonding of the Au-S polar and covalent bond, has a bond strength of ~ 44 kcal/mole[15] making it more chemically

stable, compared to the ionic $CO_2^-Ag^+$ bond which has a bond energy of 33 kcal/mole[16]. Another possibility that governs the type of bond and thus the ordering of SAMs and is governed by the metal substrate is the surface-binding mode which may consist of tri-, bi- or mono-dentate bonds. For example, it was revealed that alkanoic acids bind to AgO and ZrO_2 through a bidentate surface bond and more weakly to aluminum or copper oxide via a monodentate attachment.[12, 17-18b] Tao[12] suggested that the carboxylic head group of alkanoic acids binds through two oxygen (i.e., bi-dentate bond) on AgO surface giving more ordered monolayer. While on Al_2O_3, the gauche conformations develop around the CO_2 head group that binds to the surface asymmetrically (eg., mono-dentate linkage). Guerrero et al.[19], used diffuse reflectance infra-red Fourier transform and ^{31}P solid-state magic angle spinning nuclear magnetic resonance spectroscopies to propose a tridentate bonding mode for diethylphosphonate molecules on TiO_2 surfaces. The X-ray photoelectron spectroscopy (XPS) showed that treated Au surface with Au_2O_3 can give simultaneously ionic and covalent binding through the tail group with –OH, -COOH and $–PO_3H_2$ and the head group SH, respectively of functionalized thiols.[20]

1.1.3 Spacer of SAMs

Besides the nature of the bond, the spacer between the head and the terminal group is the second molecular part that gives to SAMs a characteristic property. The simple case is the alkyl chain spacer where the van der Waals interactions are the major forces, of the order of 10 kcal/mol[5]. When the SAMs are formed, the bond energy associated with the self-adsorption of the surfactants on the substrate can bring the chains close enough to maximize lateral van der Waals interactions, and thus allowing highly ordered SAMs. Studies[21] have shown that the longer alkyl chains (i.e., $n > 9$) form thermodynamically stable highly ordered monolayers whereas the shorter alkyl chains gives rise to more defects resulting in less ordered SAMs. As the length of the alkyl spacer, linking the carboxylic acid to gold substrate, is increased, the alkyl chains form a more crystalline structure and a more ordered monolayer.[5] Shorter alkyl chains have less van der Waals interactions, that are a function of the chain length, and thus they are more disorder. The spacer length is not the only factor that can influence the molecular assembly of surfactants. The investigation of perfluorinated[22, 23] or aromatic[24, 25] SAMs

have also been studied. Due to the F-F repulsive interactions, the long perfluorocarbon chains have a helical rather than an all-trans conformation resulting in a stiffer, cylindrical molecule than the corresponding hydrocarbon.[26] In the case of aromatic spacers, the quality of the SAMs was found to be dependent on the dipole group present and the length of the aliphatic chain above the aromatic group.[25]

1.1.4 End group of SAMs

The properties of alkanethiol monolayers are determined principally by the third and the most studied molecular part of SAMs, the tail group, X (Figure 1.1). In addition to chain packing, the end groups will influence the surface property which can be easily accomplished by varying X group. A good example is the change from a hydrophobic tail group such as CH_3 to a hydrophilic tail group such as OH.[27,28] Thus, it is important to understand how substitution of the end group will influence the molecular packing. Several studies were performed to explore the packing arrangement of X-functionalized SAMs.[29-35] SAMs composed of alkanethiols with polar end groups such as X = OH, NH_2, COOH, SO_3H and PO_3H_2 have technological importance in applications such as control of ionic binding,[36] and in studies of biocompatibility. [20, 28, 37, 38] Consequently, there is much interest in whether these form dense and ordered packing. The existence of hydrogen bonding interactions in SAMs within these polar end groups is the main driving force for the dense and ordered packing.[39] Study of hydroxy-terminated SAMs indicated that these monolayers exhibit a packing density with the same molecular area as CH_3C_nAu SAM (22 $Å^2$ per molecule) since OH is not a bulky group. For the COOH-terminated long chains SAMs infrared studies[40] suggest similar molecular orientation (i.e., 30° from the surface normal), with hydrogen bonding between terminal COOH groups resulting in sideways dimer formation.

1.2 MONOLAYER-PROTECTED CLUSTERS (MPCs)

Stable alkanethiol-capped nanoparticles also know as monolayer-protected clusters (MPCs) can be regarded as three-dimensional (3D) self-assembled monolayer structures, in comparison to alkanethiol self-assembled monolayers (SAMs) on flat gold surfaces (two-dimensional, 2D). MPCs are considered 3D SAMs because they can be

studied as a bulk in solid or in solution and because each monolayer is confined upon a molecule-sized spatial element.[41] Two structural features may cause structural and reactivity differences between monolayers of the same alkanethiol on flat gold surfaces versus 3D SAMs. The first is the MPCs surface's high radius of curvature. The methylene units of the alkane chains become progressively less densely packed and more mobile as one moves further away from the core.[42] The second is the highly faceted morphology of the 3D SAMs that on a flat surface would be regarded as defect sites.[41] Initial studies have demonstrated that 3D SAMs undergo order/disorder transitions closely related to those in the 2D SAMs.[43, 44] The Au-S surface bonding[45] and terminal group reactivities[46] of these MPCs are also similar to those of 2D SAMs. Both H-bonded and free CO_2H are detected by vibrational spectroscopy in 2D SAMs, while in the 3D SAM case there is more extensive H-bonding probably due to the inter- as well as intra-particle hydrogen bonds.[47]

A widely used synthetic approach to prepare nanoparticles is based on the Brust method,[48] where the dodecanethiol was showed to stabilize 1-3 nm gold particles. The synthesis was performed in two-phases, toluene and water. Tetraoctylammonium bromide was used to transfer tetrachloroaurate ($AuCl_4^-$) from aqueous phase to the toluene solvent where the $C_{12}H_{25}SH$ is soluble. The gold salt was then reduced by sodium borohydride resulting in Au^0 cluster that contains one third of the gold atoms at the surface and bound to a thiol molecule. Furthermore, monolayer protected clusters of various sizes with relatively high monodispersity were obtained when two-phase or one phase (methanol) method was used.[50] Alkanethiolate MPCs differ from conventional colloids[49] in that they can be repeatedly isolated from and redissolved in common organic solvents without irreversible aggregation or decomposition.

MPCs are generally stabilized with thiol-based ligands that are known to covalently bind to metals, with their properties primarily determined by the terminal functional group. Murray et al.,[50, 51] prepared MPCs having carboxylic acid functionalized alkanethiolate ligand shells that were quite soluble in water. Other water soluble MPCs have been studied over the past several years, including poly(ethylene glycol),[52] 4-hydroxythiolphenol,[53] mercaptobenzoic acid,[54] mercaptosuccinic acid,[55] 5-mercapto-2-benzimidazole sulfonic acid sodium salt (MBS),[56] and sodium 2-

mercaptoethanesulfonate (MES).[57] Solubilities of 4- hydroxythiolphenol, mercaptobenzoic acid and mercaptosuccinic acid functionalised nanoparticles are both limited and pH-dependent. The sulfonic acid functionalised MPCs are freely water soluble and stable at low pH value.[57,58] The negatively charged acid functionalised MPCs showed potential applications in biological chemistry[49] due to the water solubility. The alkyl chains of these MPCs have a high degree of conformational order due to strong hydrogen bonding.[42, 47]

1.3 SOLID-STATE NMR

1.3.1 Characterization of modified surfaces

A wide range of physical methods is now available for the surface studies of compounds such as surfactants, polymers or lipids. X-ray photoelectron spectroscopy (XPS), infrared spectroscopy (IR), atomic force microscopy (AFM), scanning tunnelling microscopy (STM) and dynamic contact angle measurements are used to determine structural parameters such as layer thickness, surface density, stability and morphology, and molecular orientation and molecular lattice. Methods based on nuclear magnetic resonance (NMR) spectroscopy reveal a variety of dynamic and structural information for complex surfactant systems. Investigation of specific nuclei such as ^{13}C or ^{31}P which provide information about the molecular dynamics and organization in their local environment, is the main advantage of NMR methods. On the other hand, the low sensitivity of NMR technique (i.e., natural abundance of ^{13}C is 1.11 %) in addition to the small amount of compound provided by a monolayer complicates the study of SAMs. However, signal enhancing techniques such as cross-polarization (CP) and study of small particles can achieve sufficient sensitivity. Therefore, 3D SAMs facilitate the study of modified surfaces by NMR.

Besides the low natural abundance of some nuclei, the low sensitivity in NMR arises due to the relatively small spacing of the energy levels of nuclear spins, ΔE. For spin $I = ½$ nuclei the energy separation is linearly dependent on the magnetic field strength (B_o) according to the Hamiltonian of the Zeeman interaction[59]

$$H_Z = -\mu_Z B_o = \gamma \hbar B_o I_Z, \qquad (1.1)$$

where γ is the gyromagnetic ratio of the nucleus, μ_Z is the magnetic moment of a spin, and I_Z can assume the values ½ or - ½. The transition of the spin occurs (i.e., resonance) by irradiation with a radio frequency pulse of the Larmor frequency $\omega_L = \gamma B_o$. At equilibrium the population ratio is given by a Boltzman distribution:[59] $N_\beta = N_\alpha \exp(-\Delta E/ kT)$, leading to an excess fraction of spins in the ground state given by

$$\frac{N_\alpha - N_\beta}{N_\alpha + N_\beta} \approx \frac{\Delta E}{2kT} = \frac{\gamma \hbar B_o}{2kT} \tag{1.2}$$

This fraction can be very low, i.e. about 10^{-5} to 10^{-4} at room temperature and a field of 9.4 T, so that the number of spins which can be excited and detected, is extremely small. The small fraction accounts in large part for the insensitivity of NMR relative to other spectroscopic methods

1.3.2 Cross-Polarization Magic Angle Spinning (CPMAS)

To obtain highly resolved solid-state NMR spectra, usually three techniques are combined [60]: (i) cross-polarization (CP), (ii) magic-angle spinning (MAS), and (iii) high power heteronuclear decoupling. Besides the resolution, CP and high power hetero-nuclear decoupling increase the signal of low abundance nuclei. The most common CPMAS experiment, achieved via the Hartmann-Hahn match[61] is run under the pulse sequence shown in Figure 1.2.

The pulse sequence starts with a single pulse applied at the ^1H frequency which transforms the magnetization along the z-axis into the x-y plane creating transverse magnetization. The pulse sequence is then followed by spin-lock cross-polarization in both nuclei channels. In CP the dipolar interaction is employed to transfer the magnetization from abundant nuclei, I, such as ^1H and ^{19}F to the rare nuclei, S, such as ^{13}C, ^{31}P and thus enhancing the signal. In principle, CP results in a signal enhancement given by γ_I/γ_S (where I and S are both spin-1/2 nuclei), where γ_I is the magnetogyric ratio of the abundant nuclei and γ_S is that of the rare nuclei. When setting up a CP experiment such as the one shown in Figure 1.2, one must ensure that the Harmann-Hahn match condition is satisfied,[59]

$$\gamma_I B_I = \gamma_S B_S. \quad (1.3)$$

I and S spins now have the same precession frequency around their respective B_1 magnetic fields which are turned on for a period known as the contact time (Figure 2), or mixing time, which is on the order of milliseconds. It is during this time that

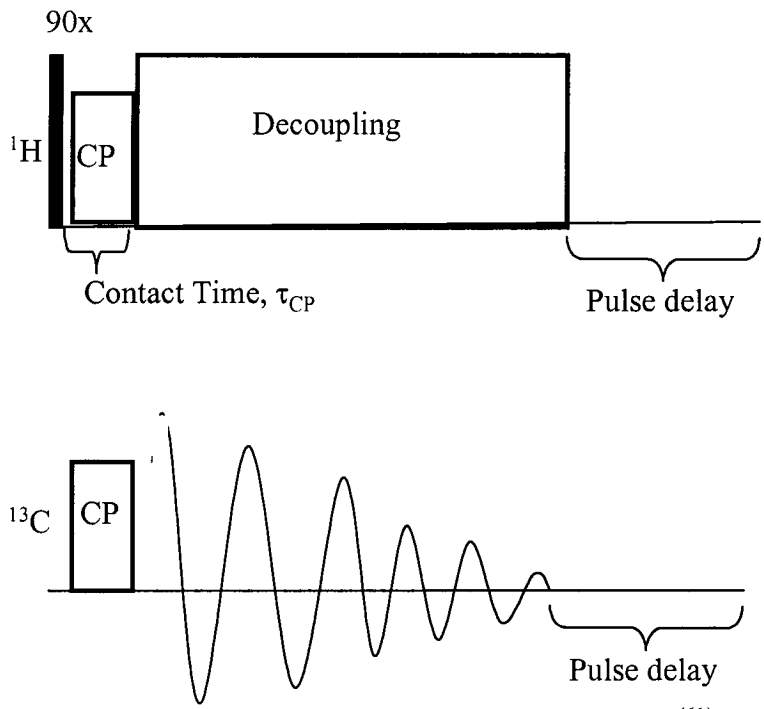

Figure 1.2 The sequence of the Cross-Polarization (CP) experiment.[61]

magnetization is transferred from the I spins to the S spins. The degree to which the S spins have been magnetized depends on the contact time. The rate of CP is initially governed by T_{IS}, a time constant which is proportional to the second moment of the dipolar coupling between the I and S spins.[62] At longer contact times, however, spin-lattice relaxation of the S and I spins in the rotating frame ($T_{1\rho S}$, $T_{1\rho I}$) dominates. The ^{13}C magnetization, $M(t_{CP})$, can be plotted as a function of contact time which will be fit to the following expression:

$$M(t_{CP}) = (M_0/\lambda)\ \{1-\exp(-\lambda t_{CP}/\ T_{IS})\}\ \exp(-t_{CP}/\ T_{1\rho I}) \qquad (1.4)$$

Where $\lambda = 1 + (T_{IS}/\ T_{1\rho S}) - (T_{IS}/\ T_{1\rho I})$. Because cross polarization requires the existence of a dipolar coupling which is strongly distance dependent, the value of t_{CP} can often identify which carbons are strongly coupled (i.e., are close) to protons and which are not.[63] For rigid systems, carbons bonded directly to protons can cross polarize more rapidly than those not bonded to protons or those bonded to protons in mobile systems where dipole-dipole couplings are weak and motionally averaged.

After the CP is applied, a Free Induction Decay (FID) is then acquired in the ^{13}C channel (Figure 1.2) during which high-power proton decoupling field is turned on. During the irradiation of the ^{1}H resonance frequency, the heteronuclear coupling between ^{1}H and ^{13}C is eliminated, leading to narrower linewidths. For solids, decoupling of abundant spins such as protons requires much more power than is generally required for solution samples thus the decoupler can be only switched on for a relatively short time.

If the CP sequence shown in Figure 1.2 would be performed with out spinning the sample, a powder-pattern spectrum would result. The shape of the spectrum depends on the nature of the internal interaction present such as direct and indirect spin-spin coupling and anisotropic nuclear magnetic shielding, and the quadrupole interaction in the case of a spin > 1/2 nuclei.[60] Under the slow magic-angle spinning (MAS), the powder-pattern spectrum breaks up into a centerband at the isotropic chemical-shift frequency and series of peaks separated by the spinning frequency, which are know as spinning sidebands.[60] When the spinning speed frequency exceeds the powder-pattern frequency region due to internal interactions, the isotropic line shape results and thus increasing the spectrum resolution. MAS consists of mechanically spinning the sample around an axis making an angle of 54.7° (i.e, magic angle) with the direction of the magnetic field B_o. At the magic angle, $\theta = 54.7°$, the term $3\cos^2\theta - 1 = 0$, and thus leading to zero dipolar and CSA interactions.

1.3.3 Chemical Shift Interaction (CSA)

NMR experiments on isotropic samples achieve narrow, resolved peaks either via rapid tumbling of molecules in solution or as it was mentioned previously via the MAS technique. Although this narrowing enhances resolution and sensitivity, it also sacrifies information by averaging various orientation-dependent spin interactions such as dipolar coupling or chemical shift anisotropy (CSA). The chemical shift anisotropy powder pattern contains orientation-dependent information. Depending on the local symmetry at the nuclear site, the magnitude of the chemical shift will vary as a function of the orientation of the molecule with respect to the external magnetic field. Typical powder patterns, an axially asymmetric and an axially symmetric, are shown in Figure 1.3. The isotropic chemical shifts are indicated by dashed lines.

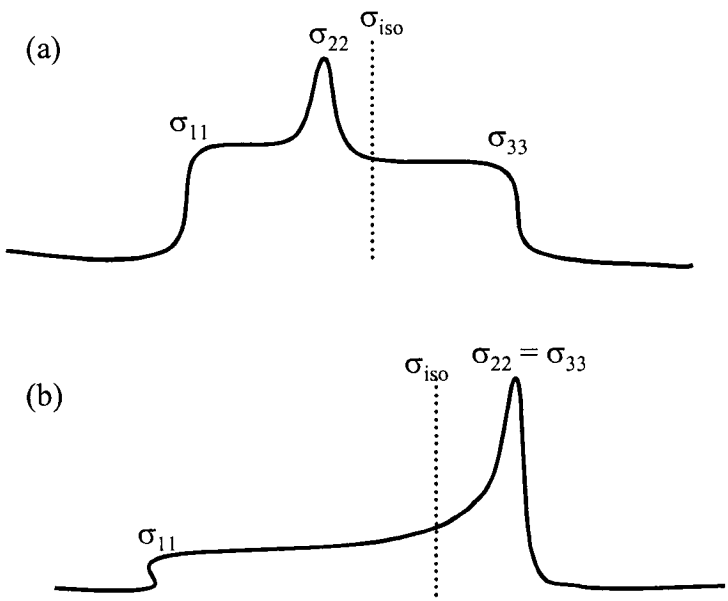

Figure 1.3 CSA powder pattern for (a) an axially asymmetric and (b) an axially symmetric tensor. The principal values of the shift tensors σ_{11}, σ_{22} and σ_{33} are shown. The isotropic chemical shift σ_{iso} is denoted by the dotted line.

The chemical shift interaction is described by a second-rank tensor with three principal components $\delta_{11} \geq \delta_{22} \geq \delta_{33}$ where δ_{11} is the chemical shift when the applied magnetic field, B_o, is along the direction of least shielding, and δ_{33} is the chemical shift when B_o is aligned with the most shielded direction. In the axially symmetric case, $\delta_{22} =$

δ_{33} (Figure 1.3b). The line shape can be described by three derived parameters: the isotropic chemical shift, δ_{iso}, the chemical shift anisotropy, $\Delta\sigma = \delta_{33} - \frac{1}{2}(\delta_{11} + \delta_{22})$ and the chemical shift asymmetry, $\eta = |\delta_{22} - \delta_{11}| / |\delta_{33} - \delta_{iso}|$ where η can take any value between 0 and 1, where 0 represents axial symmetry.[64]

In the sequence shown in Figure 1.2, the high-power proton decoupling completely removes dipolar broadening effects, and thus the powder pattern line shape reflects the pure CSA interactions. When several chemical shift tensor powder patterns from more than one unique nuclei are present, severe overlap occurs and a featureless spectrum is obtained. ^{15}N NMR and ^{31}P NMR CSA data have been more sensitive than ^{13}C NMR for biological samples (i.e., biomembranes, phospholipids or proteins) to provide information about molecular motion and the interaction with the environment.[65, 66] For example, the effect of the ^{31}P chemical shift anisotropy has been used to investigate the phospholipid headgroup interacton with cytochrome c.[65] In the case of surfactant bearing one type of nuclei (e.g., ^{15}N in $NH_2(CH_2)_xSH$ or ^{31}P in $PO_3H_2(CH_2)_xSH$), the CSA parameters can be used to study the changes upon the adsorption on a surface. The changes of the ^{31}P and ^{15}N CSA elements have shown to be sensitive to the presence of hydrogen bonding on the basis of theoretical calculations.[66]

1.3.4 Spin relaxation

Several techniques have been used in the past to reach a better understanding of the structure and dynamics of surface-bound species such as alkanethiols on gold where NMR has been shown to be particularly useful.[42] The rate of nuclear spin relaxation depends on the motion of the molecules and the working frequency of the spectrometer. In NMR relaxation measurements, these motions are probed by measuring the longitudinal relaxation time (T_1) and the transverse relaxation time (T_2). T_1 is measured by the re-establishment of the longitudinal M_z magnetization after a 180° pulse in an inversion-recovery (90°-τ-180°-τ) pulse sequence. The M_z rises back exponentially to the Bolzman equilibrium magnetization $M_z(0)$ value according to this equation:[62]

$$M_z(\tau) = M_z(0)\,(1 - 2\exp(\tau/T_1)) \qquad (1.5)$$

while T_2 can be obtained from measuring the decay in transverse magnetization $M_{x,y}$ by using the Carr-Purcell technique:

$$M_y(\tau) = M_y(0) \exp(-\tau/T_2) \tag{1.6}$$

For alkanethiols adsorbed on gold nanoparticles, a distribution in relaxation times may be obtained as a result of the difference in motion between segments close to and far away from the surface. The frequency distribution characterized by an angular frequency, ω, of the motion of a randomly tumbling molecule is expressed in terms of the spectral density, $J(\omega)$, which is the Fourier transform of the autocorrelation function $g(\tau)$.[67]

$$g(\tau) = \left\langle \overline{f(t)f(t+\tau)} \right\rangle \tag{1.7}$$

$$J(\omega) = \int_{-\infty}^{\infty} g(\tau) e^{-i\omega\tau} d\tau \tag{1.8}$$

The autocorrelation function $g(\tau)$ is a time-dependent relation expressing the average period of time, represented by the bracket, between changes in the orientation of a molecule at initial position and after time τ. The function f is related to spherical harmonics, describing the position and the motion of the molecule. In an isotropic system, for example rotational tumbling of a small spherical molecules, has the functional form of a Lorenzian line shape[67]

$$J(\omega) = A \frac{\tau_c}{1 + \omega^2 \tau_c^2} \tag{1.9}$$

Where A is a constant that depends on the relaxation mechanism and τ_c is the correlation time for the molecular motion.

For a ^{13}C nucleus relaxed by N equivalent protons at a fixed distance $r_{C\text{-}H}$ it can be shown that[67]

$$\frac{1}{NT_1} = \frac{1}{10} \frac{\gamma_H^2 \gamma_C^2 \hbar^2}{r_{C-H}^6} \{J_0(\omega_H - \omega_C) + 3J_1\omega_C + 6J_2(\omega_H + \omega_C)\} \tag{1.10}$$

where the J_0, J_1, and J_2 are of the form of equation (1.9) and prescribe the components of the motional frequencies at $(\omega_H - \omega_C)$, ω_C, and $(\omega_H + \omega_C)$; ω_H and ω_C are the resonant frequencies of the ^1H and ^{13}C, and γ_H and γ_C are the corresponding gyromagnetic ratios. The value of T_1 can be quantitatively solved using Bloembergen, Purcell, and Pound (BPP) theory, [68] and show that spin-lattice relaxation times can be simplified in terms of correlation time for the molecular motion according to the following equation:[62]

$$\frac{1}{T_1} \alpha \frac{\tau_c}{1+\omega_o^2\tau_o^2} \tag{1.11}$$

If the value of the molecular correlation time is such that $\omega_o\tau_c \cong 1$, then T_1 is most efficient (i.e., the T_1 relaxation time is at a minimum). If the molecular motions are slower or faster than the Larmor frequency (ω_o), the T_1 relaxation time becomes longer. As the molecular motion depends on the temperature, the variation of T_1 with temperature

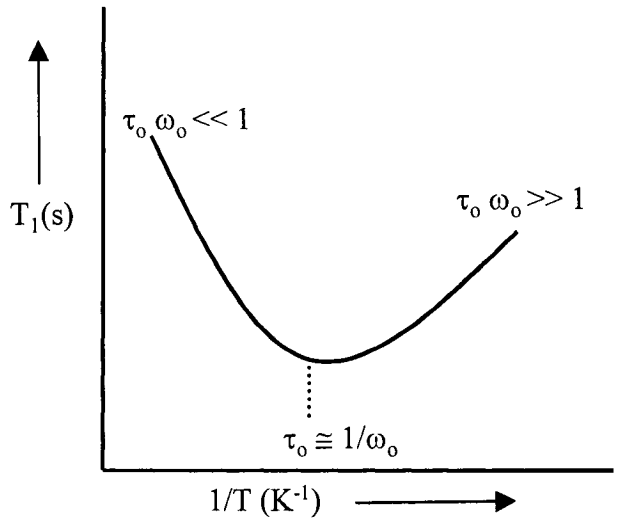

Figure 1.4 Typical plot of temperature variation of the T_1 spin-lattice relaxation time.

can exhibit a minimum if at a certain temperature the condition $\omega_o\tau_c \cong 1$ is satisfied, as shown by the Figure 1.4. If the T_1 values are decreasing with the increase of the temperature, then we are on the right side of the curve which corresponds to the slow motion regime ($\tau_o\ \omega_o >> 1$), usually present in slowly rotating macromolecules. In the fast motional regime or extreme narrowing condition ($\tau_o\ \omega_o << 1$), T_1 values increase as the temperature increases, usually observed for rapidly tumbling small molecules.

The carbon T_1 values were measured by Torchia method[69] which involves inversion-recovery pulse sequence with ^{13}C CP MAS detection as shown in Figure 1.5. In this sequence, the proton spins are inverted with a 180° pulse, and after a variable decay period, τ, the remaining magnetization is transferred to the carbon spins by cross polarization. The proton is phase shifted 90° and rotates the carbon magnetization from the z axis to the x axis.

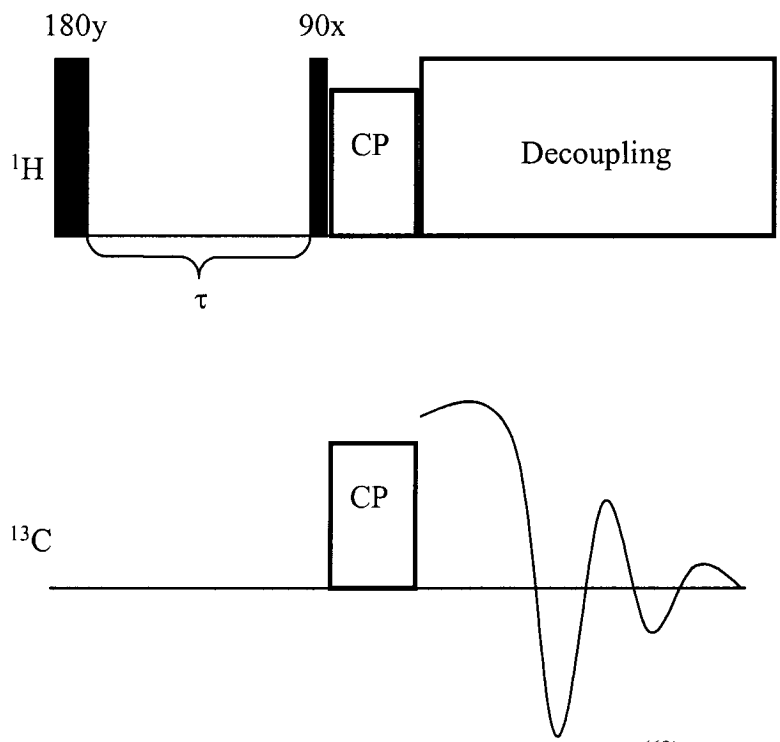

Figure 1.5 The sequence for measuring carbon T_1 relaxation times.[69]

1.3.5 Dipolar dephasing

The dipolar dephasing sequence that was used to study the mobility in the ω-functionalized alkanethiolate chains adsorbed on gold nanoparticles is shown in Figure 1.6. The pulse sequence is described by Alemany[70]. In this pulse sequence, after the cross polarization, the proton decoupler is switch off for a variable time T_{dd}, during which the carbon spins rapidly dephase due to heteronuclear dipolar interactions. A 180° pulse along the spin-locked coordinate was inserted halfway through the T_{dd} period to remove linear phase distortions and refocus long-term chemical shift spin order.

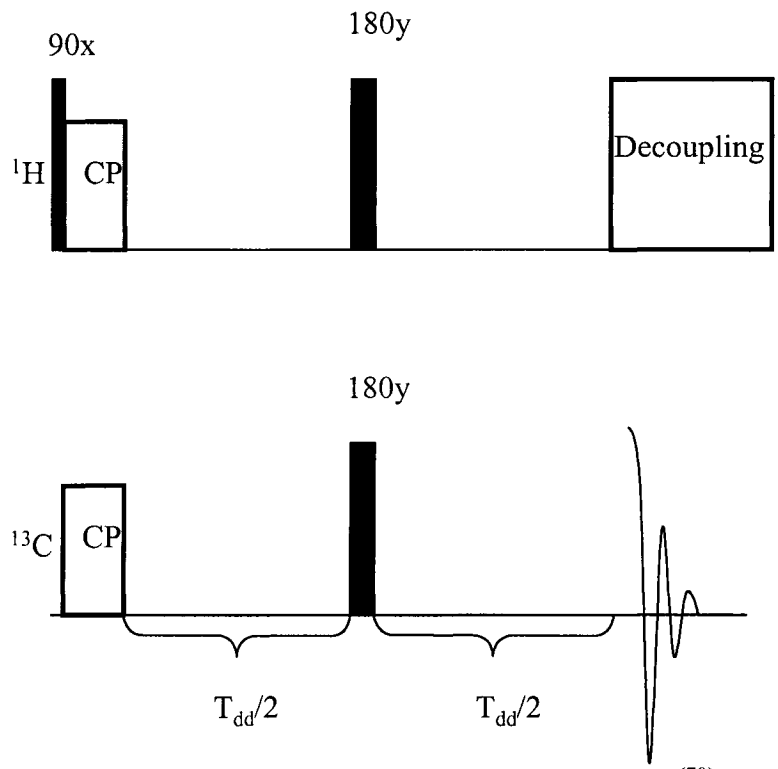

Figure 1.6 The sequence for measuring dipolar dephasing times, T_{dd}.[70]

Dipolar dephasing experiments measure how fast a polarized carbon loses its magnetization after the proton locking is terminated. Figure 1.7 shows a typical dipolar dephasing experiment for alkanethiols on Au nanoparticles.[42] The decay rate of carbon signal intensity depends on the dipole-dipole interactions between proton and carbon.

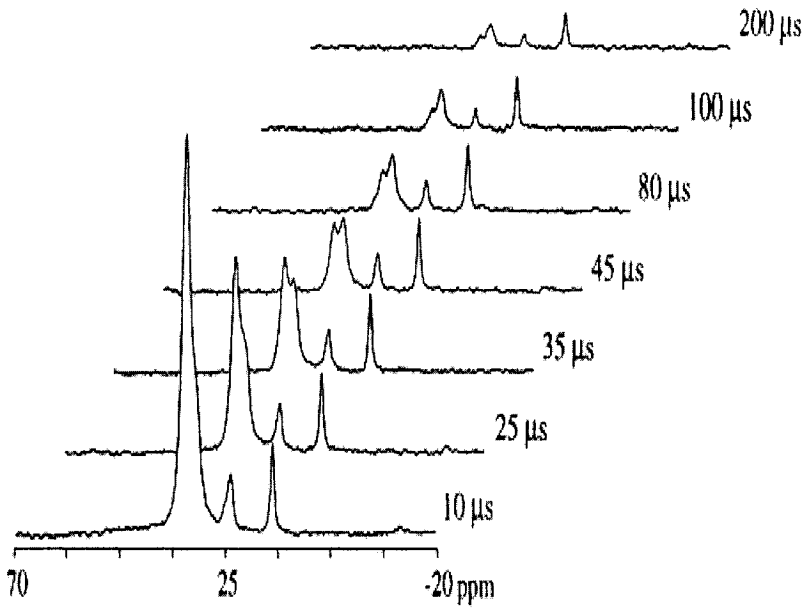

Figure 1.7[42] Dipolar dephasing spectra of octadecanethiol on gold MPCs.

Generally, rigid molecules, dephasing is most rapid for those carbons having directly bonded protons, such as CH and CH_2, due to the strong dipolar coupling. In the example of octadecathiol adsorbed on gold (Figure 1.7), the methyl end group decays much slower due to their weaker dipolar coupling than the interior methelynes that are more rigid. The decrease of signal intensity during the dephasing time T_{dd} is characterized by a constant T_2. In the case of weak dipolar interactions due to molecular motion, the data was fit to a first-order (Lorentzian) decay,[70]

$$I_L = I_{0L} \exp\{-T_{dd}/T_{2L}\}, \tag{1.12}$$

where T_{dd} is the delay time and T_{2L} is the Lorentzian decay constant. For rigid solids, the fast decays are often best fit by a second-order (Gaussian) decay,

$$I_G = I_{0G} \exp\{-T_{dd}^2/2T_{2G}^2\}, \tag{1.13}$$

where T_{2G} is the Gaussian decay constant. Sometimes the nucleus can exhibit two different motions which are best fit by a two-component Gaussian-Lorentzian decay,

$$I = I_{0G} \exp\{-T_{dd}^2/2T_{2G}^2\} + I_{0L} \exp\{-T_{dd}/T_{2L}\}. \quad (1.14)$$

1.4 SCOPE OF THE THESIS

The present research was inspired by the fact that negatively or positively charged particles, soluble in water, can be coated with polyelectrolytes.[71] Studies on the interactions between polyelectrolytes and oppositely charged colloids are of interest in diverse areas of science and technology.[72] However, before investigating the large area of particle-particle interactions between the functionalized nanoparticles and the polyelectrolytes, the influence of the charged groups on the chain order and packing is examined. Questions arise as to the extent to which gold nanoparticles functionalized with negatively charged and a hydrogen bonding functionalities affect the structural and dynamic behavior. We compare the behavior of gold nanoparticles functionalized with self-assembled monolayers of sodium, 10-mercaptodecanesulfonate and 11-mecraptoundecanylphosphonic acid to simple alkanethiols Au nanoparticles. Having the phosphorus NMR active nuclei on the end group of the nanoparticles will allows us to further explore the extent of hydrogen bonding found in nanoparticles functionalised with polar end groups.

The thesis is divided into four chapters:

Chapter one presents a general introduction to the three major components that affect the packing in self assembled monolayers and in functionalized gold nanoparticles. Only the solid state NMR techniques that were used to characterized the gold nanoparticles were described. The introduction of each subsequent chapter specifically addresses the topics covered in that chapter.

Chapter two studies the behavior of water soluble sulfonate functionalized monolayer protected clusters (SO_3-MPCs) synthesized from sodium, 11-mercapto-

decanesulphonate and are compared to simple alkanethiolate gold nanoparticles. ^{1}H and ^{13}C NMR spectroscopy, transmission infrared spectroscopy, transmission electron microscopy, differential scanning calorimetry, thermogravimetry, UV-Vis and Zeta potential were used to characterized SO_3-MPCs.

Chapter three demonstrates the changes of ^{31}P chemical shift present in 11-mercaptoundecanylphosphonic acid and in PO_3-MPCs in solution and solid state. In addition of techniques used for SO_3-MPCs characterization, mass spectrometry, optical microscopy and ^{31}P-NMR spectroscopy were employed. The chain order and dynamics of PO_3-MPCs were compared to CO_2-MPCs and CH_3-MPCs.

Chapter four consists of the overview, conclusions and future work.

1.5 REFERENCES

1. Langmuir, I. *J. Am. Chem. Soc.* **1917**, 39, 1848.
2. Blodgett, K. B. *J. Am. Chem. Soc.* **1935**, 57, 1007.
3. Bigelow, W.C.; Pickett, D. L.; Zisman, W. A. *J. Colloid Interface Sci.* **1946**, 1, 513.
4. Nuzzo, R. G.; Allara, D. L. *J. Am. Chem. Soc.* **1983**, 105, 4481.
5. Ulman, A. *An introduction to ultrathin organic films : from Langmuir-Blodgett to self-assembly*, Academic Press : New York. **1991**.
6. Strong, L.; Whitesides, G. M. *Langmuir* **1988**, 4, 546.
7. Chidsey, C. E. D.; Loiacono, D. N. *Langmuir* **1990**, 6, 682.
8. Nuzzo, R. G.; Korenic, E. M.; Dubois, L. H. *J. Chem. Phys.* **1990**, 93, 767.
9. Li, J.; Liang, K. S.; Camillone, N.; Leung, T. Y. B.; Scoles, G. *J. Chem. Phys.* **1995**, 102, 501.
10. Ulman, A. *Chem. Rev.* **1996**, 96, 1533.
11. Gao, W.; Dickinson, L.; Grozinger, C.; Morin, F. G.; Reven, L. *Langmuir* **1996**, 12, 6429.
12. Tao, Y.T. *J. Am. Chem. Soc.* **1993**, *115*, 4350.
13. Allara, D. L.; Nuzzo, R. G.; *Langmuir* **1985**, 1, 45.
14. Allara, D. L.; Nuzzo, R. G.; *Langmuir* **1985**, 1, 52.

15. Dubois, L. H.; Nuzzo, R. G. *Annu. Rev. Phys. Chem.* **1992**, 43, 437.

16. Canning, N. D. S.; Madix, R. J. *J. Phys. Chem.* **1984**, 88, 2437.

17. Schlotter, N. E.; Porter, M. D.; Bright, T. B.; Allara, D. L. *Chem. Phys. Lett.* **1986**, 132, 93.

18. Tao, Y.T.; Lee, M.T.; Chang, S.C. *J. Am. Chem. Soc.* **1993**, *115*, 9547.

19. Guerrero, G.; Mutin, P. H.; Vioux, A. *Chem. Mater.* **2001**, 13, 4367.

20. Tsai, M.-Y.; Lin, J.-C. *J. Colloid Interface Sci.* **2001**, 238, 259.

21. Porter, M. D.; Bright, T. B.; Allara, D. L.; Chidsey, C. E. D. *J. Am. Chem. Soc.* **1987**, 109, 3559.

22. Wallance, R. M.; Chen, P. J.; Henck, S. A.; Webb, D. A. *J. Vac. Sci. Technol. A* **1995**, 13, 1345.

23. Chau, L. K.; Porter, M. D. *Chem. Phys. Lett.* **1990**, 167, 198.

24. Zamborini, F. P.; Campbell, J. K.; Crooks, R. M. *Langmuir* **1998**, 14, 640.

25. Evans, S. D.; Urankar, E.; Ulman, A.; Ferris, N. *J. Am. Chem. Soc.* **1991**, 113, 4121.

26. Schmidt, M. E.; Shin, S.; Rice, S. A. *J. Chem. Phys.* **1996**, 104, 2101.

27. Bain, C. D.; Biebuyck, H. A.; Whitesides, G. M. *Langmuir* **1989**, 5, 723.

28. Olbris, D. J.; Ulman, A.; Shnidman, Y. *J. Phys. Chem.* **1995**, 102, 6865.

29. Kim, Y.-T.; McCarley, R. L.; Bard, A. J. *J. Phys. Chem.* **1992**, 96, 7416.

30. Dishner, M. H.; Hemminger, J. C.; Feher, F. J. *Langmuir* **1996**, 12, 6176.

31. Wolf, H.; et al. *J. Phys. Chem.* **1995**, 99, 7102.

32. Delamarche, E.; Michel, B.; Biebuyck, H. A.; Gerber, C. *Adv. Mater.* **1996**, 8, 719.

33. Sprik, M.; et al. *Langmuir* **1994**, 10, 4116.

34. Poirier, G. E.; Pylant, E. D.; White, J. M. *J. Chem. Phys.* **1996**, 105, 2089.

35. Dhirani, A.-A.; Zehner, R. W.; Hsung, R. P.; Guyot-Sionnest, P.; Sita, L. R. *J. Am. Chem. Soc.* **1996**, 118, 3319.

36. Sun, L.; Johnson, B.; Wade, T.; Crooks, R. M. *J. Phys. Chem.* **1990**, 94, 8869.

37. Miller, C.; Cuendet, P.; Gratzel, M. *J. Phys. Chem.* **1991**, 95, 877.

38. Nuzzo, R. G.; Dubois, L. H.; Allara, D. L. *J. Am. Chem. Soc.* **1990**, 112, 558.

39. Brewer, N.J.; Beake, D.B.; Leggett, G.J. *Langmuir* **2001**, 17, 1970.

40. His, A.; Liedberg, J. *J. Colloid Interface Sci.* **1991**, 144, 282.

41. Hostetler, M. J.; Stokes, J. J.; Murray, R. W. *Langmuir* **1996**, 12, 3604

42. Badia, A.; Gao, W.; Singh, S.; Demers, L.; Cuccia, L.; Reven, L. *Langmuir* **1996**, 12, 1262.

43. Badia, A.; Singh, S.; Demers, L.; Cuccia, L.; Brown, G. R. Lennox, R. B., *Chem. Eur. J.* **1996**, 96, 2657.

44. Hostetler, M. J.; Green, S. J.; Stokes, J. J.; Murray, R. W. *J. Am. Chem. Soc.* **1996**, 118, 4212.

45. Badia, A.; Demers, L.; Dickinson, L.; Morin, F. G.; Lennox, R. B.; Reven, L. *J. Am. Chem. Soc.* **1997**, 119, 11104.

46. Ingram, R. S.; Hostetler, M. J.; Murray, R. W.; *J. Am. Chem. Soc.* **1997**, 119, 9175.

47. Schmitt, H.; Badia, A.; Dickinson, L.; Reven, L.; Lennox, R. B. *Adv. Mater.* **1998**, 10, 475.

48. Brust, M.; Walker, M.; Bethell, D.; Schiffrin, D. J.; Whyman, R. *J. Chem. Soc., Chem. Commun.* **1994**, 801.

49. Hayat, M. A., Ed. *Colloidal Gold: Principles, Methods, and Applications*; Academic Press: New York, **1989**; Vols. 1-2.

50. Templeton, A. C.; Chen, S.; Gross, S. M.;Murray, R. W. *Langmuir* **1999**, 15, 66.

51. Templeton, A. C.; Cliffel, D. E.; Murray, R. W. *J. Am. Chem. Soc.* **1999**, 121, 7081.

52. Wuelfing, W. P.; Gross, S. M.; Miles, D. T.; Murray, R. W. *J. Am. Chem. Soc.* **1998**, 120, 12696.

53. Chen, S. *Langmuir* **1999**, 15, 7551.

54. Johnson, S. R.; Evans, S. D.; Brydson, R. *Langmuir* **1998**, 14, 6639.

55. Chen, S.; Kimura, K. *Langmuir* **1999**, 15, 1075-1082.

56. Li, X.-M.; Paraschiv, V.; Huskens, J.; Reinhoudt, D.N. *J. Am. Chem. Soc.* **2003**, 125, 4279.

57. Woehrle, G. H.; Warner, M. G.; Hutchison, J. E. *J. Phys. Chem. B.* **2002**; 106, 9979.

58. Shon, Y.-S.; Wuelfing, W.P.; Murray, R.W. *Langmuir*, **2001**, 17, 1255.

59. Becker, E. D. *High resolution NMR, theory and chemical applications*. 3^{ed}., Academic Press, Toronto, **2000**.

60. Fyfe, C. A. *Solid state NMR for chemists*. CFC Press, Guelph, Ontario, Canada, **1983**.

61. Hartmann, S. R.; Hahn, E. L. *Phys. Rev.* **1962**, 128, 2042.

62. Abragam, A. *The principles of nuclear magnetism, Oxford University Press*, **1961**.

63. Voelkel, R. *Angew. Chem. Int. Ed. Eng.* **1988**, 27, 1468.

64. Hodgkinson, P.; Emsley, L. *J. Chem. Phys.* **1997**, 107, 4808.

65. Pinheiro, T. J. T.; Watts, A. *Biochemistry* **1994**, 33, 2451

66. Potrzebowski, M. J.; Assfeld, X.; Ganicz, K.; Olejniczak, S.; Cartier, A.; Gardiennet, C.; Tekely, P. *J. Am. Chem. Soc.* **2003**, 125, 4223.

67. Bovey, F. A.; Jelinski, L. W. *J. Phys. Chem.* **1985**, 89, 571.

68. Jelinski, L. W.; Melchior, M. T. *High-resolution NMR of solids. In NMR spectrscopy techniques*, 2nd ed., Bruch, M. D., Ed.; Marcel Dekker, Inc., New York, **1996**.

69. Torchia, D. A. *J. Magn. Reson.* **1978**, 30, 613.

70. Alemany, L. B.; Grant, D. M.; Alger, T. D.; Pugmire, R. J. *J. Am. Chem. Soc.* **1983**, 105, 6697.

71. Mayya, K.S.; Schoeler, B.; Caruso, F. *Adv. Funct. Mater.* **2003**, 13, 183.

72. Strauss, J. K.; Maher III, L. J. *Science* **1994**, 266, 1829.

Chapter 2

Sulfonate-Monolayer Protected Clusters

2.1 INTRODUCTION

Well-stabilized metal nanoparticles with narrow size distribution have been of great interest for applications in electronic and optical devices[1], catalysis[2] and chemical sensors.[3] Various particle sizes can be synthesized by controlling the experimental conditions such as the temperature, pH, type of reducing agent, the rate of addition of the reducing agent and the type of stabilizing ligand.[4,5] Murray and co-workers[4] achieved some control of the particle size through variation of the gold-to-thiol ratio. An increase in the concentration of gold salt, keeping the gold-to-thiol ratio constant, leads to larger average particle sizes and polydispersity.[5] Colloids that possess very small particles size, (< 10 nm), are more stable and soluble.[6] In this chapter, the gold-to-thiol ratio and the metallic salt concentration will be varied to obtain the desired small and monodispersed particles.

The polydispersity of particles can be controlled by experimental parameters but it can also be achieved by other techniques. A heating treatment strategy was used by Maye et al.[7] to manipulate the size monodispersity and shape of the particles. Another method called digestive ripening which leads to monodispersed and spherical particles was reported by Prasad et al.[8]

Well-stabilized metal colloids can be obtained by varying the stabilizing ligands. Previous studies have shown that nanoparticles with longer alkanethiol ligands have better stability than with short alkanethiols.[9] Stabilizing ligands with a wide range of tail groups were introduced to improve the stability of the nanoparticles in solution as well as in the dry form. In this study, negatively charged, water soluble, sulfonate functionalised gold nanoparticles were synthesized and the stability as a function of ionic strength and pH was assessed.

Stabilizing ligands with bulky, charged terminal groups will have an effect on physical properties of the nanoparticles since the chain packing density and the dynamic

behavior are expected to be different from simple alkane chains. Solid-state NMR has been shown to be useful for structural and dynamic studies of alkanethiol-capped gold nanoparticles.[10] The dynamic behavior and the ordering of the sulfonate-modified thiol chains is of interest for comparison with other analogous functionalized alkanethiols.

The main motivation for preparing these water soluble and highly charged gold nanoparticles is to understand some of the molecular details of particle-particle interactions in assemblies of inorganic nanoparticles. A convenient route for surface modification consists of coating the particles with charged polymers. Layer-by-layer deposition of oppositely charged polymers to create uniform polymer coatings has been successfully extended to a wide range of colloidal substrates such as latexes.[11] For nanometer size particles, steric effects become important. Polyelectrolyte multilayers have been deposited on gold particles as small as 7 nm.[12] Stable multilayers are produced only when gold nanoparticles contain covalently immobilized anionic groups. Consequently, the chain order and packing of the sulfonate monolayer-protected clusters (SO_3-MPCs) will have an influence on the particle-particle interaction between the negatively charged sulfonate head groups and the oppositely charged polymers. The attempt to coat the SO_3-MPCs with the polycation, polydiallyldimethylammonium chloride (PDADMAC) will be examined.

Self-assembled monolayers on flat gold surfaces are considered to be two-dimensional (2D) SAMs whereas nanoparticles can be regarded as 3D SAMs. 2D or 3D SAMs with different chemical functional groups have been prepared using various methods. One approach involves doing chemistry work on the tail group of thiol chains already attached on a gold SAMs.[13, 14] Another approach uses the adsorption of dialkyl disulfides on SAMs or nanoparticles, and the resulting 2D and 3D SAMs were then compared to the corresponding alkanethiolates.[15, 16] Organic thiosulfates, known as bunte salts, is an alternative way to produce the same thiols on 2D or 3D SAMs. Lukkari et al.,[17] showed that alkylthiosulfates can be used to generate 2D SAMs on flat gold surfaces. Murray et al.,[18] demonstrated that using the Brust synthesis, MPCs prepared from dodecanethiol or from its corresponding bunte salt are identical in composition, Au-S bonding and monolayer architecture. However, under the same experimental conditions, larger MPCs are synthesized from bunte salt.

The purpose of the work presented in the following chapter is to establish the extent to which the sulfonate modified gold nanoparticles affect the properties of the previously studied functionalized alkanethiols. Sulfonated surfaces have found extensive application in biomaterials[19] and in various surface-controlled processes. Previous studies[20-23] describe useful properties of SAMs that incorporated mercaptoalkane sulfonate. Due to high charge and hydrophilicity, mercaptodecane sulfonate SAMs behave as a molecular sieve that is selectively permeable to inorganic cations.[23] Turyan and Mandler reported however, that these SO_3-SAMs are disorganised. Caruso[24] used 35 nm size SO_3-MPCs to encapsulate polyelectrolytes in a layer-by-layer sequence, yielding gold nanoparticles coated with uniform polyelectrolyte multilayers. Synthesis of SO_3-MPCs from short chain 3-mercapto-1-propanesulfonic acid was reported by Murray[25] to study its luminescence. However, the dynamic studies of SO_3-MPCs have not yet been reported.

2.2 EXPERIMENTAL

2.2.1 Chemicals

1,10-dibromodecane (97%), thiourea (99+%), hydrogen tetrachloroaurate (III) trihydrate, sodium borohydride (99%) and low molecular weight poly(diallyldimethyl-ammonium chloride) (PDADMAC), were purchased from Aldrich. Cellulose dialysis tubing with MWCO = 12000 (flat width of 25 mm, d = 16 mm) was obtained from Sigma. Sodium sulfite (98.8%) and sodium thiosulfate pentahydrate (99.7%) as well as petroleum ether, NaCl, NaOH, H_2SO_4, HCl, and HNO_3 were purchased from Fisher Scientific. Ethanol (Brampton Ont., 95%) was received from Commercial Alcohols Inc. All chemicals were used as received. 400 mesh carbon coated copper grids were purchased from Electron Microscopy Sciences. Pre-treated distilled water was further purified with the bench milli-Q® system (Millipore Co.) to give resistivity $\geq$ 18.2 MΩcm and pH of 5.5-5.7.

2.2.2 Synthesis of SO_3-functionalized surfactant

The synthesis of $HS(CH_2)_{10}SO_3H$ was slightly modified from the one reported by Turyan and Mandler.[20]

Sodium 10-Bromodecanesulfonate (I)

39.6 g of 1,10-dibromodecane (0.132 mol) was added to a triple neck 250 ml round-bottom flask and dissolved in 100 ml 95% ethanol and 80 ml water. To this stirring and refluxing solution, 3.33 g of $NaSO_3$ (0.026 mol) dissolved in 40 ml of water was gradually added through the separating funnel for 1.5-2 hrs. The mixture continued to reflux for an additional 4 hrs. The reaction was transferred to a 500 ml separatory funnel and the unreacted 1,10-dibromodacane was collected and stored. The remaining aqueous solution was then extracted with (3 × 25 ml) petroleum ether. The lower phase was concentrated by vacuum to ~50 ml, cooled down on ice and collected by suction filtration. The white solid was used directly without any further purification in the thiuronium conversion. (60-80% yield). ^{1}H NMR (270 MHz, D_2O): δ 3.44 (t, 2H, $BrCH_2$), 2.83 (t, 2H, CH_2SO_3Na), 1.78 (q, 2H, $BrCH_2CH_2$), 1.66 (q, 2H, $CH_2CH_2SO_3Na$), 1.34 (m, 4H, CH_2), 1.24 (m, 8H).

10-S-Thiouronium Decanesulfonate (II)

6.56 g of compound I (0.0203 mol), 1.54 g of thiourea (0.0203 mol), 25 ml of water, and 25 ml of 95% ethanol were stirred and refluxed for 6 hrs. The ethanol was removed by vacuum and the solution was cooled down on ice. The cold-precipitated white solid was isolated by suction filtration and twice washed with water. (20-50 % yield) ^{1}H NMR (270 MHz, DMSO-d_6): δ 9.04 (s, 4H, NH_2), 3.13 (t, 2H, SCH_2), 2.41 (t, 2H, CH_2SO_3Na), 1.56 (m, 4H, CH_2), 1.25 (m, 12 CH_2).

Sodium, 10-mercaptodecanesulfonate (IIIa)

10 % of NaOH (1 g of NaOH in 10 ml water) was added to 1.10 g of compound II (3.71 mmol) to let it stir and reflux for 3hrs under Argon stream. The solution was cooled down over night. To the stirred solution containing white crystals, dil.H_2SO_4 (0.7 ml of conc. H_2SO_4 to 5 ml of water) was added drop wise until the pH 7 was obtained. The

clear solution was cooled down on ice. Snow like precipitate was quickly transferred and collected by suction filtration and used in synthesis of SO_3-functionalized gold nanoparticles. (80-95 % yield) ^{1}H NMR (270 MHz, D_2O): δ 2.85 (t, 2H, CH_2SO_3Na), 2.50 (t, 2H, HS*CH_2*), 1.70 (q, 2H, *CH_2*CH_2SO_3Na), 1.57(q, 2H, *CH_2*CH_2SH), 1.2-1.4 (m, 12H, CH_2). ^{13}C NMR (270 MHz, D_2O): δ 51.4 (s, CH_2SO_3Na), 33.3 (s, $HSCH_2$), 28.8-28.4 (4 s, CH_2), 28.0 (s, *CH_2*$CH_2CH_2SO_3Na$), 27.8 (s, $HSCH_2CH_2$*CH_2*), 24.3 (s, *CH_2*CH_2SO_3Na) 24.1 (s, $HSCH_2$*CH_2*). ESI: 275 (M^-), 253 (M-Na), 219 (M^--HS, -Na). Elem. Anal. (found/calculated): C, 41.8/43.5, H, 7.5/7.6. No melting below 250°C was observed.

Bunte salt of decanesulfonate(IIIb)

Sodium, 10-bromodecanesulfonate (2.09g, 6.5 mmol) in 50 ml ethanol and 50 ml water and $Na_2S_2O_3·5H_2O$ (1.62g, 6.5 mmol) in 50 ml water were placed in a 250 ml round bottom flask to let it stir and reflux for 11 hrs. The solvent was removed by vacuum to give white solid. The crude product was dissolved in hot ethanol to remove soluble impurities by suction filtration. The collected solid was used in colloid synthesis. (20% yield) ^{1}H NMR (270 MHz, D_2O): δ 3.06 (t, 2H, NaO_3SSCH_2), 2.86 (t, 2H, CH_2SO_3Na), 1.72 (q, 4H, CH_2), 1.21-1.41 (m, 12H, CH_2). ^{13}C NMR (270 MHz, D_2O): δ 51.4 (s, CH_2SO_3Na), 35.3 (s, NaO_3SSCH_2), 28.7- 28.0 (6 s, CH_2), 24.2 (2s, CH_2).

2.2.3 Synthesis of SO_3 monolayer-protected gold clusters (SO_3-MPCs)

The synthesis strategy, was modified from the one for synthesizing 3-mercaptopropanesulfonic acid monolayer-protected gold clusters by Murray.[25] In a typical reaction, either 160 mg of compound IIIa (0.59 mmol) or 210 mg of compound IIIb (0.57 mmol) were co-dissolved with 75 mg of $HAuCL_4·3H_2O$ in 35 ml of 6:1 milli-Q/acetic acid and stirred for 30 min. To the rapidly stirring solution, 15 ml of freshly prepared $NaBH_4$ (143 mg, 3.8 mmol in milli-Q) was added within less than 30 sec. The whole reaction vessel was stirred for an additional 100 min, and the pH was then adjusted to 1 by dropwise addition of concentrated HCl. The solution was loaded into 20 cm segments of cellulose dialysis membranes and slowly stirred in a 4 L beaker of milli-Q water. The milli-Q water was replaced twice a day after at least 8 hrs for a period of 3

days. The SO_3-MPCs were collected from the dialysis bags and the solvent was removed by vacuum (<40 °C) or by freeze drying.

In the SO_3-MPCs synthesis where the surfactant IIIa was used, two aspects of the reaction conditions were varied. First, the mole ratio of sodium, 10-mercaptodecanesulfonate to $HAuCl_4 \cdot 3H_2O$ and second, the concentration of gold was different.

2.2.4 Deposition of PDADMAC on SO_3-MPC

The 2 nm-diameter sulfonate-modified gold nanoparticles were coated with a layer of poly(diallyldimethyl-ammonium chloride) (PDADMAC), according to the Caruso paper[12]. An ionic strength of 20 mM NaCl was used and milli-Q water was used instead of 0.1M TRIS.

2.2.5 Instrumentation

Solution-state NMR Spectroscopy

Characterization of compounds through out the synthesis and the study of the bulk thiols and thiol-derivatized gold colloids in solutions were performed on a JOEL ECLIPSE-270 spectrometer at 25 °C.

Solid-state NMR Spectroscopy

Solid-state 67.92 MHz ^{13}C NMR spectra were run on a Chemagnetics CMX-270 spectrometer with 4 mm (Chemagnetics/Varian) double tuned magic angle spinning (MAS). A spin rate of 6 kHz, an average of 100-1000 scans and pulse delay of 2 s were typically used to acquire ^{1}H-^{13}C CP/MAS spectra. The ^{1}H 90° pulse widths were between 3 and 4 μs and a contact time of 1 ms was used. For the variable-temperature CP-MAS experiments, the sample temperature was controlled to within ± 2°C by a Chemagnetics temperature controller. Before any sample was run, the reference hexamethylbenzene (HMB) was used to calibrate the spectrometer by adjusting the 180° pulse and setting its methyl peak at 17.3 ppm.

For the carbon T_1 measurements, the Torchia inversion-recovery sequence[26] was used with the initial ^{13}C magnetization generated by cross polarization. A pulse delay of 5 T_{1H} was used to allow the return of magnetization to equilibrium.

The dipolar dephasing experiments were performed using the decoupling pulse sequence[27] and T_{dd} was measured as described in introduction.

Transmission Electron Microscopy (TEM)

Samples for TEM were prepared by placing a drop of aqueous colloidal solution on carbon-coated copper grids (400 mesh), waiting 5 min, and removing the excess solution by touching a small piece of filter paper to the edge of the grid. The copper grids were then dried over night in the air. The phase-contrast images of the particles were obtained with a top-entry JOEL JEM-2000 FX electron microscope operating at 80 keV and fitted with an Electron Dispersive Spectrometer (EDS). Size distributions of the particles were determined from diameters of at least 100 particles, selected from three typical regions at magnification ranging from 100 kX to 340 kX. A CCD camera (Gatan BioScan Camera Model 792) was used to obtain the images where the DigitalMicrograph™ software version 2.4.3 was used to obtain better contrast and brightness. Sigma Scan version 4.1 was then used to obtain the size diameter of the particles.

UV-Visible Spectroscopy

UV-Vis spectra were obtained using a double beam Cary 300 Bio UV-Vis spectrophotometer. The dilute solutions of gold colloids were acquired from 900 to 300 nm with a scan rate of 300 nm/min, using a quartz cell with a path length of 1 cm. The milli-Q water was used as reference.

Fourier Transform Infrared Spectroscopy (FT-IR)

Transmission spectra for the bulk samples and the nanoparticles were acquired on a photoacoustic Bio-Rad FTS6000 spectrometer containing a MTEC300 photoacoustic cell from MTEC Photoacoustics, Inc. The infrared spectra were obtained after purging the cell with helium gas and were background corrected using a carbon black reference. Spectra were obtained for 32 to 64 scans at a resolution of 4 cm^{-1}.

Differential Scanning Calorimetry (DSC)

DSC Q1000 fitted with autosampler and finned air cooling system was calibrated against the indium reference at the same settings; under nitrogen atmosphere, heat-cool rates of 5 °C/min and a high volume stainless steel pan, using 2- 8 mg samples.

Thermogravimetry Analysis (TGA)

TGA analyses were performed with a TGA Q500 with an autosampler and two mass flow controllers. 5-10 mg of accurately weighed samples were recorded starting from room temperature to 550 °C under N_2 and than under O_2 up to 700 °C, at 20 °C/min.

Zeta-potential Analysis

The charge of the SO_3-modified gold particles before and after the deposition of the polyelectrolyte, was monitored by the ZetaPlus analyzer (Brookhaven Instruments Corp., N.Y.). All measurements were performed in 1mM NaCl, milli-Q water (pH ~ 5.7) at 25 °C. The electrophoretic potential was taken from the average of three runs of ten measurements.

2.3 RESULTS AND DISCUSSION

2.3.1 Synthesis of MDS and SO_3-MPC

To reduce the formation of the disulfonic acid in the first step of sodium, 10-mercaptodecanesulfonate (MDS) synthesis, a large excess of 1,10 dibromodecane is necessary and sodium sulfite should be preferentially added dropwise over a period of time.[28] NaOH or NH_3 can be used to convert thiouronium compounds into mercaptants. In the case of NaOH, used here, the thiol is readily obtained however a byproduct, dicyandiamide, $(NH_2CN)_2$, is produced which is difficult to remove.[29] From the elemental analysis, 0.1 to 0.7% of N was found in the samples which was probably due to the dicyandiamide impurity. The presence of this impurity was not detrimental to this study since the compound was removed by dialysis when MDS was adsorbed on gold and the elemental analysis of gold colloids indicated no nitrogen containing impurities. The sodium, 10-mercaptodecanesulfonic acid was hygroscopic and was only soluble in water

where it formed micelles above a certain concentration and behaved as a soap which maked it very difficult to crystallize. The ^{1}H-NMR spectra of the MDS and its Bunte salt are given in Figures 2.1 and 2.2.

The gold nanoparticles stabilized by sodium, 10-mercaptodecanesulfonate have been prepared in milli-Q/acetic acid solvent since MDS is only soluble in water. Due to the hydrolysis of $NaBH_4$,[30] (equation 2.1), the reaction mixture reached a pH of 10 in pure water forming irreversible black aggregates, as opposed to the final pH 4.8 when in presence of acetic acid. The irreversible aggregates were also produced when $NaBH_4$ was

$$NaBH_4 + 4H_2O \longrightarrow H_3BO_3 + NaOH + 4H_2 \qquad (2.1)$$

added to a control sample (i.e., no MDS), showing the importance of the stabilizing ligand. Co-dissolution of $AuCl^-$ and MDS in milli-Q/acetic acid solvent resulted in a pale yellow/brown color. When $NaBH_4$ was added dropwise, the color of the mixture immediately darkened and a strong emulsion resulted. The excess of unreacted thiol, acetic acid and other impurities was removed by dialysis.

2.3.2 Transmission Electron Microscopy

From the TEM pictures in Figure 2.3, the results clearly show that a decrease in the MDS:$AuCl_4^-$ ratio and an increase in the $AuCl_4^-$ concentration, lead to larger average particles sizes and higher polydispersities, consistent with previously reported results for less bulky substituents.[14] The EDS analysis performed on individual particles showed that the constituent element was Au. The morphology of the gold particles obtained in this study was mostly spherical. For larger clusters with a diameter of 3.5 ± 1.5 nm and 5.7 ± 1.9 nm, the color of the dispersed colloid in solution were found to be red and light pink, respectively and when in dry form, their dark free powder displayed a distinct golden tinge. Smaller particles with an average diameter of 3.0 ± 1.2 nm and 1.8 ± 0.4 nm have an appearance of finely divided black powder with no waxy texture and red and brownish colors, respectively when dispersed in water. The smallest particles show extremely high water solubility even at high concentration, which will be particularly useful for biological applications and biosensers.[31, 32] Water was the only solvent where

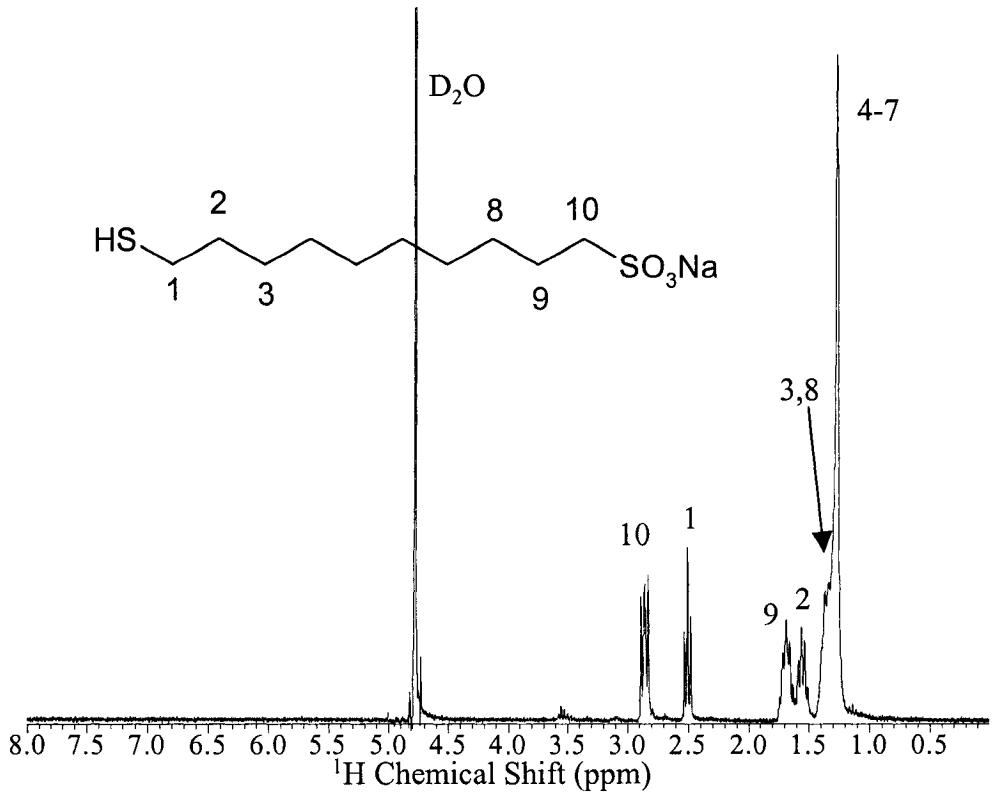

Figure 2.1 ^{1}H-NMR spectrum of sodium, 10-mercaptodecanesulfonic acid in D_2O.

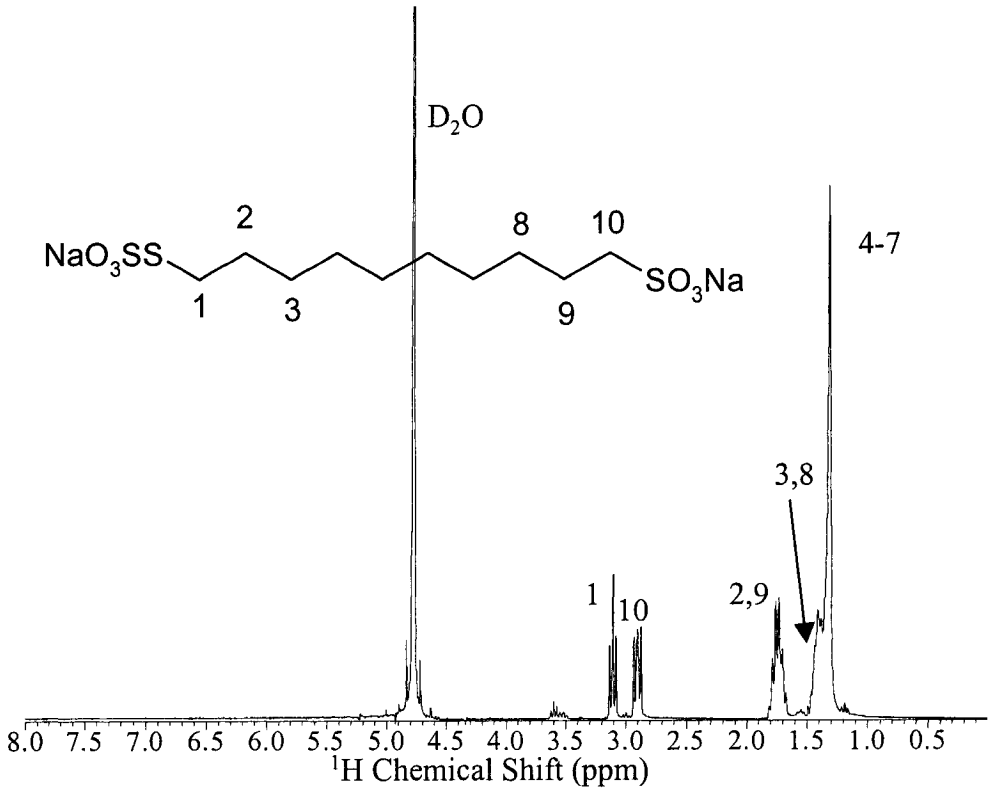

Figure 2.2 ^{1}H-NMR spectrum of Bunte salt sodium decanesulfonate in D_2O.

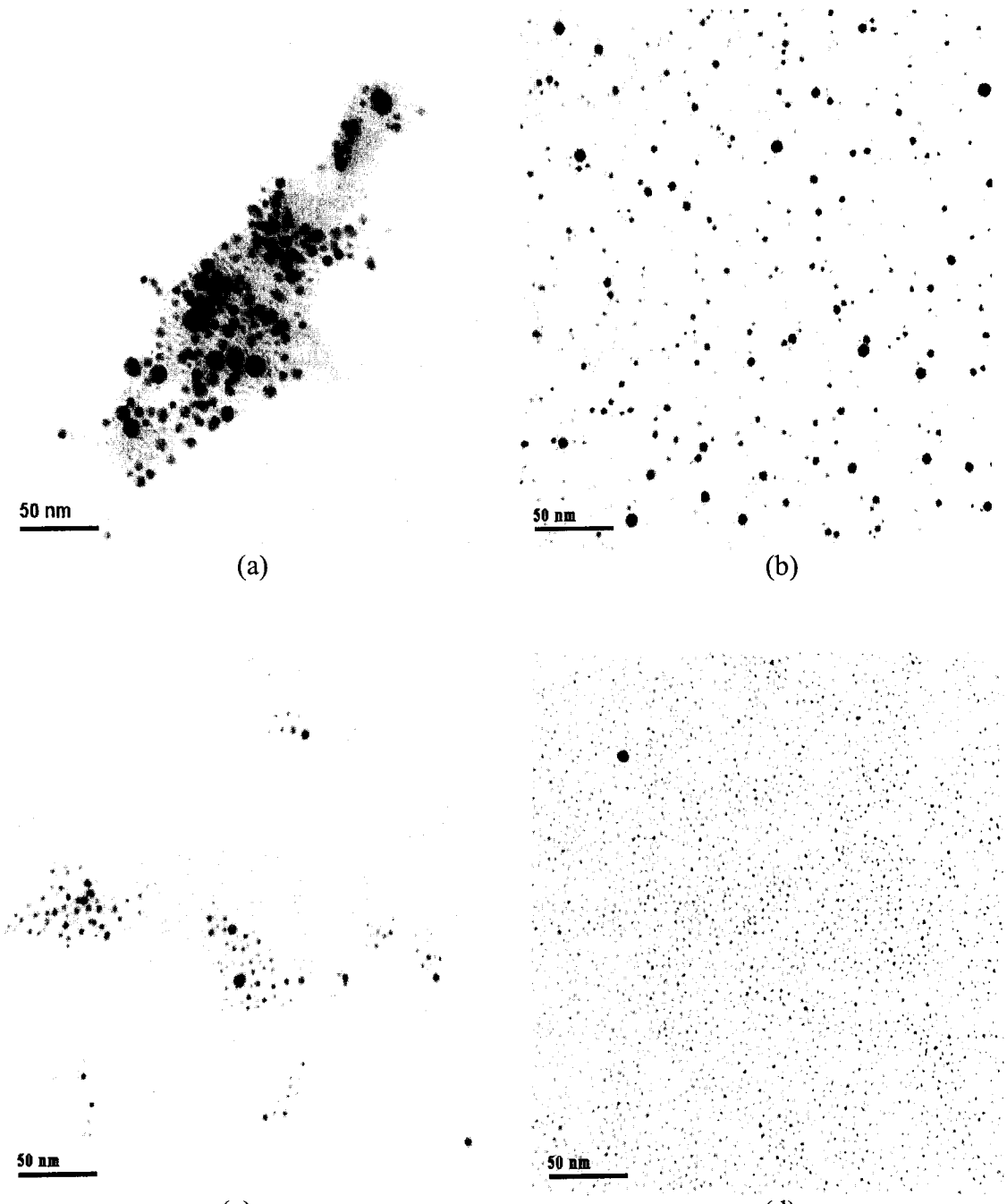

Figure 2.3 TEM micrographs of SO_3-MPCs prepared by varying two experimental conditions: MDS:Au ratio and [Au]. (a) 5.7 ± 1.9 nm, 1:3, 15.7 mM. (b) 3.5 ± 1.5 nm, 2:1, 15.7 mM. (c) 3.0 ± 1.2 nm, 3:1, 15.7 mM. (d) 1.8 ± 0.4 nm, 3:1, 3.8 mM.

the isolated SO_3-MPCs were soluble, showing very specific solubility character. In other common polar solvents, such as methanol, ethanol, acetonitrile and acetone these particles were insoluble.

2.3.3 Solution ^{1}H-NMR

The ^{1}H-NMR spectra of SO_3-MPCs (i.e., 3:1, MDS:Au, [Au] = 3.8 mM) synthesized from bunte salt of decanesulfonate (Figure 2.4a) are nearly identical to those of SO_3-MPCs (2:1 MDS:Au, [Au] = 15.7 mM) synthesized from sodium, 10-mercaptodecanesulfonate (Figure 2.4b). Three broad peaks at 2.7-2.9, 1.6-1.8 and 1.1-1.4 ppm arise from the methylene protons CH_2SO_3, $CH_2CH_2SO_3$ and from the middle chain, respectively. The peak broadening effect[4, 10] is typical for alkanethiolate-MPCs and demonstrates that SO_3-modified alkanethiolate chains are attached to the gold clusters. Furthermore, the absence of methylene peaks at 2.5 ppm observed in free MDS or 3.1 ppm in free Bunte salt and 1.6 ppm in both, is an indication that no free surfactant is present. The methylene groups closest to the gold interface are the most densely packed with a solid-like mobility. The other contribution to the broadening of these resonances has been shown to be a large chemical shift distribution, due to slightly different bonding environment on the faces, edges and corners of the nanoparticles.[33] Figure 2.5 shows a 3.0 ± 1.5 nm SO_3-MPCs (3:1 MDS:Au, [Au] = 15.7 nm) where the small sharp multiplets are due to the free impurities. The 5.7 ± 1.9 nm SO_3-MPCs prepared from 1:3 MDS:Au ratio and a 15.7 mM of gold salt showed no ^{1}H-NMR due to the settling of the particles.

2.3.4 UV-Vis characterization

The size distribution and the stability can be also qualitatively obtained from the intensity and energy of the surface plasmon (SP) resonance band typically encountered in metal nanoparticles.[34] Figure 2.6 displays the relation between the intensity of SP resonance band and the particle size for the SO_3-MPCs prepared under different conditions. The shape and position of the SP band are consistent with TEM images in Figure 2.3 and are in agreement with those previously reported for particles of similar sizes.[4] Due to their large particle size, the 5.7 nm gold nanoparticles settled down instead of being dispersed in solution giving a very faint pink color and no visible SP

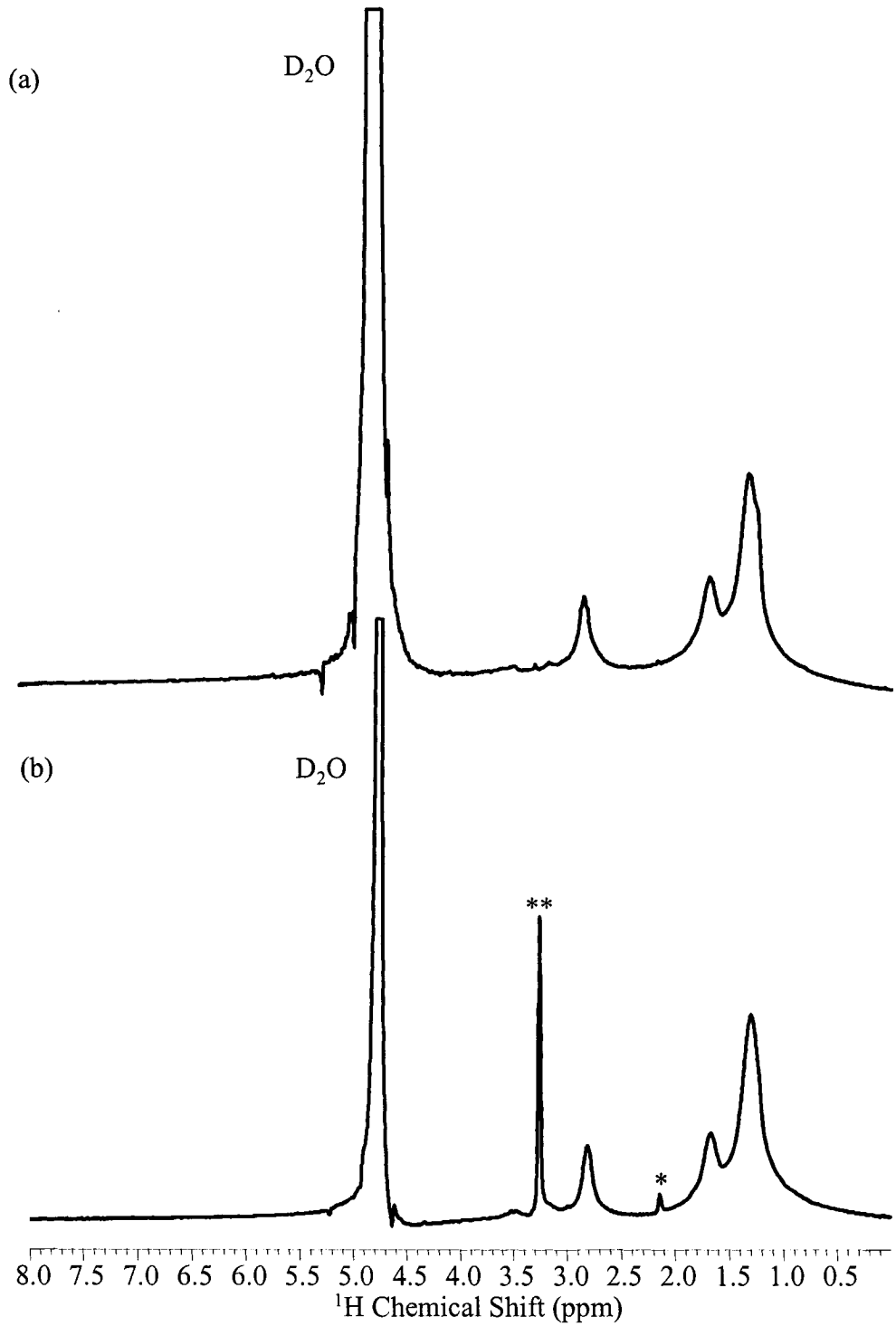

Figure 2.4 The ^1H-NMR spectra of SO_3-MPCs in D_2O synthesized from (a) Bunte salt of decanesulfonate (1.8 ± 0.4 nm) and (b) from sodium, 10-mercaptodecanesulfonate (3.5 ± 1.5 nm). Line broadening of 1 Hz was used. The acetone(*) and methanol (**) peaks were present.

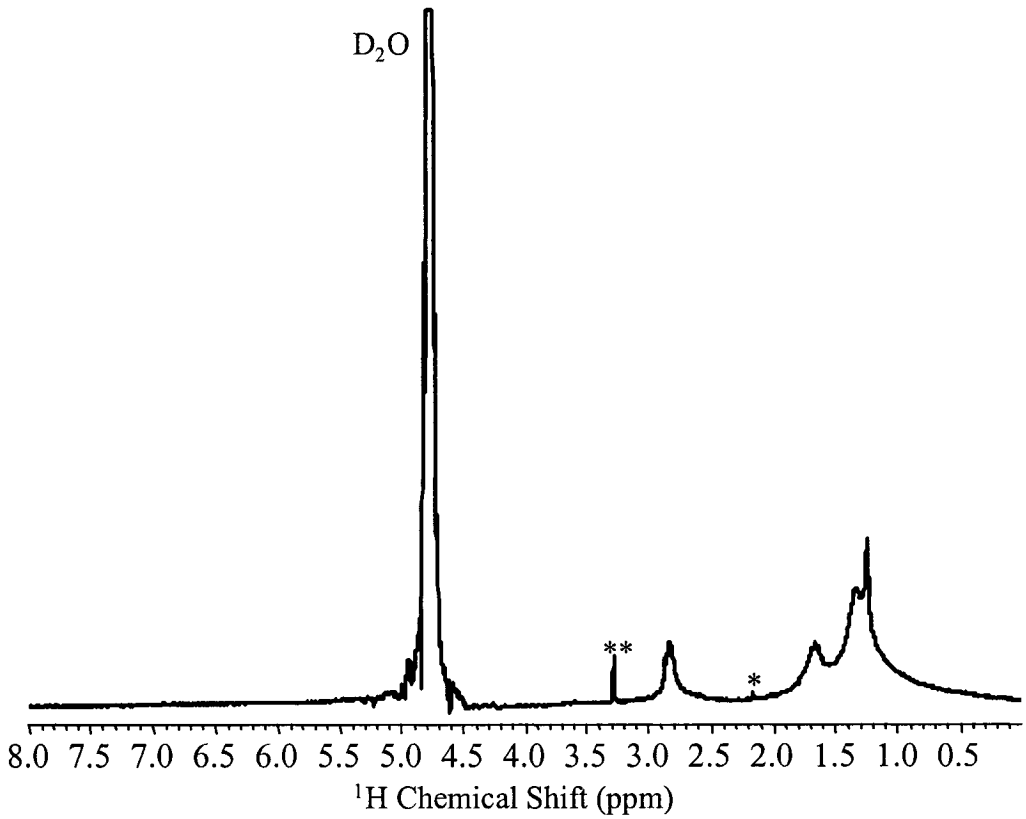

Figure 2.5 The ^{1}H-NMR spectrum of 3.0 ± 1.2 nm diameter SO_3-MPCs prepared using 3:1 MDS:Au, [Au] = 15.7 mM. Spectrum shows sharp peaks due to unbound impurities. Acetone (*) and methanol (**) were present. Line broadening of 1 was used.

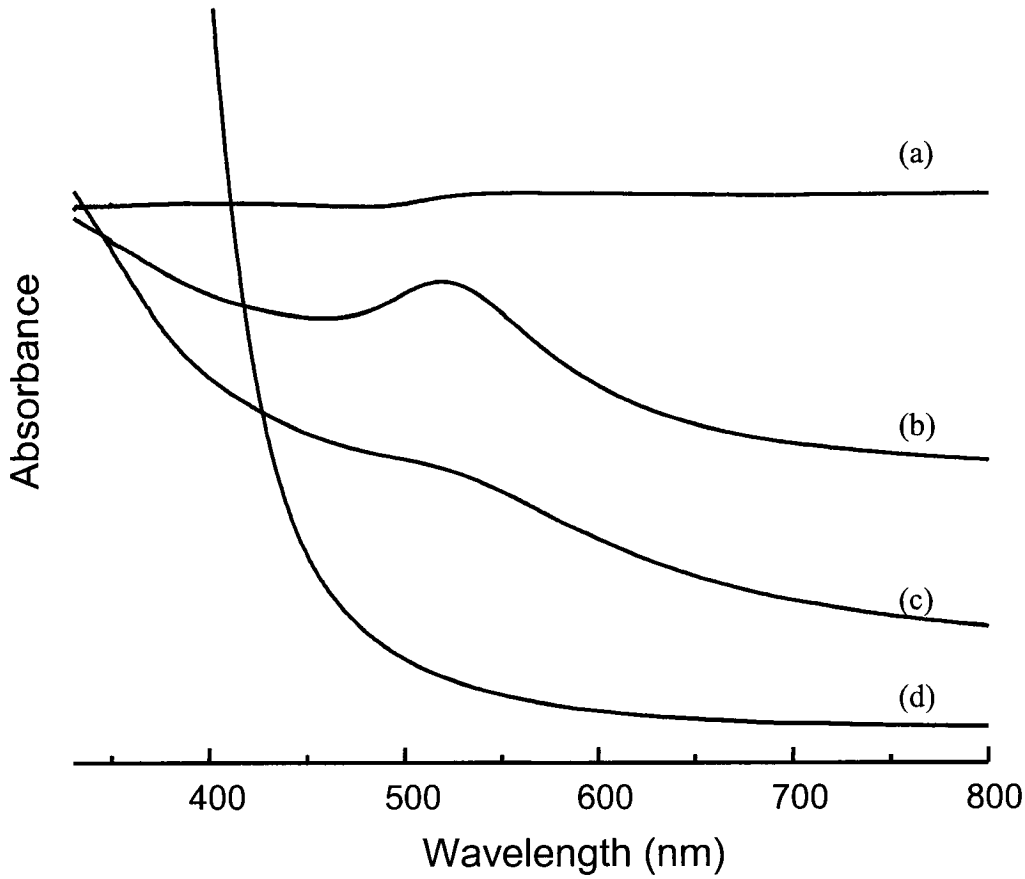

Figure 2.6 UV-Vis spectra of various sizes of SO_3-MPCs synthesized with various MDS:Au ratio and Au concentration. (a) 5.7 ± 1.9, 1:3, 15.7 mM. (b) 3.5 ± 1.5, 2:1, 15.7 mM. (c) 3.0 ± 1.2, 3:1, 15.7 mM. (d) 1.8 ± 0.4, 3:1, 3.8 mM.

band. In contrast, the 3.5 nm particles gave a strong SP resonance band with a λ_{max} of 520 nm. A less defined SP band (i.e., shoulder) was observed for smaller particles, whereas for the smallest clusters no SP band was detectable as an indication of quantum size effects explained by Mie theory.[35]

The red shift of the SP band in the UV-Vis spectrum is a good indication of the aggregation of the particles and thus their stability can be monitored. The thermodynamic stability of nanoparticles can be affected by the packing of the chains which in turn depends on the functionality of the tail group. Water soluble MPCs are particularly important in biolabeling experiments[36] where excess buffer can lead to complications. The stability of the SO_3-MPCs as a function of ionic strength and pH was displayed in Figures 2.7 and 2.8. At low electrolyte concentration (i.e., 0.1 M NaCl), the 3-3.5 nm particles were stable for a few days, whereas the 1.8 nm particles did not aggregate even after few months. As the ionic strength was increased, the particles became less stable, and formed larger clusters in a shorter period of time. The UV-Vis spectrum of the SO_3-MPCs in 3 M NaCl displays additional broad bands at 600 nm and 650 nm, suggesting that large aggregates were required to produce the dramatic color change.[37]

The stability of SO_3-MPCs as a function of pH was also examined. The UV-Vis spectra at three different pH values were recorded and are shown in Figure 2.8. Alkylsulfonic acids are know to behave as strong acids (i.e., $CH_3CH_2SO_3H$ has a pK_a of –1.68),[38] and thus are expected to be highly charged even at low pH, giving a little aggregation.

The spectra obtained in Figure 2.8 as a function of solution pH are almost identical showing little evidence for aggregation of the particles. The SO_3-MPCs also have good thermal stability. When dispersed in water and heated at 60 °C for 8 hrs, the ^{1}H-NMR spectra looked exactly the same as before heating, free of sharp peaks and no shift in the plasmon absorption band was observed. Similar thermal stability was observed for the short chain O_3SC_3S/Au nanoparticles.[39] Hutchison et al., claim that on top of the high thermal stability, the particles showed remarkably good pH and electrolyte stability. They found that the particles where stable in saturated NaCl solutions for several days, which was not the case for the long chain SO_3-MPCs.

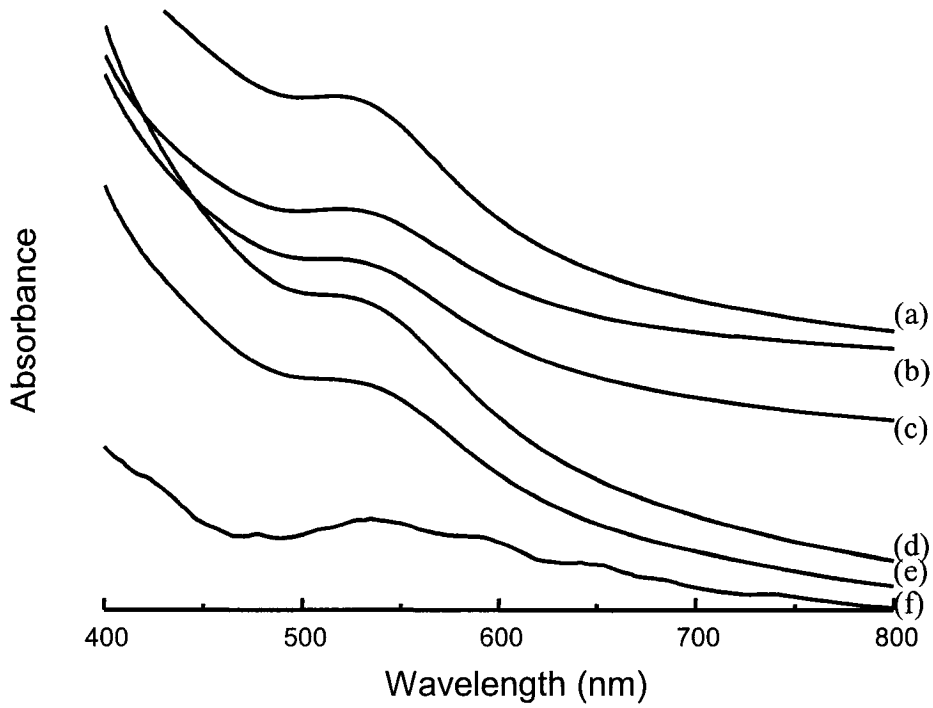

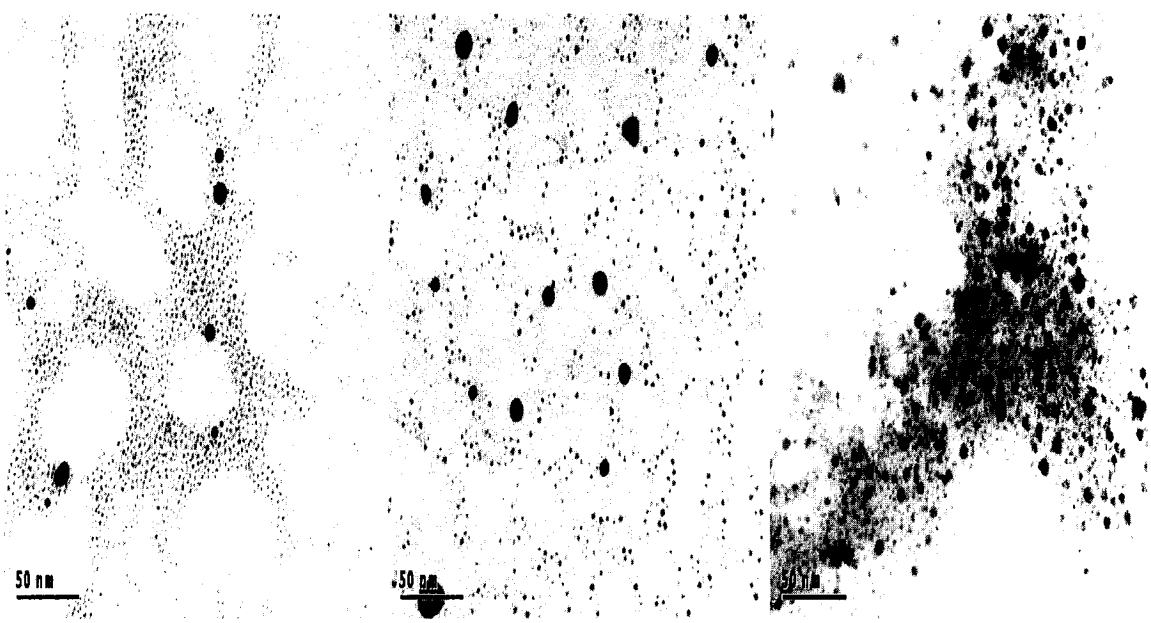

Figure 2.7 The surface plasmon absorption band of 3.0 nm diameter SO_3-MPCs, using various NaCl concentration; (a) no NaCl, (b) 0.1 M, (c) 0.5 M, (d) 1 M, (e) 2 M and (f) 3M. TEM micrographs visualizing the aggregation for 0.1, 0.5 and 1M NaCl.

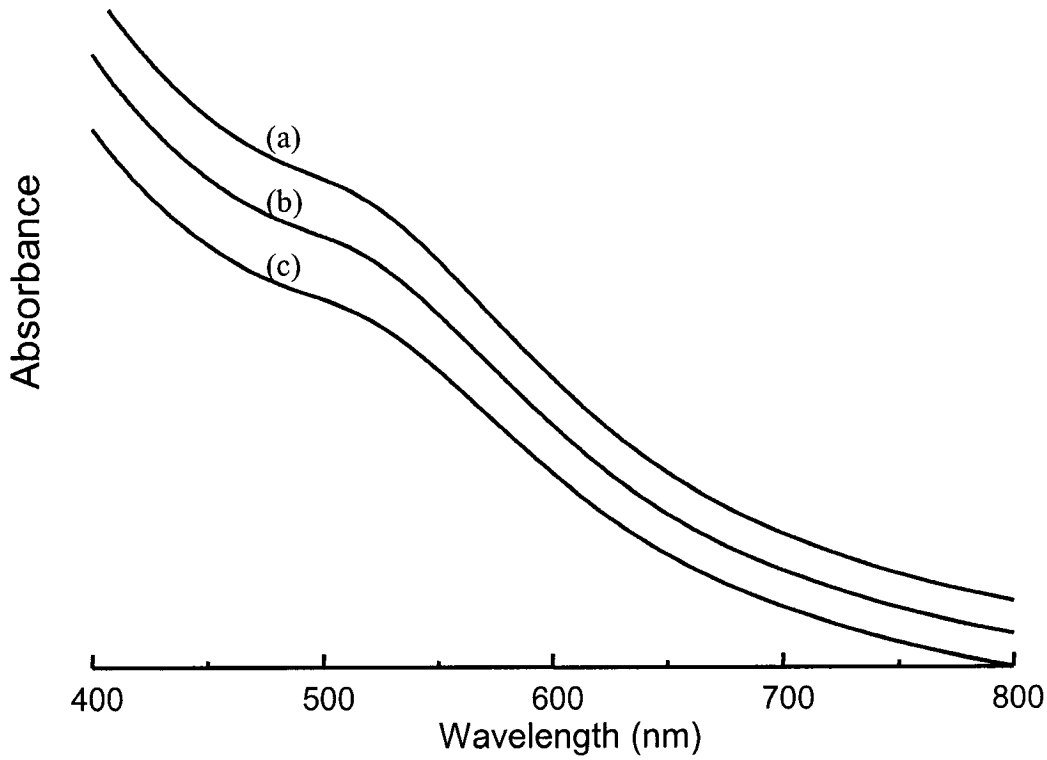

Figure 2.8 Uv-Vis spectra of 3.0 nm-diameter SO_3-MPCs as a function of solution pH (a) 10 (b) 7 and (c) 2.

2.3.5 Thermogravimetric analysis

Thermogravimetric analyses (TGA) were performed on the unbound MDS along with different SO_3-MPCs sizes to determine the organic weight fraction. Figure 2.9 shows the TGA curves of the free bulk and the SO_3-MPCs (i.e., 2:1 MDS:Au, [Au] = 15.7 mM). Sodium, 10-mercaptodecanesulfonate had large degradation stage which started at 350 °C and ended at 500 °C. The gradual loss at the beginning of the heating was associated with the loss of water. At 750 °C, an additional ~ 7 % of the mass was lost under the oxygen and a large non-volatile residue (i.e., ~ 40 %) was still not volatilized at 1000 °C. The TGA curve of the MDS was consistent with a thermal degradation of

Table 2.1 Average particle size, UV-Vis and organic fraction data of gold nanoparticles protected by sodium, 10-mercaptodecanesulfonate prepared by using various thiol:Au ratio and Au concentration.

MPC (thiol:Au, [Au])	TEM (d ± st.dev., nm)	UV-Vis λ_{max} (nm)	TGA % organic
1:3, 15.7 mM	5.7 ± 1.9	Agglomerates	3.1
2:1, 15.7 mM	3.5 ± 1.5	516	18.4
3:1, 15.7 mM	3.0 ±1.2	Shoulder, 490-580	49.7
3:1, 3.8 mM	1.8 ± 0.4	No S.P. band	32.4

poly(vinyl sulfonic acid) in sodium form.[41] The analysis of the residue showed that inorganic components, such as sulfite and sulfate ions were present. Wilkie et al., proposed the degradation pathway for the formation of inorganic products.[41] Table 2.1 tabulates the organic weight loss when SO_3-MPCs of different sizes were heated under

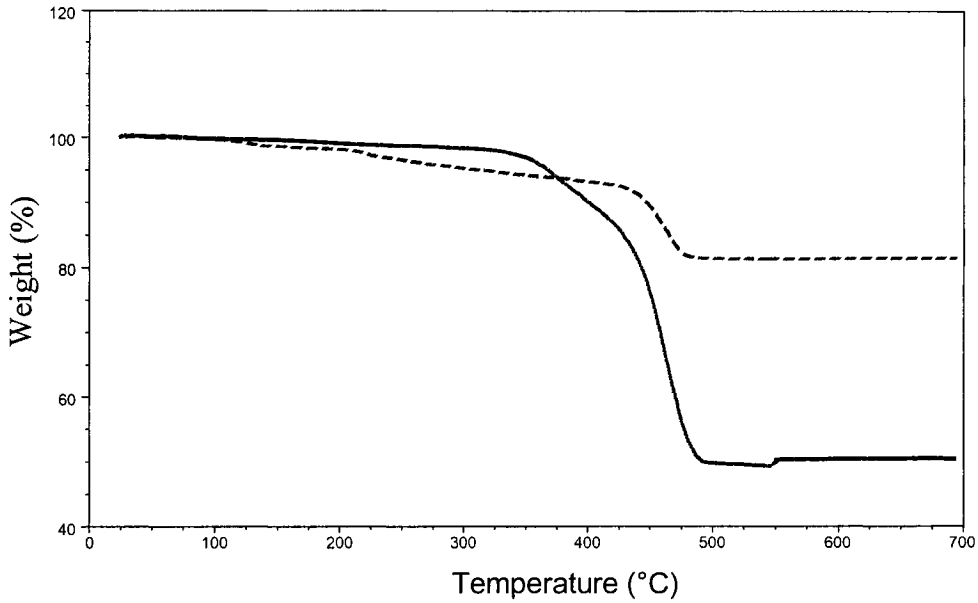

Figure 2.9 Comparison between TGA curve of unbound thiol, MDS, (solid line) and TGA curve of 3.5 nm-diameter SO_3-MPCs (dashed line) at 20 °C/min under nitrogen and oxygen.

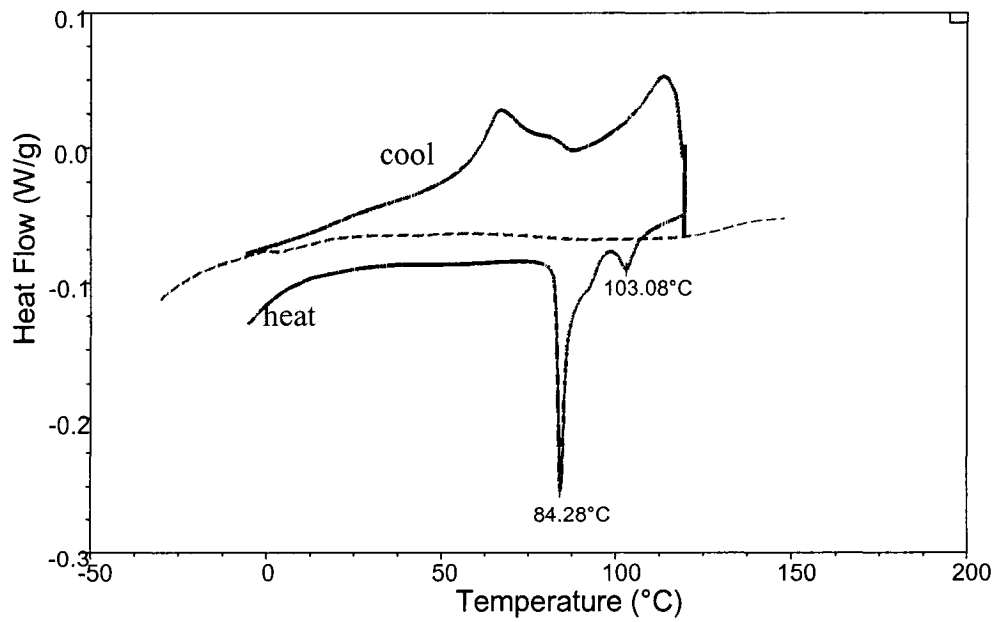

Figure 2.10 Heating and cooling curves of unbound thiol, MDS (solid line) and heating curve of 1.8 nm-diameter SO_3-MPCs (dashed line). The MDS shows solid-solid transition at 84 °C.

the TGA conditions. When SO_3-MPCs were burned under N_2 only (up to 1000 °C), no loss was observed after 450 °C and black solid residue was found in the pan. Only when N_2 was switched to O_2 at 550 °C, a gold-color solid product resulted. The TGA curve of 3.5 nm SO_3-MPCs was shown in Figure 2.9 where the main mass loss occured at ~ 450 °C. For the 5.7 nm SO_3-MPCs only small % organic mass fraction was burned which indicates that not all the Au surfaces were covered by the MDS. The SO_3-MPCs colloid of 3.5, 3.0 and 1.8 nm in diameter resulted in a coverage of 214, 332 and 61 MDS chains and a corresponding area per chain of 18.0, 8.52 and 16.7 $Å^2$. The % organic of 3.0 nm SO_3-MPCs were considerably higher which was probably due to unbound surfactant, Figure 2.5. The results of the footprint size for 3.5 and 1.8 nm SO_3-MPCs were reasonable and comparable to the results for 2.1 nm $C_{14}S$-MPCs[9] and 1.8 nm tiopronin-MPCs[30] which generated footprints of 17.2 and 18 $Å^2$/chain, respectively. TGA data of 2.2 nm SO_3-MPCs synthesized from 2-acryloamido-2-methyl-1-propanesulfonic acid yielded 30.2 % organic mass loss with a coverage of 111 chains.[41]

Differential scanning calorimetry (DSC) was previously used to study the phase behavior of thiol-derivatized Au nanoparticles in terms of the temperature and the enthalpies of the phase transitions.[9] The endotherms which increase in temperature and in enthalpy with increasing chain length are associated with the order/disorder transition of the alkyl chain observed by solid-state NMR.[9] The DSC curves of the bulk thiol and the SO_3-MPCs (dashed line) were extrapolated in Figure 2.10. The heating curve for the DSC of the bulk surfactant showed two endotherm peaks, a larger one at 84 °C and a smaller one at 103 °C (i.e., water loss) with enthalpies of 8.5 J/g and 1.0 J/g. The larger enthalpy phase transition was associated with an order/disorder transition which was observed by solid-state NMR. To confirm this, the sodium, 10-mercaptodecanesulfonate was heated in the rotor and spectra were recorded at temperatures around the DSC endotherm, this will be discussed later. The melting of the MUP solid was not detected below 250 °C thus the DSC peak at 84 °C does not correspond to an enthalpy of fusion.

Since the enthalpy decreased with decreasing chain length, short chain simple alkanethiol, $C_{12}S$/Au, nanoparticles showed a broad and small endotherm signal in the DSC curve at ~ 0 °C compared to the $C_{18}S$/Au nanoparticles which showed a distinct DSC transition at ~ 55 °C.[9] The DSC curve for the 1.8 nm SO_3-MPCs in Figure 2.10

(dashed line) shows no enthalpy signal even though the order/disorder transition was observed in solid-state NMR, which will be discussed later. Due to the short chain, C10, and possibly water being adsorbed which could affect the baseline, no endotherm was observed.

2.3.6 PAS-FTIR

Infrared spectroscopy provides structural and conformational information for the monolayers of MPCs. Solid-state FTIR spectra of free sodium, 10-mercaptodecane-sulfonate and SO_3-MPCs (3:1 MDS:Au, [Au] = 3.8 mM) are compared in Figures 2.11a and 2.11b, respectively. The bands observed at ~2920 and 2850 cm^{-1} are assigned to symmetric and antisymmetric C-H stretching vibrations, respectively. These bands are very sensitive to the degree of organization of the monolayer and have been used in previous IR studies to provide conformational information of the methylene chain ordering.[42] A shift to a lower wavenumber is characteristic of a trans conformation. The symmetric and asymmetric methylene vibrations of the bulk surfactant are located at 2924 and 2853 cm^{-1}, respectively. A shift to lower wavenumbers observed for SO_3-MPCs (i.e., s. str. = 2920, as. str. = 2851 cm^{-1}) and the narrower line width are indicative of chain organization. The sulfonate (i.e., S=O=S) group vibrations, at 1215 (as.) and 1067 cm^{-1}(s.) in MDS show the presence of the sulfonic acid functionality.[41, 43] The absence of the S-H stretching vibration at 2561 cm^{-1} in the SO_3-MPCs spectrum suggests that the MDS surfactant is chemisorbed via its thiol group, which has already been observed for other thiols.[43] Methylene scissoring at 1466 cm^{-1} and the scissoring of the methylene group next to the Au-S bond at 1419 cm^{-1} further confirms the attachment of MDS to Au.[44] The region of 600-750 cm^{-1} provides conformational information about C-C bonds adjacent to the C-S bond in the alkanethiols.[42] As can be seen from the bulk spectrum, the gauche and trans conformation of the S-C-C chain at 640 cm^{-1} and 725 cm^{-1}, respectively are both present in the sample. In the case of the SO_3-MPCs, the intensity of the gauche band is no longer observed which can be explained by highly ordered chains at the gold surface. The shift of the trans peak (i.e., 721 cm^{-1}) to lower wavenumber is associated with the removal of electron density from the C-S bond due to the Au surface.[42]

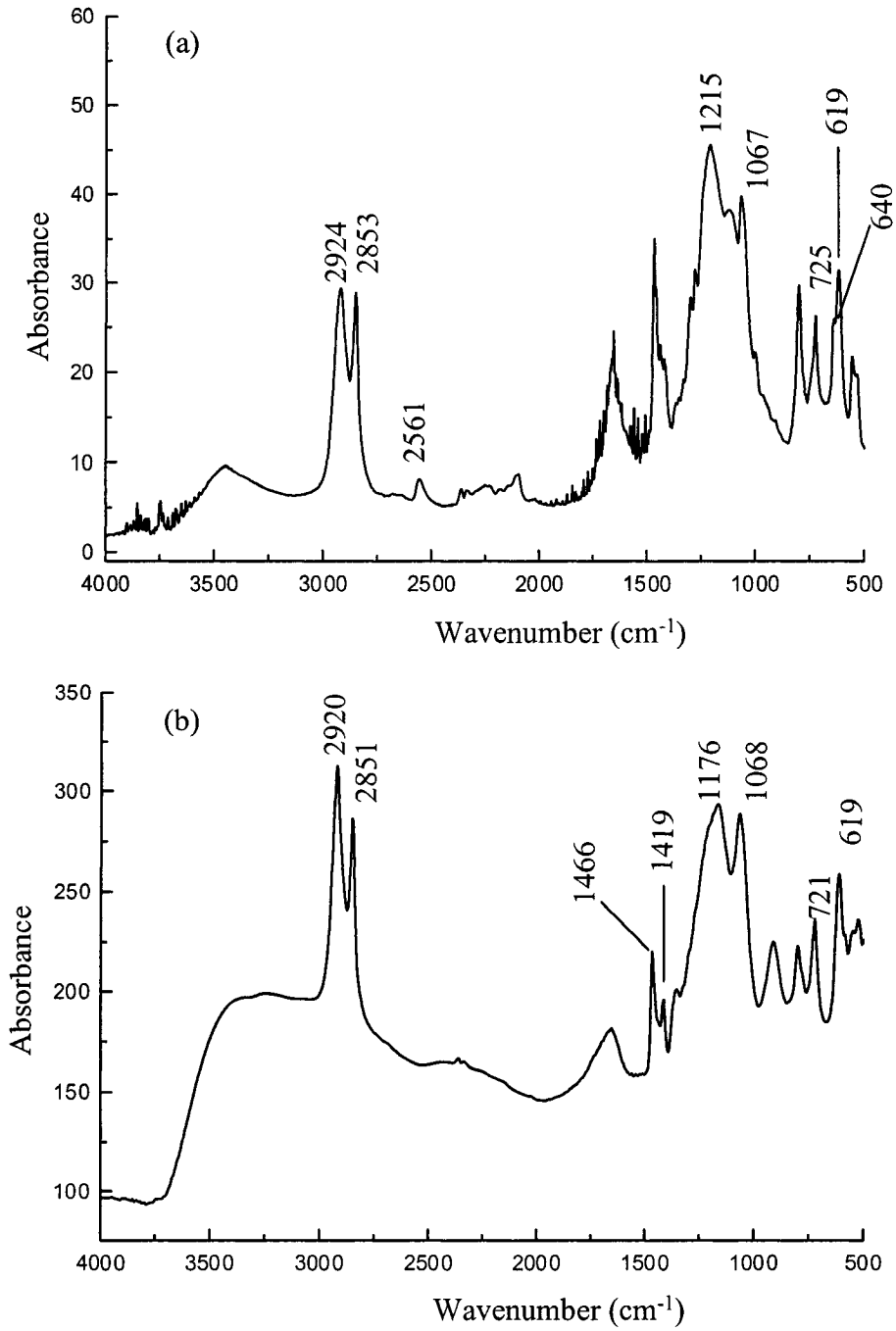

Figure 2.11 PAS-FTIR spectra of (a) sodium, 10-mercaptodecanesulfonic acid and (b) 1.8 nm-diameter SO_3-MPCs.

2.3.7 Solid-State NMR

^{13}C-NMR

The ^{13}C-NMR spectra of the unbound surfactant, and 1.8 nm SO_3-MPCs in D_2O and 1.8 nm SO_3-MPCs in solid-state were given in Figure 2.12. As observed in ^{1}H-NMR spectrum, the ^{13}C-NMR spectroscopy of SO_3-MPCs showed broadening of the signals in contrast to the ^{13}C-NMR spectrum of unbound MDS surfactant. Once again this broadening of the peaks was believed to arise from, a reduced chain mobility and distribution of shifts due to different Au-thiolate chemisorption, especially for carbons closest to the Au/thiol surface.[4, 10] The absence of the first two carbons adjacent to the sulfur head group in Figure 2.12b, clearly indicated by C2 (33.3 ppm), shows that SO_3-MPCs are free of unbound surfactant. In addition to the distribution of shifts, the broadening in solid state is due to the CSA and dipolar interaction. The methylene groups in alkyl chains can have trans or gauche conformations.[45] In solid state, these conformations are reflected in the chemical shifts. Whereas liquid-like disordered chains give an average shift of 30-31 ppm, the all-trans chains in crystalline form are shifted to 33-34 ppm. Self-assembled monolayers of long chain alkanethiols are mostly in an all-trans conformation at room temperature (i.e., C4-C15 in $C_{18}S/Au$ = 33.8 ppm) whereas the monolayers of short chain thiols do not crystallize at room temperature (i.e., C4-C5 in C_8S/Au = 31.1 ppm).[10] The interior methylenes signals of the MDS bulk in D_2O ranges from 28.0 to 28.8 ppm, and are moved downfield to 30.3-29.0 ppm when adsorbed on the gold, showing a broad resonance at 36 ppm due to C1 and C2.

The solid-state ^{13}C CPMAS NMR spectrum of SO_3-MPCs is shown in Figure 2.12c. At 25 °C, the interior methylene chains of SO_3-modified alkanethiol capped nanoparticles show a chemical shift at 33.2 ppm which indicates that they are mostly in the trans conformation. However, the large linewidth shows a significant population of gauche conformers, and indicates that ordered and disordered regions are in close proximity.[45] The higher population of all-trans component in 1.8 nm SO_3-MPCs of 10 carbons present at 25 °C confirms the FTIR data. By comparison to the simple alkanes, C_xS/Au where $x < 14$, the solid-state revealed that liquid-like population of gauche conformations are mostly present at room temperature.[10, 33] The higher population of trans conformers in SO_3-MPCs at room temperature may be due to the small particle size

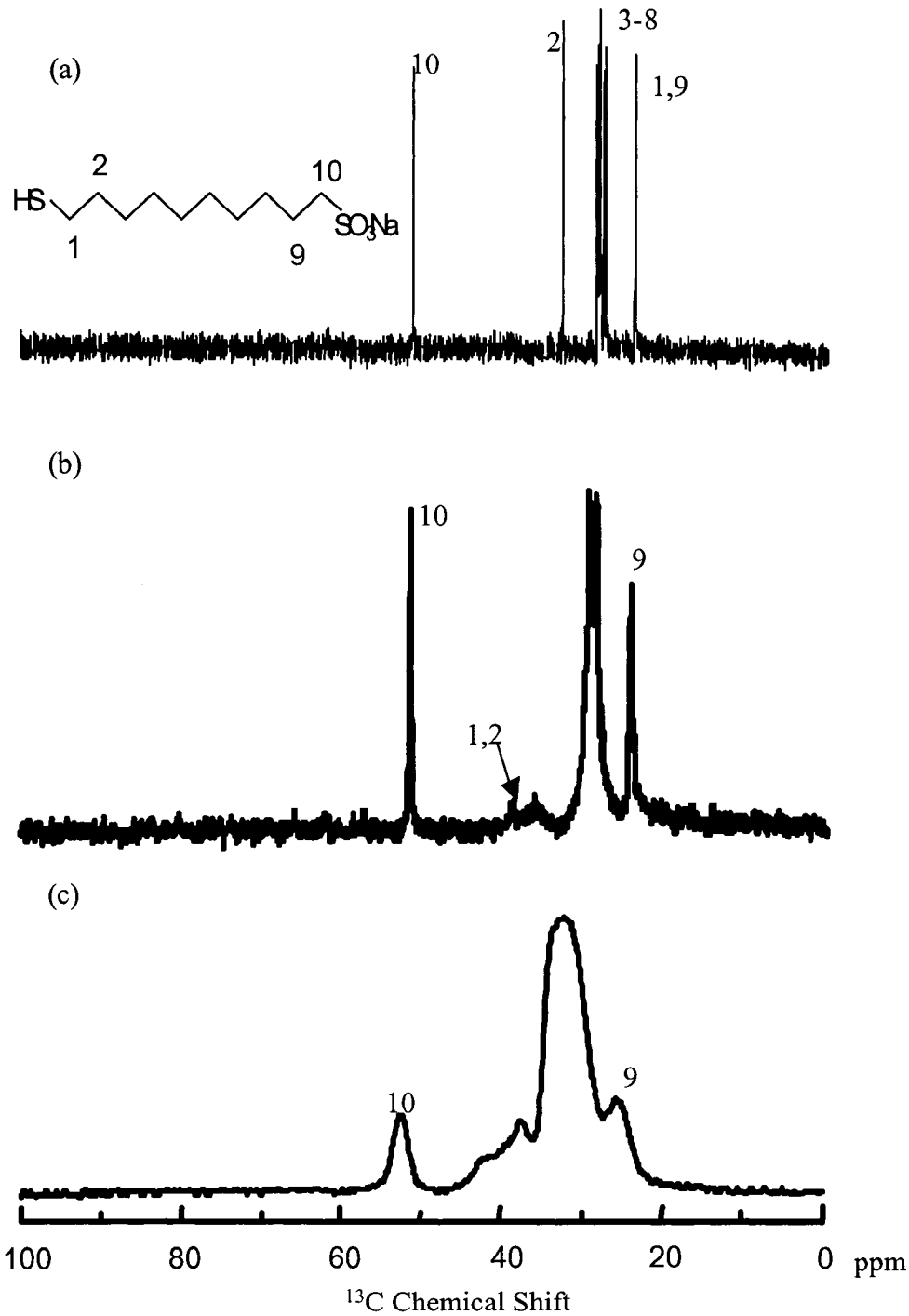

Figure 2.12 ^{13}C NMR spectra of (a) unbound thiol sodium, 10-mercaptodecane-sulfonic acid and (b) 1.8 nm-diameter SO_3-MPCs in D_2O and (c) in solid-state.

and the nature of the sulfonate terminal group. A smaller particle size would give a higher chain packing due to more efficient intercalation of chains between neighboring particles but this would be counteracted by the higher surface curvature.[33] The dialysis of the SO_3-MPCs should remove the excess sodium and it is possible that a portion of the end groups are in the acid form rather than in the Na form, but this remains to be confirmed. In the latter case, hydrogen bonding interactions among the end groups, which have been shown to promote conformational order,[51] would be possible. The salt form of the bulk surfactant showed no melting up to 250 °C and only decomposition occurred around 350 °C. However, variable temperature solid-state NMR studies, discussed next, showed that conformational disordering of the bulk surfactant occurs at 84 °C and in the case of SO_3-MPCs, the chains start to disorder slightly above the room temperature.

Variable temperature

The variable temperature ^{13}C solid-state NMR spectra of the bulk surfactant are shown in Figure 2.13. At room temperature, the MDS displays a dominant peak at 33 ppm, associated with methylene carbons in the trans conformations. Heating the sample before the DSC transition (Figure 2.10), solid-state spectrum at 74 °C showed that some gauche defects started to appear, as indicated by the shoulder at 31.1 ppm. At 84 °C, the 33 ppm peak shifted to 31 ppm signalling the disorder of the chains. The ^{13}C solid-state CPMAS NMR spectrum of the MDS at 100 °C, above the first DSC transition, was consistent with the presence of a significant population of gauche conformations. At 100 °C, the peaks were more narrow, due to enhanced mobility which coincided with the small endotherm in DSC, attributed to the desorption of water.

The variable temperature ^{13}C solid-state CPMAS NMR spectra for SO_3-MPCs are shown in Figure 2.14 along with the corresponding temperatures. The similar behavior of order/disorder transition was observed as previously reported in $C_{18}S$/Au and $HOC_{16}S$/Au systems.[10] This transition was displayed by a decrease of the trans component at 33 ppm and a gradual growth of gauche component at 31 ppm. In the case of SO_3-MPCs, above 45 °C, the chains were mostly disordered, and little change was observed as the sample was heated to 70 °C. The spectrum returned to its original state upon cooling. $C_{14}S$/Au and $HOC_{16}S$/Au show an order/disorder transition at ~ 22 °C and ~ 70 °C, respectively

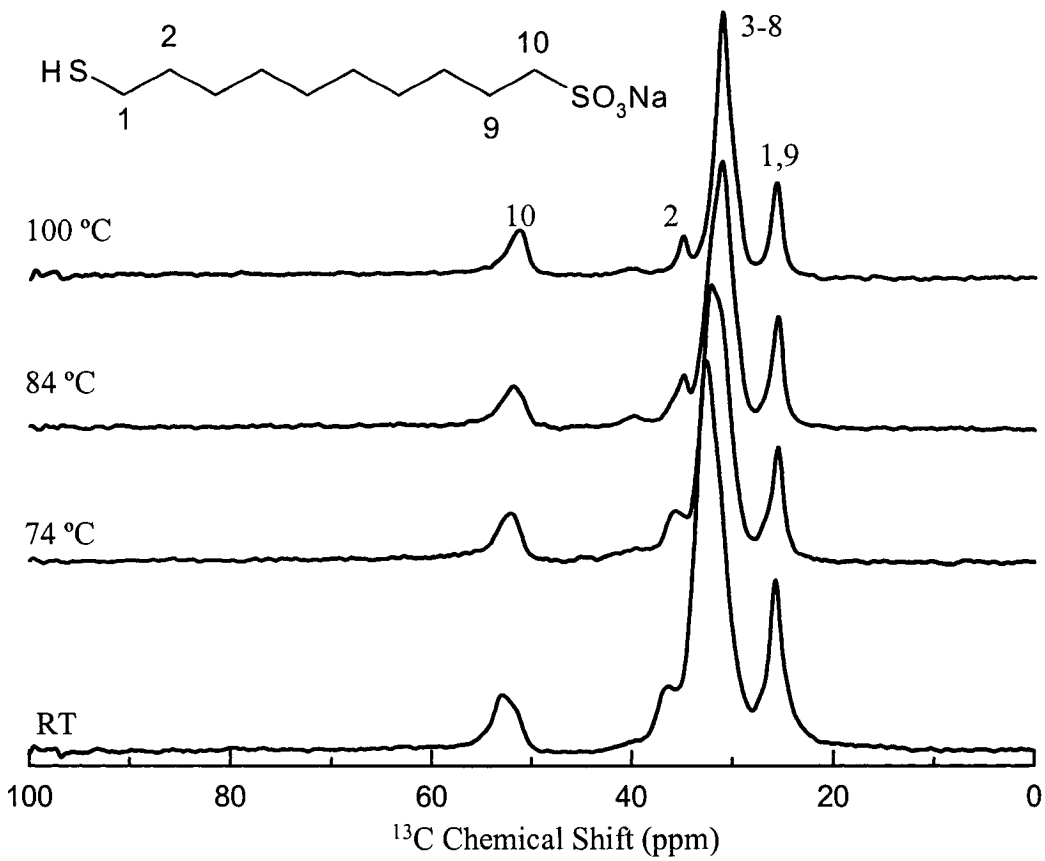

Figure 2.13 Variable temperature solid-state ^{13}C CP/MAS NMR spectra of sodium, 10-mercaptodecanesulfonic acid.

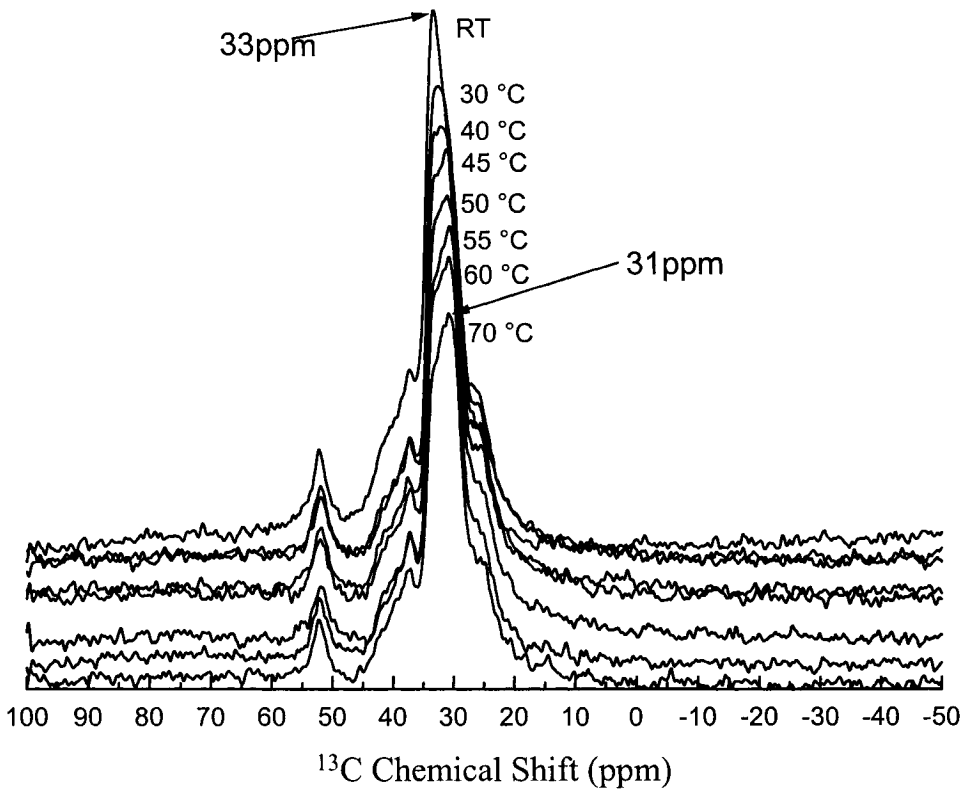

Figure 2.14 Variable temperature solid-state ^{13}C CP/MAS NMR spectra of 1.8 nm diameter SO_3-MPCs.

which correspond to a melting of chains observed by an endotherm peak in DSC.[10] As comparison to the SO_3-MPCs, the order/disorder transition was observed at ~35 °C, slightly higher than $C_{14}S$/Au and much lower than $HOC_{16}S$/Au nanoparticles. Such transitions in solid-state NMR can be sometimes seen as endotherms in DSC. The enthalpic contribution was chain length dependent and the magnitude of the enthalpy increased with increasing chain length. The SO_3-MPCs did not show such a DSC endotherm (Figure 2.10), probably due to the short chain, C10, and its hygroscopic characteristic where the baseline drifts as water desorbs.

Dynamic studies

The SO_3-modified capped gold nanoparticles were further studied by T_1 relaxation and dipolar dephasing experiments. In highly crystalline solids, the carbon T_1 values can be quite long whereas in mobile or amorphous solids T_1 values are relatively small. The spin-lattice relaxation data for the SO_3-MPCs were shown in Table 2.2 where they were compared to other thiol/gold systems. The best results were obtained by fitting the data by a biexponential equation, where the short decay time was 0.65 s (39 %) and a longer decay time of 11.5 (61%) was found for the 33 ppm peak. The different times can be associated with different chain mobilities as both disordered and rigid components were present. The terminal methylene group, nearest to the sulfonate tail group displayed faster T_1 values, 0.51 s (59 %) for the fast decay and 10.2 s (41 %) for the slow decay, showing more mobility at the end of the chains. The SO_3 tail group must somehow reduce the chain mobility since similar T_1 values were recorded for $C_{18}S$/Au, which is a much longer chain. Longer T_1 values were measured for the $HOC_{16}S$/Au where the presence of hydrogen bonding at the tail groups slowed down significantly the chain mobility.[10]

Another highly useful technique for detecting the relative molecular mobilities is the ^{13}C-^{1}H heteronuclear dipolar dephasing experiment. As reported previously,[27] mobile methyl carbons usually experienced a weaker ^{13}C-^{1}H heteronuclear dipolar coupling as indicative by the decay times of 50-120 μs whereas rigid methylene carbons experienced

Table 2.2 Comparison of solid-state carbon T_1, dipolar dephasing time and the order/disorder temperature of SO_3-MPCs to other thiol/gold systems.

	$^{C}T_1$(s)	T_{dd}(μs)	Order/disorder transition (°C)[c]
$HO_3SC_{10}S$/Au			
C4-C8	12[a]	24[b]	~35
C10	10[a]	27[b]	
C_8S/Au[(d)]			Disordered
C4-C5	0.45	114	at RT
C8	0.44	242	
$C_{18}S$/Au[(d)]			
C4-C16	12	16	~45
C18	1.82	190	
$HOC_{16}S$/Au[(d)]			
C4-C15	37	17	~70
C16	0.2	102	

[a] Long $^{C}T_1$ values were used which were obtained from the biexponential fit. [b] T_{dd} value were derived from a fit of a Gaussian decay as described in the chapter 1. [c] Temperatures were obtained from the solid-state NMR spectra at which the intensity of gauche and trans peak is equal. [d] Data from reference 10.

stronger heteronuclear dipolar where the range of decay times was usually 10-30 μs. The dipolar dephasing experiment of SO_3-MPCs was shown in Figure 2.15 and the data is tabulated in Table 2.2. As in previous dipolar dephasing experiments,[(46)] the rigid 33 ppm component demonstrated fast decay which was characterized by the Gaussian decay constant. The highly mobile 31 ppm component became more visible and slowly decayed away with the Lorentzian decay constant. This pattern was also observed in SO_3-MPCs where at 35 μs the 33 ppm peak has mostly decayed away. The interior methylenes and the C10 at the end of the chain fitted a Gaussian decay, with constants of T_{dd} = 24 μs and T_{dd} = 27 μs, respectively. In contrast to $HOC_{16}S$/Au nanoparticles, the methylene chain end was described by the Lorentzian decay, with T_{dd} = 102 μs.[(10)] The increase in the mobility of the chain ends in SO_3-MPCs was observed but the distribution of the mobility

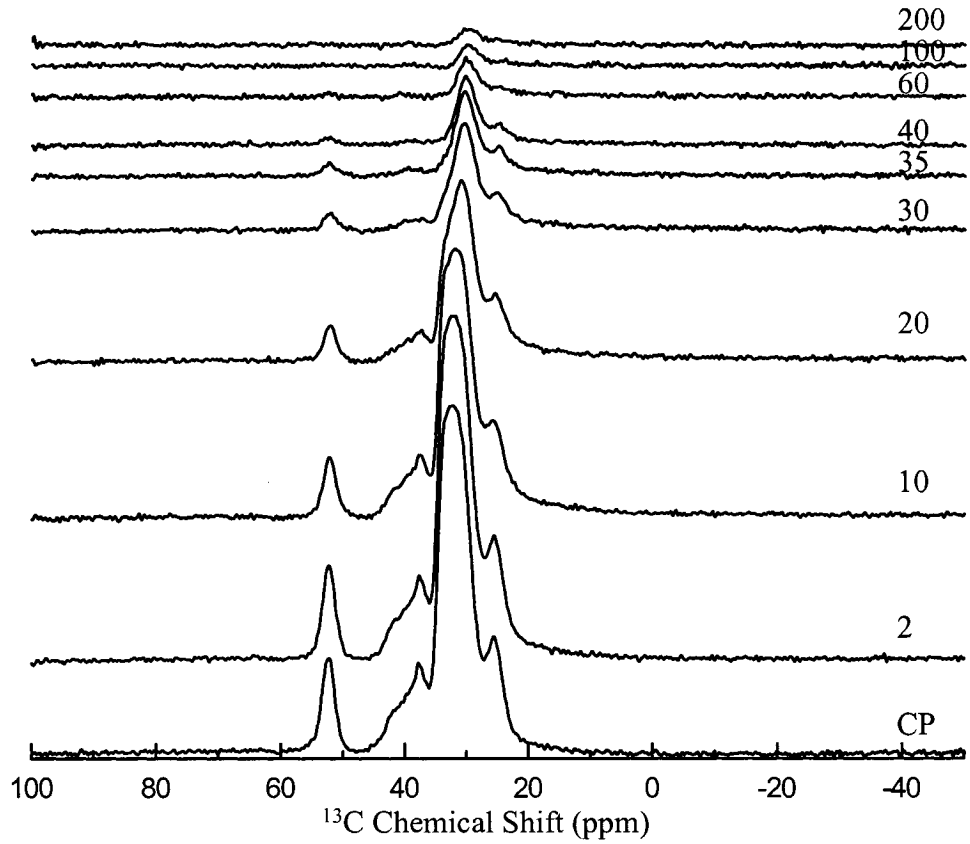

Figure 2.15 Dipolar dephasing spectra of 1.8 nm diameter SO_3-MPCs at selected dephasing times (μs), indicated next to the respective spectrum.

along the chain was much less pronounced than in $HOC_{16}S$/Au and $C_{18}S$/Au nanoparticles.

2.3.9 Encapsulating SO_3-MPC with PDADMAC

Electrostatic self-assembly (ESA) uses electrostatic interactions between a charged surface and oppositely charged polyelectrolytes to build thin layers.[47] Polyelectrolytes are deposited in an alternating, layer-by-layer (LbL) fashion. Initially, planar supports for ESA were studied most often, but recently there has been an interest of coating small charged species such as proteins, clays and nanoparticles.[48] Colloidal gold is of particular interest as a substrate for ESA because its properties are intermediate between small molecules and bulk metal. However, factors governing the controlled LbL adsorption of polyelectrolytes, makes coating of nanoparticles very challenging. Theoretical calculations have been performed to investigate the key factors such as particle size, polymer chain length, and the ionic strength, that affect adsorption onto high-curvature surfaces.[49] The high surface curvature of nanoparticles should strongly affect the adsorption of polymers and polyelectrolytes on these particles. Based on theoretical predictions by Kunze and Netz for the salt-induced DNA-histone complexation[50], Mayya et al.,[12], showed that 7 nm diameter CO_2-modified gold nanoparticles were uniformly coated by two oppositely charged polyelectrolytes. Very small particles do not allow the adsorption of all the polyelectrolyte due to the monomer-monomer repulsion which results in extended tails in the solution.[49] Negatively charged 1.8 nm diameter SO_3-modified gold nanoparticles had an initial ξ-potential value of -35 ± 1 mV, a typical value for negatively charged gold nanoparticles.[12] Due to their small particle size, no surface plasmon absorption band was observed. The oppositely charged polyelectrolyte had been deposited on the negatively charged gold surface by means of electrostatic and hydrophobic particle-particle interactions. ξ-potential measurements indicated a clear charge inversion (37 ± 2 mV) , which suggested PDADMAC adsorption, as seen previously on larger particles.[12] A well defined plasmon absorption band at a maximum wavelength of ~ 560 nm was observed in the UV-Vis. The appearance of the SP band at a large red-shift suggested that larger colloids were produced and causing the particles to aggregate. Closer examination of TEM micrographs of the PDADMAC-

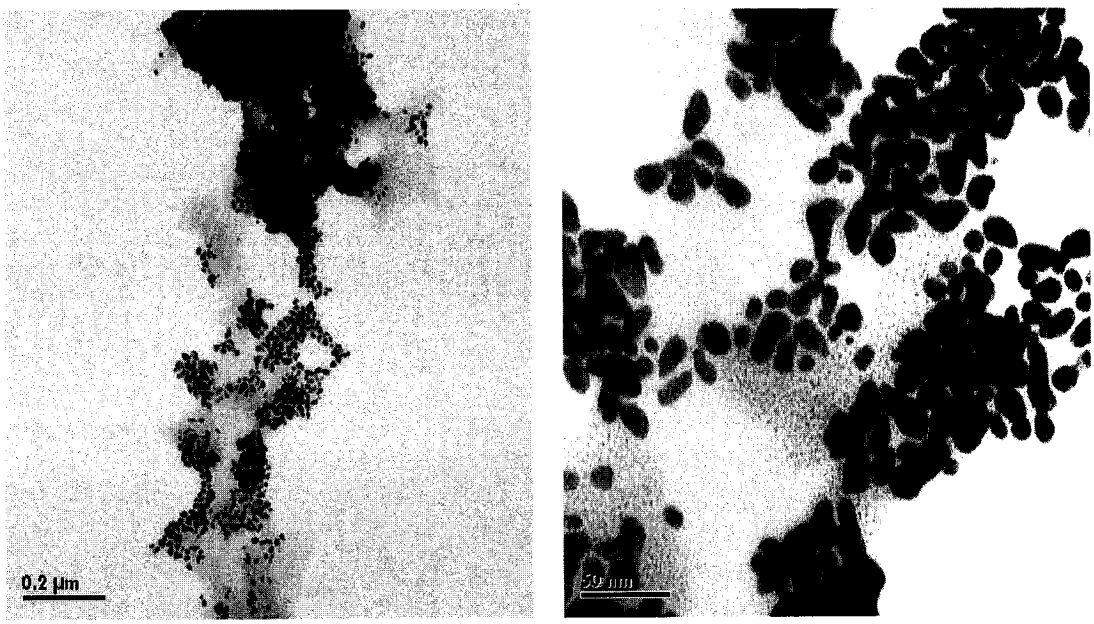

Figure 2.16 TEM micrographs of PDADMAC-coated 1.8 nm diameter SO_3-MPCs. On the left, region with 200 nm scale bar is shown and on the right the closer look up of the non-aggregated region with a scale bar of 50 nm is shown.

coated nanoparticles in Figure 2.16, showed that the average particle size increased to ~ 12 nm forming irregular 3D aggregates. The increase in size of the particles can be attributed to the formation of extended tails of the polyelectrolyte which in turn results in a multiple adsorption of SO_3-MPCs.

2.4 CONCLUSIONS

Water-soluble well-stabilized gold nanoparticles were readily obtained using negatively charged sulfonate stabilizing ligands. Sulfonate-monolayer protected clusters (SO_3-MPCs) were generated from sodium, 10-mercaptodecanesulfonate surfactant and by solution ^{1}H-NMR they show indistinguishable behavior from those SO_3-MPCs prepared from Bunte salt. The combined results from TEM and UV-Vis established that the smallest clusters with lowest dispersity were obtained using low concentration of gold and high surfactant to gold ratio. Both FTIR and NMR spectra indicated the SO_3-MPCs with highly ordered chains at room temperature. Variable temperature solid-state ^{13}C-NMR, relaxation and dipolar dephasing experiments showed that the introduction of a terminal SO_3 group on a C10 alkylthiolate chain was found to induce conformational order and rigidity compare to gold nanoparticles capped with alkylthiolate chain (C_{12}-C_{18}). Extended tails of PDADMAC resulted in a multiple adsorption of 1.8 nm SO_3-MPCs due to their small particles size.

2.5 REFERENCES

1. Novak, J. P.; Brousseau, L. C.; Vance, F. W.; Johnson, R. C.; Lemon, B. I.; Hupp, J. T.; Feldheim, D. L. *J. Am. Chem. Soc.* **2000**, 122, 12029.

2. Hoffman, A. J.; Mills, G.; Yee, H.; Hoffman, M. R. *J. Phys. Chem.* **1992**, 96, 5546.

3. Huisman, B.-H.; Rudkevich, D. M
.; Van Veggel, F. C. J. M.; Reinhoudt, D. N. *J. Am. Chem. Soc.* **1996**, 118, 3523.

4. Hostetler, M. J.; Wingate, J. E.; Zhong, C.-Z.; Harris, J. E.; Vachet, R. W.; Clark, M. R.; Londono, J. D.; Green, S. J.; Stokes, J. J.; Wignall, G. D.; Glish, G. L.; Porter, M. D.; Evans, N. D.; Murray, R. *Langmuir* **1998**, 14,17.

5. Liz-Marzán, L. M.; Philipse, A. P. *J. Phys. Chem.* **1995**, 99, 15120.

6. Mayer, A. B. R.; Mark, J. *E. Eur. Polym. J.* **1998**, 34, 103.

7. Maye, M. M.; Zhong, C.-J.; *J. Mater. Chem.* **2000**, 10, 1895

8. Prasad, B. L. V.; Savka, I. S.; Sorensen, C. M.; Klabunde, K. J. *Langmuir* **2002**, 18, 7515.

9. Badia, A.; Singh, S.; Demers, L.; Cuccia, L.; Brown, G. B.; Lennox, R. B. *Chem. Eur. J.***1996**, 2, 359.

10. Badia, A.; Gao, W.; Singh, S.; Demers, L.; Cuccia, L.; Reven, L. *Langmuir* **1996**, 12, 1262.

11. Goldenberg, L. M.; Jung, B.-D.; Wagner, J. S.; Pulke, B.-R.; Görnitz, E. *Langmuir* **2003**, 19, 205.

12. Mayya, K.S.; Schoeler, B.; Caruso, F. *Adv. Funct. Mater.* **2003**, 13, 183.

13. Nagtegaal, M.; Stroeve, P.; Ensling, J.; Gűtlich, P.; Schurrer, M.; Voit, H.; Flat, J.; Käshammer, J.; Knoll, W.; Tremel, W. *Chem. Eur. J.* **1999**, 5, 1331.

14. Templeton, A.C.; Wuelfing, W.P.; Murray, R.W. *Acc. Chem. Res.* **2000**, 33, 27.

15. Ulman, A. *Chem. Rev.* **1996**, 96, 1533.

16. Shon, Y.-S.; Mazzitelli, C.; Murray, R.W. *Langmuir* **2001**, 17, 7735.

17. Lukkari, J.; Meretoja, M.; Kartio, I.; Laajalehto, K.; Rajamäki, M.; Lindström, M.; Kankare, J. *Langmuir* **1999**, 15, 3529.

18. Shon, Y.-S.; Gross, S. M.; Dawson, B.; Porter, M.; Murray, R. W. *Langmuir* **2000**, 16, 6555.

19. Okkema, A. Z.; Giroux, T. A,; Grasel, T. G.; Cooper, S . L. *Mater. Res. SOC. Symp. Proc.* **1989**, 110, 91-96.

20. Turyan, I.; Mandler, D. *J. Am. Chem. Soc.* **1998**, 120, 10733.

21. Lin, J.-C.; Chuang, W.-H. *J. Biomed. Mater. Res.* **2000**, 51, 413.

22. Lestelius, M.; Liedberg, B.; Tengvall, P. *Langmuir* **1997**, 13, 5900.

23. Turyan, I.; Mandler, D. *Isr. J. Chem.* **1997**, 37, 225.

24. Gittins, D. J.; Caruso, F. *J. Phys. Chem. B* **2001**, 105, 6846.

25. Huang, T.; Murray, R.W. *J. Phys. Chem. B* **2001**, 105, 12498.

26. Torchia, D. A. *J. Magn. Reson.* **1978**, 30, 613.

27. Alemany, L. B.; Grant, D. M.; Alger, T. D.; Pugmire, R. J. *J. Am. Chem. Soc.* **1983**, 105, 6697.

28. Marvel, C. S.; Sparberg, M. S. *Org. Synth.* **1943**, 2, 558.

29. Schramm, C.H.; Lemaire, H.; Karlson, R.H. *J. Am. Chem. Soc.* **1955**, 77, 6231.

30. Schaaff, T. G.; Knight, G.; Shafigullin, M. N.; Borkman, R. F.; Whetten, R. L . *J. Phys. Chem. B* **1998**, 102, 10643.

31. Schneider, B. H.; Dickinson, E. L.; Vach, M. D.; Hoijer, J. V.; Howard, L. V. *Biosens. Bioelectron.* **2000**, 15, 13.

32. Weller, H. *Angew. Chem., Int. Engl.* **1993**, 32, 41.

33. Badia, A.; Demers, L.; Dickinson, L.; Morin, F. G.; Lennox, R. B.; Reven, L. *J. Am. Chem. Soc.* **1997**, 119, 11104.

34. Alvarez, M. M.; Khoury, J. T.; Schaaff, T. G.; Shafigullin, M. N.; Vezmar, I.; Whetten, R. L. *J. Phys. Chem. B* **1997**, 101, 2706.

35. Averitt, R. D.; Westcott, S. L.; Halas, N. J. *J. Opt. Soc. Am. B* **1999**, 16, 1824.

36. Gittins, D.; Caruso, F.; *Chem. Phys. Chem.* **2002**, 3, 110

37. Storhoff, J. J.; Elghanian, R.; Mucic, R. C.; Mirkin, C. A.; Letsinger, R. L. *J. Am. Chem. Soc.* **1998**, 120, 1959.

38. Guthrie, J. P. Can. *J. Chem.* **1978**, 56, 2342.

39. Woehrle, G. H.; Warner, M. G.; Hutchison, J. E. *J. Phys. Chem. B* **2002**, 106, 9979.

40. Jiang, D.D.; Michael. Q. Y.; McKinney, M. A.; Wilkie, C. A., *Polym. Degrad. Stab.* **1999**, 63, 423.

41. Shon, Y.-S.; Wuelfing, W. P.; Murray, R. W.; *Langmuir* **2001**, 17, 1255.

42. Bryant, M. A.; Pemberton, J. E. *J. Am. Chem. Soc.* **1991**, 113, 8284.

43. Kudelski, A. *Langmuir* **2002**, 18, 4741.

44. Bhattacharya, S.; Srivastava, A *Langmuir* **2003**, 19, 4439.

45. Clauss, J.; Schmidt-Rohr, K.; Adam, A; Boeffel, C.; Spiess, H.W. *Macromolecules* **1992**, 25, 5208.

46. Huang, Y.; Gilson, D.F.R.; Butler, I. S.; Morin, F. *J. Phys. Chem.* **1991**, 95, 2151.

47. Bertrand, P.; Jonas, A.; Laschewsky, A.; Legras, R. *Macromolecular Rapid Communications* **2000**, 21, 319.

48. Caruso, F. *Chem. Eur. J.* **2000**, 6, 413.

49. Chodanowski, P.; Stoll, S. *J. Chem. Phys.* **2001**, 115, 4951.

50. Kunze, K.-K.; Netz, R. R.; *Phys. Rev. Lett.* **2000**, 85, 4389.

51. Schmitt, H.; Badia, A.; Dickinson, L.; Reven, L.; Lennox, R. B. *Adv. Mater.* **1998**, 10, 475.

Chapter 3

Phosphonate-Monolayer Protected Clusters

3.1 INTRODUCTION

The addition of a specific functional tail group greatly affects the physical and surface properties of surfactant protected nanoparticles. Many studies have been done on differently functionalised nanoparticles.[1-6] A good example is the change from a hydrophobic tail group such as CH_3 to a hydrophilic tail group such as OH. The effect of the nature of the tail group was quantitatively investigated by various research groups using a two-component system, $HO(CH_2)_{11}SH$ and $CH_3(CH_2)_{11}SH$.[7,8] Most of these studies have focused on the growth dynamics of monolayer-protected Au clusters (MPCs) formation and few studies have explored the effect of the tail group on the molecular dynamics or the degree of ordering of the chains. An investigation of densely packed alkyl chains by solid-state NMR with different tail groups was performed by Badia et al.[5] Hydroxyl and carboxylic acid terminated alkanethiols chemisorbed on gold showed a high degree of conformational ordering compared to the simple alkanethiols. Extensive hydrogen bonding among the COOH terminal groups gave rise to a high thermal stability of the chain order.[6]

In this chapter, the synthesis of alkyl phosphonate functionalised gold nanoparticles and the solid-state NMR studies of their dynamic and structural properties are described. The synthesis and characterization of a $PO(OH)_2$ terminated SAM on a planar gold substrate have been reported. Zhang et al.[9] proposed a model in which one of the hydroxyl groups of a phosphonic SAM lies in the plane of the monolayer and takes part in intramonolayer hydrogen bonding, and the other lies out of the plane. Chemical force microscopy data further suggested that strong hydrogen bonding between neutral and ionized species on the gold tip ($PO(OH)_2$) and substrate ($PO(O^-)_2$ was formed.[9,10] An adhesion study using the contact deformation mechanics method revealed that intermolecular hydrogen bonding at the surface of $H_2O_3P(CH_2)_{11}SH$ SAM resulted in

decreased adhesion.[11] Our motivation for the choice of the phosphonic acid thiol came from the study of COOH-terminated thiols on gold nanoparticles where it was observed that CO_2-MPCs can sustain high thermal stability and showed highly ordered chains due to hydrogen bonding.[6] Therefore, we anticipate similar behavior for phosphonic acid functionalised gold nanoparticles where the PO_3H_2 end group is a hydrogen-group donor and hydrogen-group acceptor. This system also is appealing from both practical and scientific interests. Phosphonic acids exhibit a wide range of biological activity as potent antibiotics and enzyme inhibitors.[12,13] They are also used as corrosion inhibitors and adhesion promoters.[14] The nature of the strong hydrogen bond is of interest in fields such as adhesion, chemical sensors and biocompatibility. The PO_3H_2 group is well suited for ^{31}P-solid-state NMR studies which can be used to explore the extent to which the structure of the adsorbed thiols on gold can be affected by strongly interacting tail groups. Pawsey et al.,[15] have shown the utility of solid-state NMR spectroscopy for interpreting the structural information in carboxyalkylphosphonic acids bound to metal oxides. High-resolution ^{1}H solid-state NMR experiments showed that hydrogen bonding network was formed by multilayers of the diacids on the ZrO_2 nanopowder.[16]

Another very important application of ^{31}P NMR is the investigation of the head group motions of phospholipids in membrane systems and oriented bilayers.[17] Principal elements of the shielding tensors can be obtained directly from the spinning side bands that arise from slow sample spinning.[18] Since the principal elements of the chemical shift are very sensitive to changes in the molecular and electronic structure, they may be used to monitor molecular changes. As the objective of the PO_3-MPCs synthesis was to have ^{31}POOH groups at the outer surface of the nanoparticles, we wanted to know if solid-state ^{31}P NMR spectroscopy could be used as an investigative tool to provide information about the surface interactions of the phosphate groups. The ^{31}P chemical shift anisotropy (CSA) of phosphonic acids and esters have been studied by various groups.[19-24] Since the size of the asymmetry parameter (η) was found to be related to the nature of hydrogen bonding,[23] ^{31}P NMR may provide another method for detecting surface hydrogen bonding interations.

A molecule which has a polar head attached to a long hydrophobic tail is an example of a group of molecules called amphiphiles. Simple long alkyl chain phosphonic

acids and 11-mercaptoundecanylphosphonic acid (MUP) can be regarded as such molecules. These amphiphilic molecules can self-assemble to form lyotropic liquid crystals (LLC)[25] such as the well known phospholipid bilayer. Kose et al.[26] reported that n-octyl- and n-hexylphosphonic acids form widely spaced lamellar domains in the presence of water over a relatively broad composition and temperature range. The temperature dependence of the phases can be monitored by optical microscopy and differential scanning calorimetry (DSC). Such studies were performed on long-chain phosphonic acids[27] and alkyl phosphonate salts.[19] In both cases, one crystalline form was seen at 25 °C but when heated another thermodynamically less stable form was produced. In phosphonic acids, the changes from one crystalline form to the other can be associated with breaking the strong intermolecular interactions between the phosphonic acid head groups.[25] The phosphonic acid group can act as both a hydrogen-bond donor through the two P-OH groups and an acceptor via the P=O oxygen. Compared to carboxylic acid, the tridentate character of PO_3H_2 group can give rise to complicated hydrogen bonded assemblies. Mahmoudkhani and Langer[28] have shown that the PO_3H_2 group in phenylphosphonic acid forms complex hydrogen-bonded networks which result in various crystal structures.

In addition to the CSA parameters, more information about the hydrogen bonding and the $PO(OH)_2$ environment can be obtained from the isotopic ^{31}P chemical shift. In solution, the degree of intramolecular and intermolecular hydrogen bonding in phosphonic acids can affect the ^{31}P chemical shift.[29-31] Several hydrogen-bonding mechanisms were proposed to account for the solvent effect on the chemical shifts of acids and esters.[31] In non-polar solvents the intramolecular hydrogen bond is formed resulting in a deshielding of the phosphorous group. In polar solvents with hydrogen-donor properties, the intramolecular hydrogen bonding are weakened, which results in a shift to higher field.[29] The shielding effect can be explained by the involvement of the phosphoryl oxygen in a hydrogen bond, which increases the bond order of the phosphoryl group. In solid-state NMR, the change in ^{31}P chemical shift was also observed, depending on the interaction of the $PO(OH)_2$ group. In the sodium salt form, a higher shift was reported relative to the protonated form of the phosphonic acid group.[19]

Studies performed in solution of various functionalised nanoparticles are difficult to compare due to large differences in solubility and stability. Investigation of structural and dynamic properties by solid-state NMR makes the comparison of powder colloidal samples possible. A series of functionalized gold nanoparticles differing both in terminal functionality and in chain length were characterized by solid-state NMR.[5,6,32] To investigate PO_3-monolayer protected gold clusters (PO_3-MPCs) and to compare it to other systems, the chain conformation and mobility will be characterized by ^{13}C and ^{31}P CPMAS solid-state NMR.

3.2 EXPERIMENTAL

3.2.1 Chemicals

11-bromo-1-undecene (95%), triethylphosphite (98%), AIBN (98%), hydrogen tetrachloroaurate (III) trihydrate, sodium borohydride (99%) and poly(diallyldimethyl-ammonium chloride) (40 % wt) were purchased from Aldrich. Thioacetic acid (97%) was obtained from Fluka. Chloroform, methanol, acetic acid, $MgSO_4$, NaCl, HCl, and ammonium hydroxide were purchased from Fisher. Ethyl acetate and sodium bicarbonate (99.7 %) were obtained from EM Science. Ethanol, hexane and silica gel were purchased from Commercial Alcohols Inc., EMD™ and Silicycle (Quebec, QC), respectively. All chemicals were used as received. Cellulose dialysis tubing of 25 mm flat width and 16 mm in diameter (MWCO = 12000) was purchased from Aldrich. 400 mesh carbon coated copper grids were purchased from Electron Microscopy Sciences (Fort Washington, PA). Pre-treated distilled water was further purified with the bench milli-Q® system (Millipore Co.) to give resistivity ≥ 18.2 MΩcm and pH of 5.5-5.7.

3.2.2 Synthesis of 11-mercaptoundecanylphosphonic acid (MUP)

MUP compound was prepared by essentially the same method as described by Whitesides et al.[33] Some modifications were reported, especially in the last step, for the hydrolysis of the phosphate group.

Diethyl 10-undecenylphosphonate (I)

Triethyl phosphite (20.7 mL, 0.121 mol) and 11-bromo-1-undecene (11.7 g, 50 mmol) were refluxed for 24 h with nitrogen stream bubbling into the solution. The solution was then cooled, and 50 mL of water was added in one portion. The two-phase mixture was stirred for 3 h and extracted with chloroform. The $CHCl_3$ (50 mL × 2) extracts were combined and washed twice with 20 mL water, once with 20 mL brine (i.e., saturated NaCl) , and dried over $MgSO_4$. The filtered solution was concentrated by rotary evaporation to give slightly yellow colored oil (95 – 99 % yield). The product was purified by flash chromatography using a gradient of 10/1 heaxanes/ethyl acetate to neat ethyl acetate as eluent. TLC: $R_f = 0.33$ in ethyl acetate. ^{1}H-NMR (270 MHz, $CDCl_3$): δ 5.78 (m, 1H, CH_2=*CH*-), 4.90 (m, 2H, *CH_2*=CH-), 4.01 (m, 4H, OCH_2) 1.96 (q, 2H, CH_2=CH*CH_2*-), 1.40-1.70 (m, 4H), 1.10-1.30 (m, 18H). ^{31}P-NMR (270 MHz, $CDCl_3$): δ 33.3 (s, $PO(OEt)_2$). APCI: 291 (MH^+).

Diethyl 11-(acetylthio)undecanylphosphonate (II)

A solution of compound (I) (3.95 g, 13.6 mmol) in thioacetic acid (3.88 ml, 54.5 mmol) and 10 mg of AIBN was placed in a 30 mL quartz round-bottom flask and capped with a septum. After flushing the flask with nitrogen, the quartz flask was irradiated with high pressure mercury lamp (100 W) for 8 h at a distance of 5 cm.[34] The reaction was quenched with 40 mL of $CHCl_3$. The mixture was stirred while a saturated solution of sodium bicarbonate (40 mL) was added slowly. The organic phase was separated from the aqueous phase and washed with 20 mL of water and 20 mL of brine. When dried over the $MgSO_4$, the solution was concentrated to an orange oil, 2.85 g (57 % yield). To remove the impurities, the crude oil was purified by flash chromatography using a gradient of 1/1 hexanes/ethyl acetate to neat ethyl acetate as eluant to yield a slightly yellow oil. ^{1}H-NMR (270 MHz, $CDCl_3$): δ 4.01 (m, 4H, OCH_2), 2.85 (t, 2H, SCH_2), 2.29 (s, 3H, CH_3CO), 1.45-1.77 (m, 6H), 1.20-1.40 (m, 20H). ^{31}P-NMR (270 MHz, $CDCl_3$): δ 33.3 (s, $PO(OEt)_2$). APCI: 367 (MH^+), 325 (MH^+-H_2C=C=O).

Diethyl 11-mercaptoundecanylphosphonate (III)

Compound (II) (1.18 g, 3.1 mmol), 15 mL of ethanol, and 10 mL of concentrated HCl were heated under nitrogen at reflux for 7 h. The solvents were removed by vacuum leaving an oil that was resuspended in 25 mL of water to remove the excess of HCl. The reaction was concentrated again under vacuum to give a clear oil, (0.844 g, 81 % yield). ^{1}H-NMR (270 MHz, $CDCl_3$): δ 6.32 (br, H, P(O)OH), 4.10 (q, 4H, OCH_2), 2.51 (q, 2H, CH_2SH), 1.45-1.80 (m, 6H), 1.20-1.40 (m, 21H). ^{31}P-NMR (270 MHz, $CDCl_3$): δ 37.5 (s, $PO(OH)_2$, 36.3 (s, PO(OH)(OEt)), 33.5 (s, $PO(OEt)_2$). APCI: 325 (small, MH^+), 297 (strong, MH^+- CH_2CH_3), 269 (medium, MH^+-$(CH_2CH_3)_2$).

11-mercaptoundecanylphosphonic acid, MUP

Concentrated HCl (12 mL) was added to compound (III) (0.736 g, 2.3 mmol), stirred and refluxed for 19 h.[35] After the mixture was cooled, a white precipitate appeared. The solid was collected by suction filtration, washed several times with acetonitrile and dried in a vacuum to give 0.566 g (84.6 % yield). The collected solid was used in colloid synthesis. ^{1}H-NMR (270 MHz, $CDCl_3$): δ 8.25 (br, 2H, $PO(OH)_2$), 2.51 (q, 2H, CH_2SH), 1.50-1.80 (m, 6H), 1.20-1.40 (m, 15H). ^{31}P-NMR (270 MHz, $CDCl_3$): δ 37.1 (s, $PO(OH)_2$). ^{31}P-NMR (270 MHz, CD_3OD): δ 30.9 (s, $PO(OH)_2$). ^{13}C-NMR (270 MHz, CD_3OD): δ 33.9 ($HSCH_2\mathit{CH_2}$), 30.4 (d, $\mathit{CH_2}CH_2CH_2PO(OH)_2$, J^3 = 16 Hz), 29.3-28.3 (5 s, CH_2), 28.1 (s, $\mathit{CH_2}CH_2CH_2SH$), 26.8 (d, $CH_2PO(OH)_2$, J^1 = 138 Hz), 23.6 (s, $HSCH_2$), 22.6 (d, $\mathit{CH_2}CH_2PO(OH)_2$, J^2 = 5 Hz). ESI: 269 (MH^+), 267 (M^-). Elem. Anal. (found/calculated): C, 49.4/49.2, H, 9.50/9.41. The melting point of MUP was found to be 84 °C.

3.2.3 Synthesis of PO_3 monolayer-protected gold clusters (PO_3-MPCs)

The following procedure was performed based on the SO_3-MPCs synthesis described in chapter 2. In a typical reaction, 75 mg of $HAuCl_4$ $3H_2O$ was dissolved in 35 ml of solvent, methanol (30 mL)/acetic acid (5 mL), containing dissolved 184 mg of MUP. The solution was left to stir for a half hour. Freshly prepared, 145 mg of $NaBH_4$ in 15 mL of milli-Q water was added dropwise (< 30 s) to a rapidly stirring solution. After stirring for an additional 100 min, the pH was then adjusted to 1 by dropwise addition of

concentrated HCl. The black precipitate was collected on a fine glass filter and rinsed with several portions of methanol. When dry, the black particles were collected and dissolved in 20 mL dilute ammonium hydroxide milli-Q water solution. The solution was loaded into 20 cm segments of cellulose dialysis bags and slowly stirred in 4L beaker of milli-Q water. The milli-Q water was replaced twice a day with at least 8 h of interval for a period of 3 days. The PO_3-MPCs were collected from dialysis bags and the solvent was removed by freeze drying.

3.2.4 Encapsulation of PDADMAC on PO_3-MPC

The method for layer deposition of poly(diallyldimethyl-ammonium chloride), PDADMAC, on phosphonate-modified gold nanoparticles was used from published work.[36] The PDADMAC and PO_3-MPCs were prepared using 20 mM NaCl as the ionic strength.

3.2.5 Instrumentation

Solution-state NMR spectroscopy

The purity of intermediates and bulk thiol surfactant were verified by solution-state JOEL ECLIPSE-270 spectrometer at 25 °C. The $HS(CH_2)_{11}PO_3H_2$ capped gold nanoparticles were not soluble in common NMR solvents.

Solid-state NMR spectroscopy

Solid-state 67.92 MHz ^{13}C NMR and 109.34 MHz ^{31}P NMR spectra were run on a Chemagnetics CMX-270 spectrometer with 4 mm (Chemagnetics/Varian) double tuned magic angle spinning (MAS). Spin rate of 6 kHz, an average of 100-1000 scans and pulse delay of 2.5 s were typically used to acquired ^1H-^{13}C CP/MAS and ^1H-^{31}P CP/MAS spectra. The ^1H 90° pulse widths were between 3 and 4 μs and a contact time of 1 ms was used. For the variable-temperature CP-MAS experiments, the sample temperature was controlled to within ± 2°C by a Chemagnetics temperature controller. Before any sample was run, reference hexamethylbenzene (HMB) was used to calibrate the spectrometer for ^1H-^{13}C CP/MAS experiments, adjusting the 180° pulse and setting its methyl peak at 17.3 ppm. For ^1H-^{31}P CP/MAS experiments, chirophos:bis(diphenyl phosphino) butane was

used as reference, which resonates upfield at –13.0 ppm. Typically, a line broadening factor of 30 Hz was used to improve NMR signal to noise.

For the carbon T_1 measurements, the Torchia inversion-recovery sequence[37] was used with the initial ^{13}C magnetization generated by cross polarization. The relaxation delay of 5 T_{1H} was used to allow adequate signal decay between pulses.

The dipolar dephasing experiments were performed using the decoupling pulse sequence[38] and T_{dd} was measured as described in introduction.

Transmission Electron Microscopy (TEM)

Samples for the TEM were prepared by placing a drop of aqueous colloidal solution on carbon-coated copper grids (400 mesh), waiting 5 min, and removing the excess solution by touching a small piece of filter paper to the edge of the grid. The copper grids were then dried overnight in air. The phase-contrast images of the particles were obtained with a top-entry JOEL JEM-2000 FX electron microscope operating at 80 keV and fitted with an Electron Dispersive Spectrometer (EDS). Size distributions of the particles were determined from diameters of at least 100 particles, selected from three typical regions at magnification ranging from 100 kX to 340 kX. A CCD camera (Gatan BioScan Camera Model 792) was used to obtain the images where the DigitalMicrograph™ software version 2.4.3 was used to obtain better contrast and brightness. Sigma Scan version 4.1 was then used to obtained the size diameter of the particles.

UV-Visible Spectroscopy

UV-Vis spectra were obtained using double beam Cary 300 Bio UV-Vis spectrophotometer. The dilute solutions of gold colloids were acquired from 900 to 300 nm with a scan rate of 300 nm/min, using quartz cell with a path length of 1 cm. The milli-Q water was used as reference.

Fourier Transform Infrared Spectroscopy (FT-IR)

Transmission spectra for the bulk samples and the nanoparticles were acquired on a photoacoustic Bio-Rad FTS6000 spectrometer containing a MTEC300 photoacoustic

cell from MTEC Photoacoustics, Inc. The infrared spectra were obtained after purging the cell with helium gas and were background corrected using a carbon black reference. Spectra were obtained for 64 scans at a resolution of 4 cm^{-1}.

Differential Scanning Calorimetry (DSC)

The 2-8 mg of bulk MUP and PO_3-MPCs were analyzed by DSC Q1000 fitted with autosampler which was calibrated against the indium reference under the same settings. The settings were as follows: nitrogen atmosphere, heat-cool rates of 5 °C/min and high volume stainless steel pan were used.

Thermogravimetry Analysis (TGA)

TGA analysis were performed with TGA Q500 with autosampler and two mass flow controller. 5-10 mg of accurately weighed samples were recorded starting from room temperature to 550 °C under N_2 and than under O_2 up to 700 °C, at 20 °C/min.

Zeta-potential Analysis

The charge of the SO_3-modified gold particles before and after the deposition of the polyelectrolyte, was monitored by the ZetaPlus analyzer (Brookhaven Instruments Corp., N.Y.). All measurements were performed in 1mM NaCl, milli-Q water (pH ~ 5.7) at 25 °C. The electrophoretic potential was taken from the average of three runs of ten measurements.

Optical Microscopy

Microscopic observations were made with a Nikon OPTIPHOT polarizing microscope with a Linkam THMS600 hot stage. The solution samples were prepared by dispersing a drop of MUP in chloroform or in methanol on a clean microscope slide and covering it with a cover slip. The solid MUP was placed between the microscope slide and cover slip, heated to 100 °C and cool down to room temperature. A transparent thin layer was obtained which was analyzed in the hot stage device.

3.3 RESULTS AND DISCUSSION

3.3.1 Synthesis of 11-mercaptoundecanylphosphonic acid (MUP)

To synthesize the MUP surfactant, the five step procedure described by Skulason and Frisbie was first tried.[39] 11-bromoundecanol (98%, Aldrich) was used as the starting material where the alcohol group was protected as the phosphorylation was performed on the bromide. In addition to the lengthy five step procedure, significant efforts were required to recrystallize the white solid from dark brown oil. Since overnight cooling in the freezer was needed, a week of recrystallization produced only 50 mg of an off-white product. The synthesis strategy was then replaced by the procedure used by Lee et al.[33] in which 11-bromo-1-undecene was used as the starting material. The final step of the four-step synthesis required bromination by trimethylsilyl bromide (TMSB) followed by water hydrolysis. From the ^{1}H-NMR and mass spectrometry (MS), it was clearly shown that the hydrolysis was not complete. This was observed even when the TMSB/water sequence was repeated twice to maximize the completion of the hydrolysis step. Concentrated hydrochloric acid previously used in phosphonate ester hydrolysis[35, 40-42] was used instead. The ^{1}H-NMR and MS showed that hydrolysis using a stronger acid (6 M HCl) was efficient and essentially complete, and the thiol group was not affected. The ^{1}H-NMR spectrum of partially and fully hydrolyzed MUP is shown in Figure 3.1 and 3.2, respectively.

Mass Spectrometry

Electron spray ionization mass spectra (ESI-MS) in negative mode of MUP in chloroform-d and methanol are shown in Figure 3.3a and Figure 3.3b, respectively. In $CDCl_3$, the deprotonated molecular ion at m/z 267 (M^-) corresponding to the MUP followed by broad cluster population at m/z 535 (M_2^-), m/z 803 (M_3^-), m/z 1071 (M_4^-), m/z 1338 (M_5^-), m/z 1606 (M_6^-) and m/z 1874 (M_7^-) were observed at a desolvation gas temperature of 200 °C. The trimer at m/z 803 appears as the major and is the most stable cluster. Under the same ESI-MS conditions, the MUP in methanol shows only the m/z at 267 which corresponds to the deprotonated molecular monomer. It is obvious that MUP

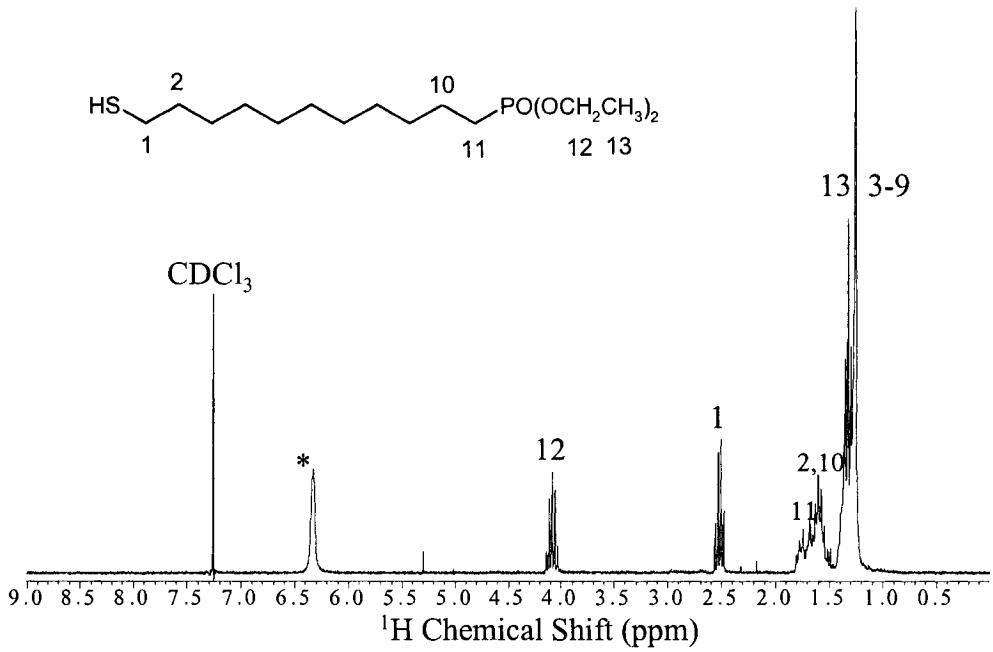

Figure 3.1 Solution ^{1}H-NMR spectrum of diethyl 11-mercaptoundecanyl-phosphonate in $CDCl_3$. The broad peak (*) at 6.32 ppm is due to the fully hydrolyzed phosphonate group.

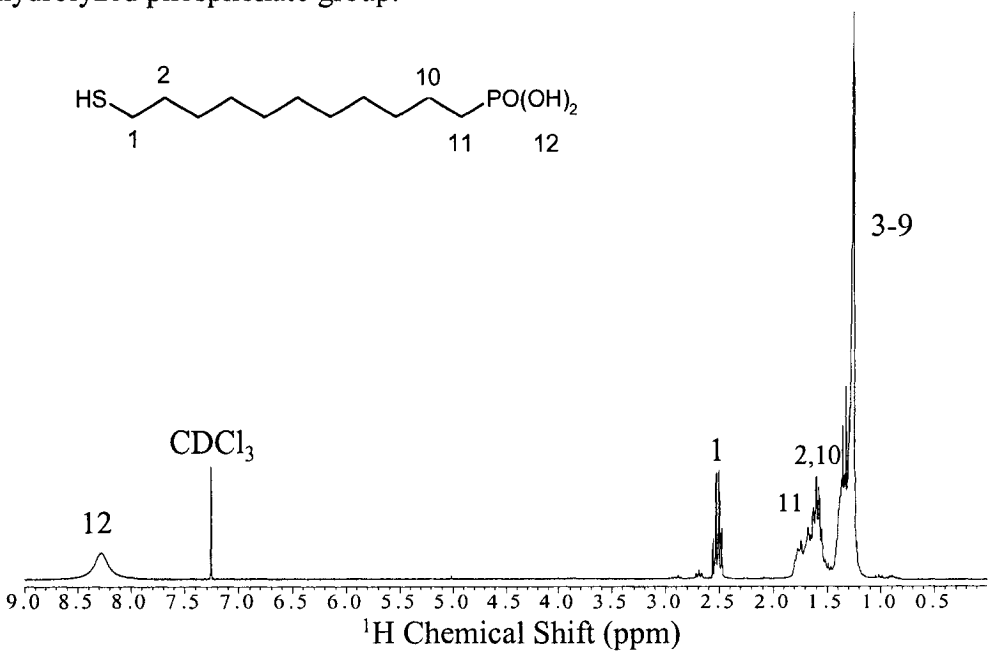

Figure 3.2 Solution ^{1}H-NMR spectrum of 11-mercaptoundecanylphosphonic acid, MUP, in $CDCl_3$.

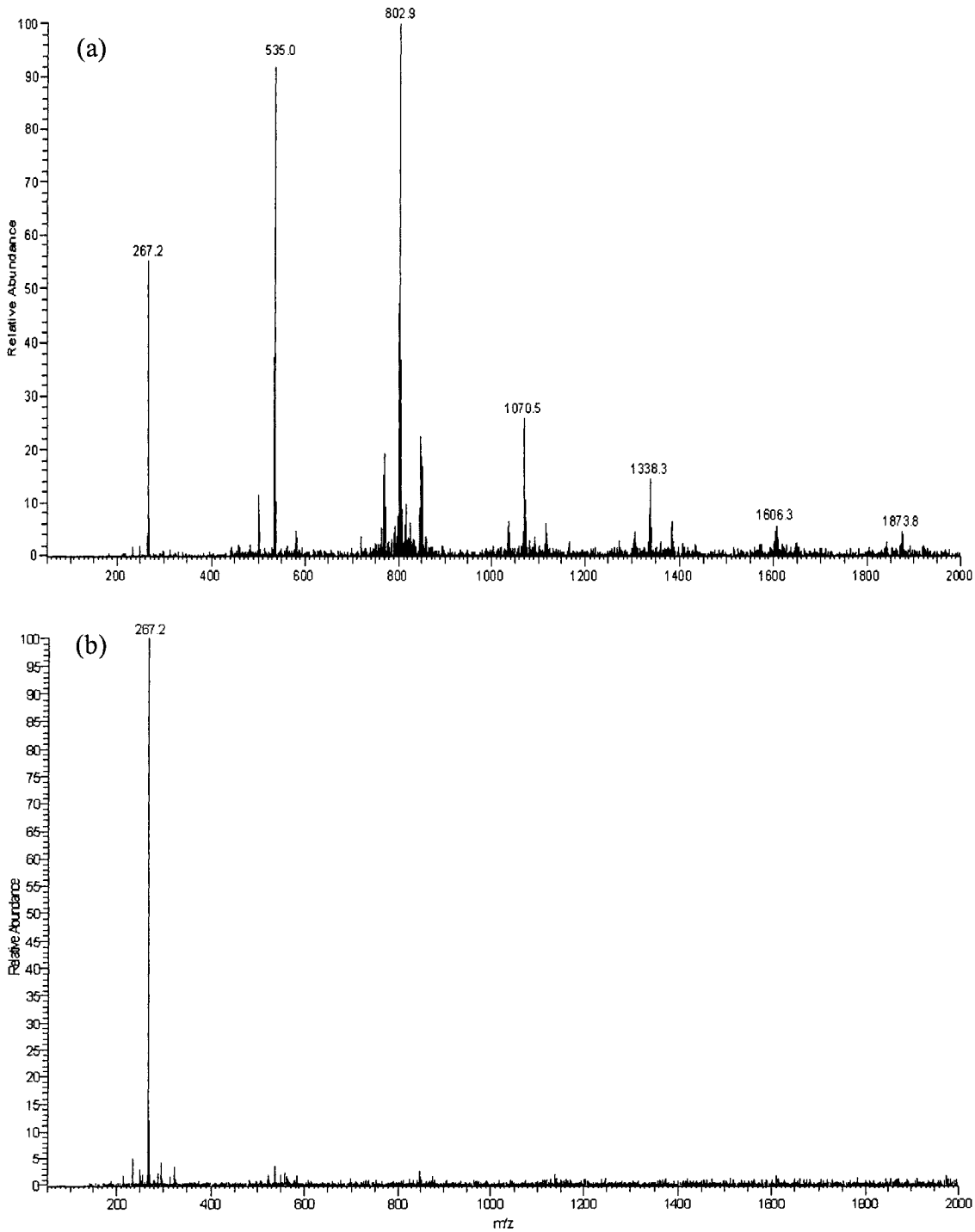

Figure 3.3 ESI mass spectra (0-2000 m/z) in negative mode of 11-mercaptoundecanyl-phosphonic acid in (a) chloroform-d and (b) methanol. Capillary tube temperature was set to 200 °C.

in chloroform forms aggregates that are stable even in the gas phase at high temperature. H-bonded clusters in chloroform were previously studied by ESI-MS.[43,44] The MS spectra does not always reflect what is present in the solution due to the dissociation during ionization. In addition, several ESI-MS conditions might influence the cluster formation affecting the rearrangement processes in the gas phase.[30] The ESI-MS studies of tert-butylphosphonic acid in chloroform were shown to form H-bonded clusters in the gas phase but did not reflect the geometry found by X-ray.[30] However, the information that can be obtained from the ESI-MS data is that chloroform favors the cluster formation presumably linked through hydrogen bonding whereas the methanol with hydrogen-acceptor property can weaken the clusters by forming an intermolecular hydrogen bonds with the phosphoryl groups.[29]

The melting point of MUP was found to be 84 °C. Due to its amphiphilic property, MUP was soluble in methanol as well as in chloroform but not in water where it formed an emulsion-like soap giving only a broad signal (1.1-1.7 ppm) in solution ^{1}H-NMR.

3.3.2 Synthesis and TEM of PO_3-MPC

11-Mercaptoundecanylphosphonic acid monolayer protected gold clusters, PO_3-MPCs, were prepared according to a procedure published by Murray[45], in a methanol/acetic acid solvent mixture. The PO_3-MPCs were synthesized using 3:1 thiol to gold ratio and a concentration of 3.8 mM for the $HAuCl_4$ $3H_2O$ solution, parameters that previously gave the 1.8 nm diameter particles for the analogous SO_3-MPCs. The brownish solution, containing thiol and gold, turned dark as soon as the reducing agent ($NaBH_4$) was added. The dried gold nanoparticles were collected as a finely divided black powder. Since an excess of $NaBH_4$ was used, these collected particles were in the sodium form and will be referred to as PO_3Na-MPCs. To remove the Na ions and other impurities, dialysis was performed on the PO_3Na-MPCs. ^{31}P solid-state NMR of the dialyzed particles showed no trace of phosphonate salt, and will be referred to as PO_3-MPCs. The PO_3-MPCs were partially soluble in methanol and chloroform, but are not very stable. High solubility and stability were found only in basic water. On average, 3.0 to 3.5 nm diameter particles were synthesized, with a highly spherical shape and

somewhat polydisperse with a relative standard deviation of 20-30%. When compared to SO_3-MPCs, the PO_3-MPCs were ~1 nm larger in core size, suggesting that the nature of the MUP surfactant or the methanol, the only differences between the two MPCs syntheses, had a definite impact on the growth dynamic of PO_3-MPCs. The TEM pictures are shown in Figure 3.4 where the 3.1 nm diameter PO_3-MPCs at pH 5.5 (Figure 3.4a) and 10.7 (Figure 3.4b) are displayed. The pKa values of 11- mercaptoundecanyl-phosphonic acid on a 2D SAM gold surface were found to be 4.5 and 8.4 using chemical force microscopy.[9,10] Thus at pH 10.7, there was little aggregation observed, as would be expected for highly charged colloids.[46] At pH 5.5 some of the phosphonic groups were protonated, resulting in interparticle interactions through intermonolayer hydrogen bonding that creates particle aggregation. The TEM pictures of heated PO_3-MPCs and the same colloids coated with PDADMAC polyelectrolyte are shown in Figures 3.4c and 3.4d, respectively. Average particle size grew to 7.2 ± 3.1 nm after heating (120 °C) the sample in the solid-state NMR rotor. This will be discussed later. The increase in particle size phenomena for Au nanoparticles from the heat treatment in solid-state[47,48] and in solution[49,50] was previously observed. The change in particle size was mainly due to recrystallization and coalescence of the particles.[48,50] The TEM of heated PO_3-MPCs shows two particle size distributions, one around 3.5 nm and the larger one at 9 nm. The histograms are given in the appendix.

From the TEM picture (Figure 3.4d) of the PO_3-MPCs coated with PDADMAC, the average diameter was found to be 3.9 ± 0.9 nm, which resulted in an increase of ~ 0.8 nm layer thickness. This increase in core size is consistent with the layer thicknesses obtained for PDADMAC/PSS layers assembled on 7 nm carboxylic acid derivatized gold nanoparticles.[36]

3.3.3 UV-Vis Spectroscopy

The surface plasmon (SP) absorption band in the 515-530 nm region of the different PO_3-MPCs is shown in Figure 3.5. The SP band of PO_3-MPCs is more detectable at pH 10.7, Figure 3.5b, than at pH 5.5, Figure 3.5a, where the broadening of the SP band is due to hydrogen bonding induced aggregation as seen in TEM pictures. The characteristic of the SP band is strongly dependent on the particle size.[36] The

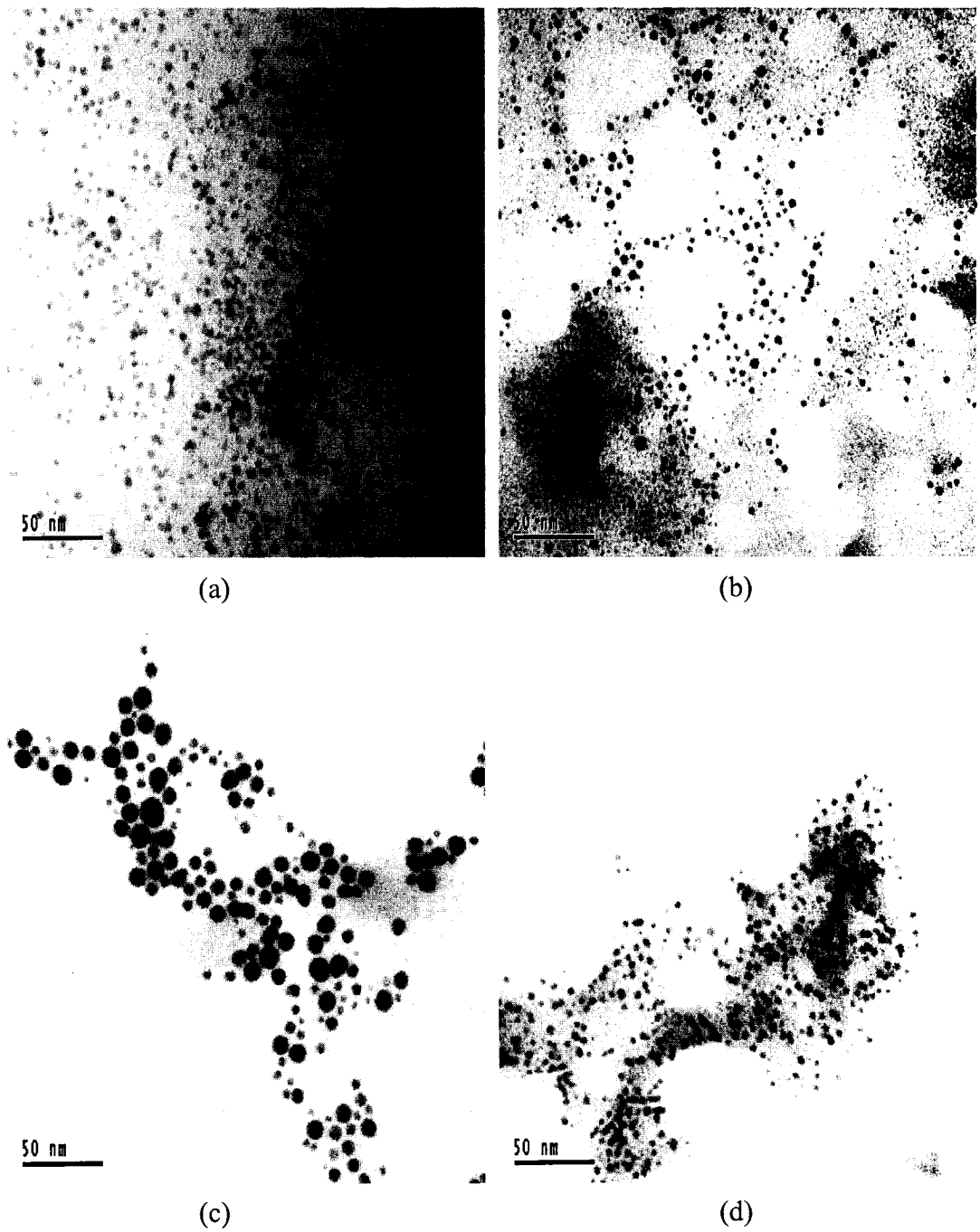

Figure 3.4 TEM micrographs of PO_3-MPCs at (a) pH = 5.5, (b) pH 10.7, 3.1 ± 0.9 nm (c) heated to 120 °C, 7.2 ± 3.1 nm and (d) coated with PDADMAC, 3.9 ± 0.9 nm

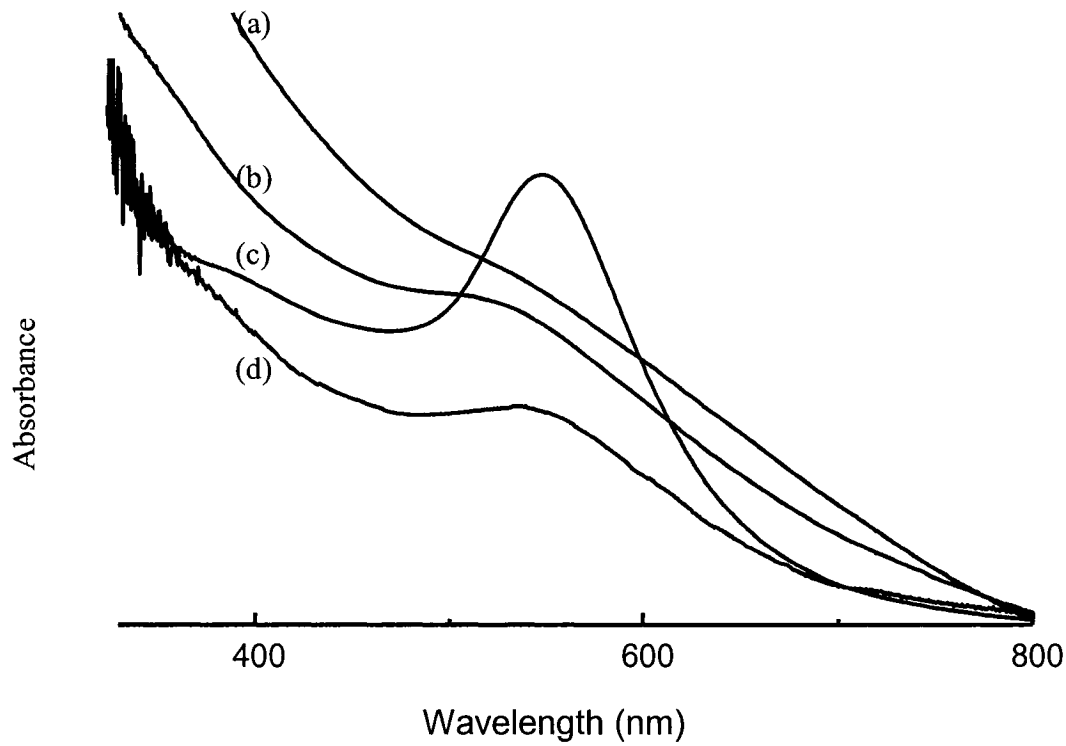

Figure 3.5 Plasmon absorption band of PO_3-MPCs (a) in milli-Q water (pH = 5.5), (b) after adjusting the pH with dil.NH_4OH to pH 10.7, (c) heated to 120°C (in milli-Q water and (d) coated with layer of PDADMAC (in milli-Q water).

shoulder with λ_{max} at ~ 520 nm for 3.1 nm-diameter PO_3-MPCs at pH 10.7 was previously observed for similar sizes of alkanethiolate gold nanoparticles.[1] The UV-Vis spectrum of the red solution of heated PO_3-MPCs (Figure 3.5c) showed a distinctive SP band at 530 nm typical for 7 nm-diameter particles.[36] Polyelectrolyte adsorption can be monitored by the λ_{max} shift in a SP band because it is sensitive to relative thickness of materials coated on a particle surface.[36] The wavelength shift in the SP band of the PDADMAC coated PO_3-MPCs (Figure 3.5d) was ~ 5 nm giving a new λ_{max} shift at 525 nm. A similar wavelength shift was observed for PDADMAC coated carboxylate-modified gold nanoparticles.

3.3.4 Thermogravimetric analysis (TGA)

Figure 3.6 compares the TGA curves between the unbound free surfactant MUP and the PO_3-MPCs. In the free thiol, the TGA curve (solid line) had two degradation steps. The first initial mass loss starts at about 200 °C and ends at about 350 °C with a ~ 10 % of the organic mass loss. In the second step, the main mass loss (~80 %) occured over the range of 350 and 500 °C. The analysis of the non-volatile residue in poly(vinylphosphonic acid) suggested the presence of phosphorus residue.[51] The TGA curve of PO_3-MPCs (dashed line in Figure 3.6) also shows two degradation steps in the temperature intervals of 200-300 °C (~ 10 % organic loss) and 300-550 °C (~ 40 % organic loss). The slightly higher temperature range at which the loss of organic from PO_3-MPCs was observed indicates that MUP bound to gold surface is more thermally stable than free MUP. After heating to 700 °C, the gold-color solid residue was found to be 51.4 % residual material. Assuming an effective footprint of about 17 $Å^2$, as found in SO_3-MPCs, and a gold diameter particle of 3.1 nm, the % fraction can be easily calculated to 20.7 %. The excess can be attributed to the free thiol and trapped water. The nature of the hydrogen bonding in phosphonic acids makes it possible that some MUP molecules were hydrogen bonded with MUP molecules bound to the surface of gold nanoparticles[39,52] which could not be removed even after several washing steps.

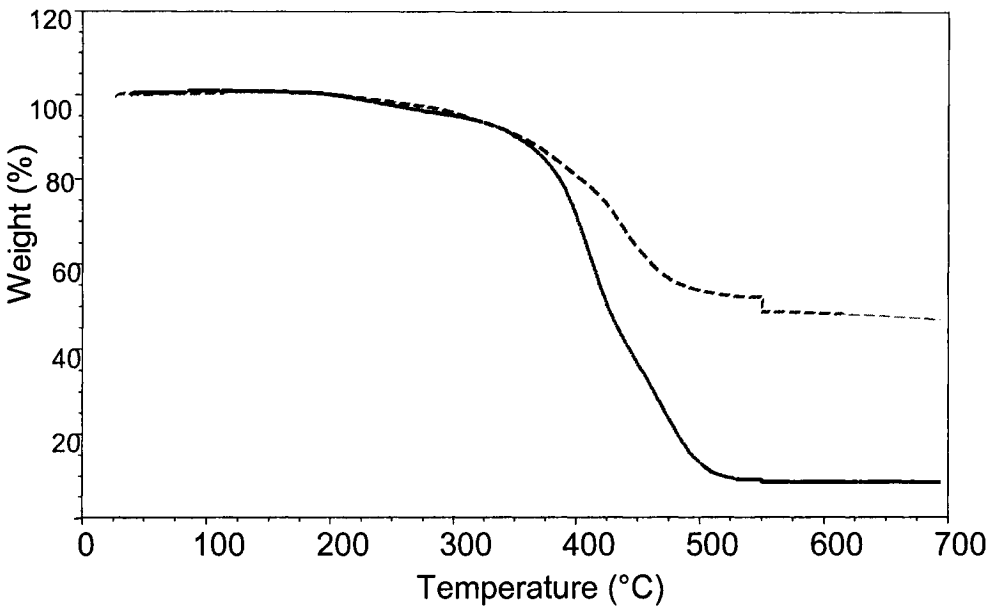

Figure 3.6 Comparison between TGA curve of unbound thiol, MUP, (solid line) and TGA curve of 3.1 nm-diameter PO_3-MPCs (dashed line) at 20 °C/min..

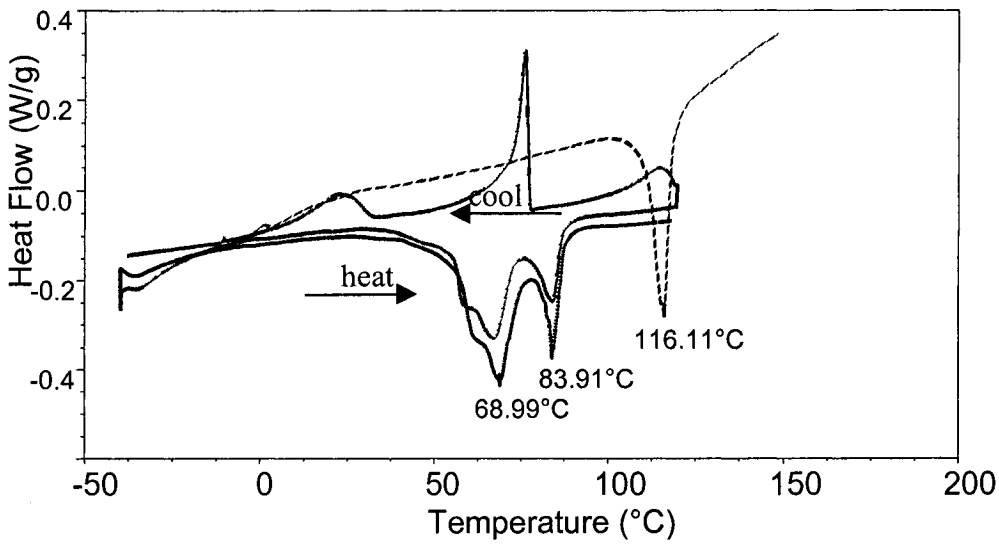

Figure 3.7 Heating and cooling curves of unbound thiol, MUP (solid line) and heating curve of PO_3-MPCs (dashed line). The MUP shows solid-solid transition at 69 °C and melting at 84 °C. PO_3-MPCs show solid-solid transition at 116 °C.

3.3.5 Differential Scanning Calorimetry (DSC)

The DSC curves of MUP (solid line) and PO_3-MPCs (dashed line) are shown in Figure 3.7. The 11-mercaptoundecanylphosphonic acid exhibits two endotherms, first one at onset temperature of 62 °C (ΔH = 66 J/g) and the smaller one at 80 °C (ΔH = 18 J/g). The first endotherm is believed to be associated with a phase transition from one crystalline form to a less thermodynamically stable form. Such transitions have been observed in long-chain phosphonic acids (i.e., $C_{12}PO_3H_2$) where the enthalpy of transition was larger than the enthalpy of fusion.[27] The second transition at 84 °C corresponds to the melting of the MUP surfactant. From the magnitude of enthalpies, the heating and cooling cycles showed that the phase transitions for the MUP are not completely reversible. The entropy of fusion is small ($\Delta S \sim 14$ J K^{-1} mol^{-1}) compared to the entropy of transition ($\Delta S \sim 53$ J K^{-1} mol^{-1}) which indicates that a major disordering process occurs prior the melting.

The endotherm at 116 °C with ΔH = 29.7 J/g, observed in the DSC curve (dashed line, Figure 3.7) of the PO_3-MPCs, corresponded to the order/disorder transition in solid-state NMR. Hysteresis was observed which coincided with the irreversible chain order/disorder process observed in solid-state NMR due to the desorption of the thiol from the gold nanoparticles.

The MUP sample was melted between the microscope slide and cover slip and cooled down to room temperature. The sample was then heated to the first transition point. Figure 3.8 shows the transformation under cross polarizers of a spherulite phase at room temperature (Figure 3.8a) into an isotropic phase (Figure 3.8b) at 70 °C. The high degree of crystallinity in MUP is reflected from the spherulite geometry similar to that observed in a simple triglyceride.[53] The polarized light intensity was lost above the second transition (84 °C) which indicates the melting. No fluid phase was detected by optical microscopy above the first transition.

3.3.6 FT-IR spectroscopy

Infrared spectroscopy is often used to determine the functionality present in unknown organic molecules. In addition, the intensity and shape of a peak and the relative position of the band are commonly used to characterize the packing and

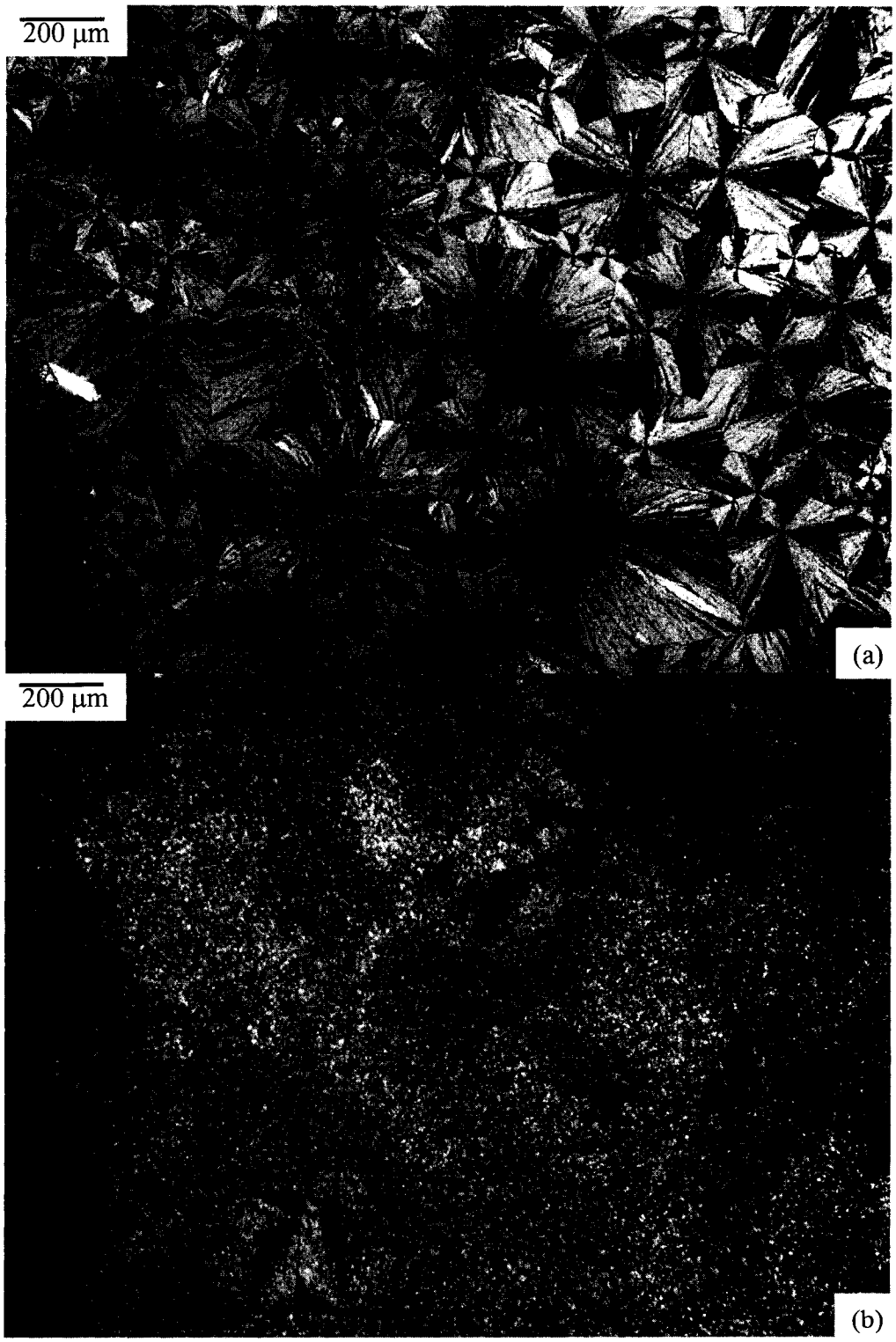

Figure 3.8 Photomicrograph (crossed polarized) of (a) MUP at room temperature (b) heated to 70 °C, above the first phase transition.

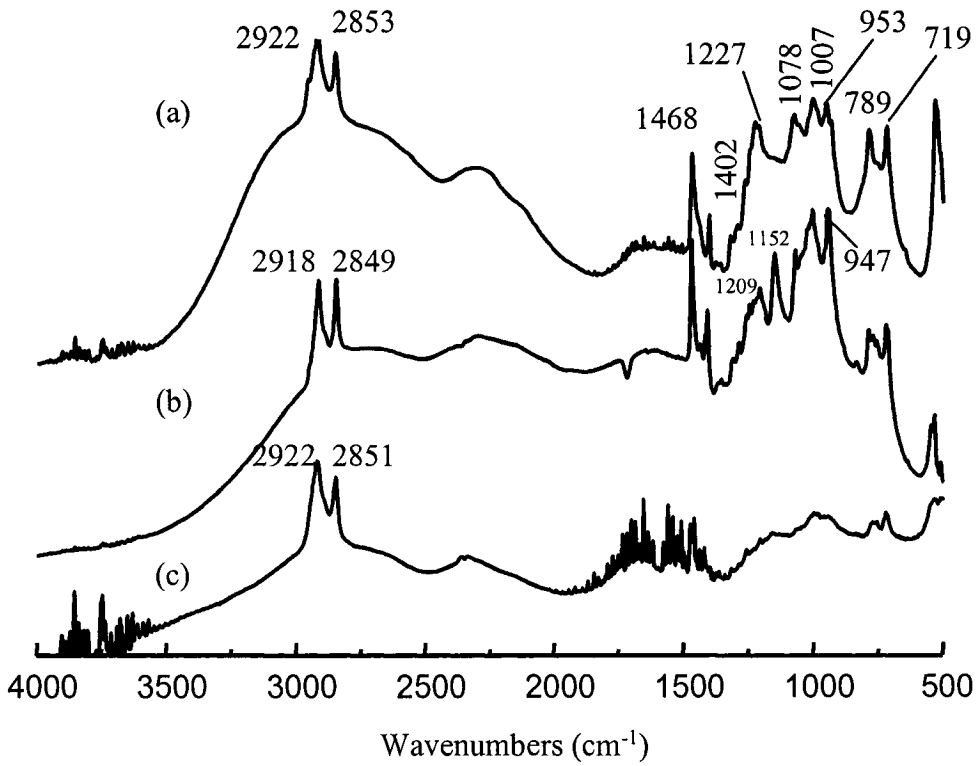

Figure 3.9 PAS-FTIR spectra of (a) bulk, 11-mercaptoundecanylphosphonic acid, (b) 3.1 nm-diameter PO_3-MPCs and (c) 3.1 nm-diameter PO_3Na-MPCs.

orientation in SAMs. Photoacoustic Fourier transform infrared (PAS-FTIR) spectra of pure MUP, PO_3-MPCs, and PO_3Na-MPCs are shown in Figures 3.9a, 3.9b and 3.9c, respectively. The CH_2 IR adsorption bands for MUP are assigned as follows: 2922 and 2853 cm^{-1} for symmetric (ν_s) and anti-symmetric (ν_{as}) stretches, and 1468 and 1402 cm^{-1} for scissoring mode (δ). All the CH_2 bands and bands at 789 and 719 cm^{-1} (ν, P-C) have been reported previously.[54] The extent of alkyl chain ordering compared to bulk sample can be estimated from the ν_a and ν_{as} stretches as reported in Table 3.1. In liquid alkanes, where there is an equilibrium population of the trans and gauche conformations, the ν_s and ν_{as} stretches appear at 2924 and 2854 cm^{-1}. The stretching frequencies ν_s and ν_{as} of PO_3-MPCs (Figure 3.9b) have been found at 2918 and 2849 cm^{-1}, indicating a high trans population. The PO_3Na-MPCs sample show stretching frequencies (ν_s = 2922 cm^{-1}, ν_{as} = 2851 cm^{-1}) slightly higher than PO_3-MPCs and is still more ordered than the bulk MUP.

Table 3.1 Comparison of stretching frequencies, ν, in various IR regions for MUP and PO_3-functionalized nanoparticles.

Compound	ν, CH (cm^{-1})		ν, P-OH (cm^{-1})			ν, P-C (cm^{-1})	
	ν_s	ν_{as}	ν_s	ν_{as}	νPO_3		
MUP, bulk	2922	2853	1078	953	1007	789	719
PO_3-MPCs	2918	2849	1070	947	1006	788	721
PO_3Na-MPCs	2922	2851	-	-	-	777	723

The IR bands on the phosphonate group were assigned on the basis of literature assignments and especially from a study of alkylphosphonic acid ($C_{18}H_{37}PO_3H_2$) adsorbed on a calcium hydroxyapatite surface.[54] The 950-1300 cm^{-1} fingerprint region of the PO_3H_2 functional group can be useful in the determination of hydrogen bonding. The IR bands of the bulk MUP at 1227 cm^{-1} (ν, P=O), 1078 and 953 cm^{-1} (ν_s, ν_{as} of POH), and 1007 cm^{-1} (ν, PO_3) are consistent with previously studied phosphonic acids.[54-57] Various studies have been carried out involving phosphonate head groups bound to

surfaces[54-56] where the disappearance of P=O stretching band along with the POH bands at ~ 950 and 1075 cm^{-1} was evidence of PO_3 interacting with a surface. Recently, D'Andreat and Fadeev suggested that the absence of the P=O band is due to the hydrogen bonding between the phosphonic acid and the modified calcium surface bearing OH groups.[54] Intermolecular associations in hydroxyalkyl phosphinic acids have also been studied by IR.[58] The appearance of the band at ~1170 cm^{-1} is associated with P=O groups involved in intermolecular hydrogen bonding. In the case of PO_3-MPCs, the PO_3H_2 group is the tail group of the functionalised alkanethiolate chain chemisorbed on the gold surface by the S-Au bond. In the IR spectrum of PO_3-MPCs (Figure 3.9b), the decrease in the P=O absorption band and the presence of the band at 1152 cm^{-1} may be an indication of the P=O groups being involved in interparticle hydrogen bonding which is also believed to be present in carboxylate functionalized gold nanoparticles.[6] The 950-1300 cm^{-1} region in PO_3Na-MPCs is broad as observed in other Na-phosphate compounds.[59]

3.3.7 Solution NMR studies of MUP

The ^{1}H-NMR spectrum of 11-mercaptoundecanylphosphonic acid in $CDCl_3$ was shown in Figure 3.2. The typical quartet at 2.5 ppm corresponds to the methylene group next to SH group indicates the thiol functionality. The ^{31}P chemical shift of the MUP in chloroform-d was 37.1 ppm whereas in methanol-d_4 the ^{31}P chemical shift was 30.9 ppm. The effect of various solvents on ^{31}P chemical shift has been previously investigated.[29-31,60] The change in ^{31}P chemical shift by several ppm indicates that phosphonic acids have a very high solvent dependence and that a drastic change in the ^{31}P environment must have occurred. The shielding in ^{31}P NMR can be attributed to CD_3OD providing intermolecular hydrogen bonding to the phosphoryl oxygen, which increases the π-bonding to phosphorus.[29,31]

The solution ^{13}C-NMR spectra of MUP in Figure 3.10 showed clearly the effect of using chloroform versus methanol solvent. At high concentration (30 mg/mL) of MUP in chloroform-d, Figure 3.10a, the three carbon signals next to the phosphonic group are broad, indicating a decrease in mobility. Such a broadening was observed in rod-like micelles of dodecyldimethylammonium chloride in D_2O[61] and for phosphatidylcholine

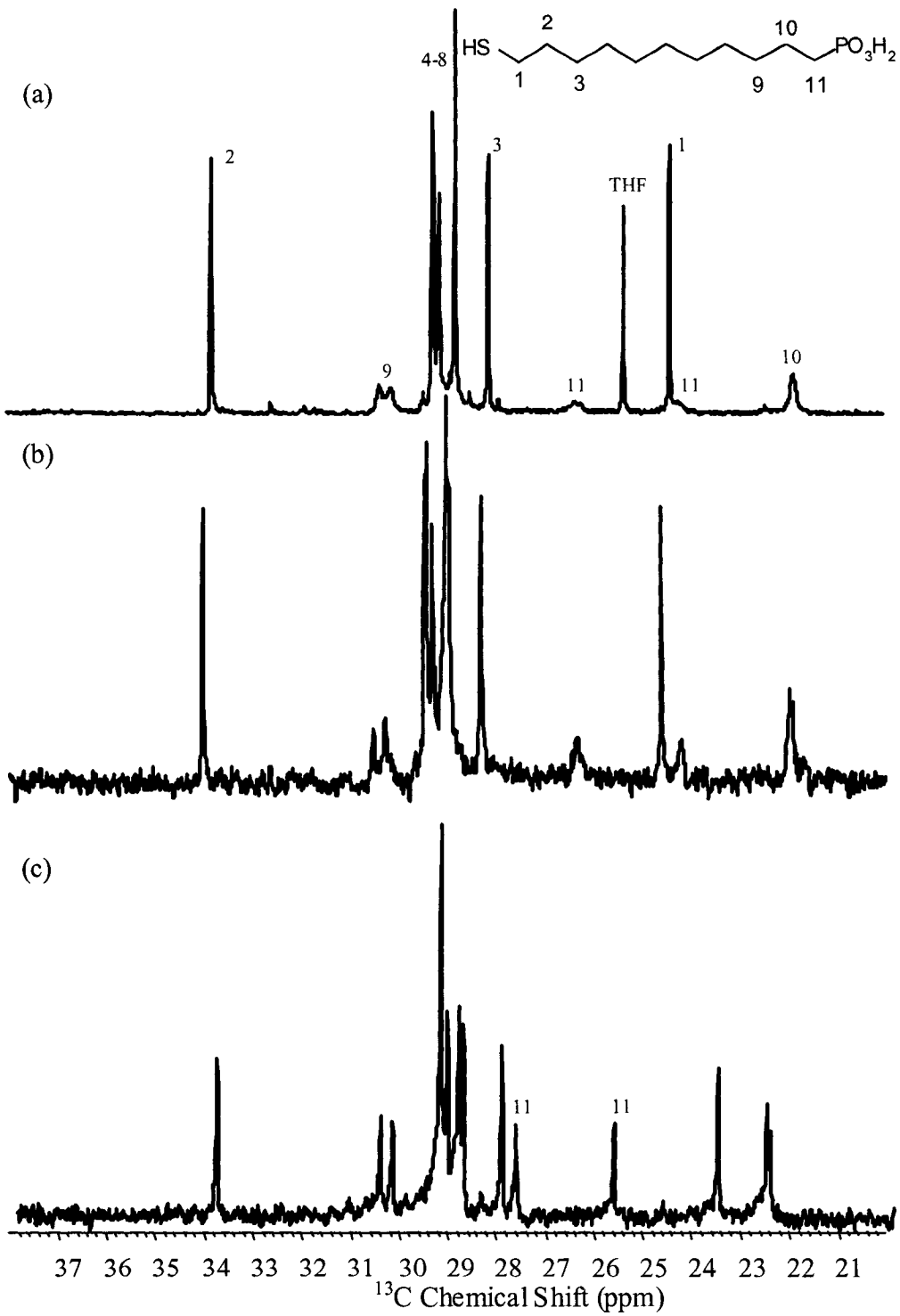

Figure 3.10 Solution ^{13}C CP NMR (20 – 38 ppm) of 11-mercaptoundecanyl-phosphonic acid in chloroform-d (a) 30 mg/ml and (b) 5 mg/ml and (c) in methanol-d_4. Peak at 25.6 ppm is due to the presence of tetrahydrofuran (THF).

inverted micelles (i.e., consisting of a hydrophilic cluster core and a hydrophobic cluster shell) in various organic solvents.[62] The change in line width of C9, C10 and C11 occurs at lower concentration of MUP in chloroform-d (5 mg/mL), Figure 3.10b, whereas in methanol-d_4 (Figure 3.10c), the peaks (C9-C11) are as narrow as the other ^{13}C signals. At a high concentration of MUP in $CDCl_3$, the phosphonate groups would interact strongly through H-bonding with each other forming inverted-like micelle clusters and limit the internal rotation of the carbons closer to the phosphate group. By decreasing the concentration of MUP in $CDCl_3$, these H-bonded aggregates are broken down into smaller clusters and likely down to monomers in very dilute solutions. The ^{13}C NMR spectrum in CD_3OD demonstrates that the motion at the head group is free and behaves more like a monomer. These results are consistent with the results found in the mass spectrometry, where the cluster formation was found in chloroform.

The PO_3-MPCs were only soluble in alkaline water giving a dark wine-colored homogenous solution. The spectrum of the gold colloids showed no signal in the solution ^1H-NMR not even the broad peak in the 1.2-1.7 ppm region which was observed in the free MUP-D_2O spectrum. An increase in average size of MPCs and in packing density along the chains can significantly broaden the signal. Intraparticle and intramonolayer hydrogen bonding may decrease the mobility enough to completely broaden out the NMR resonances. A similar phenomena is observed for the hydroxylate functionalized gold nanoparticles.[5]

3.3.8 Conformation and Dynamics of PO_3-MPC in solid-state

The solid-state ^{13}C CPMAS NMR spectrum of 11-mercaptoundecanylphosphonic acid (MUP) adsorbed on gold nanoparticles is shown in Figure 3.11c along with the solution (Figure 3.11a) and the solid-state ^{13}C (Figure 3.11b) spectrum of the unbound MUP. The ^{13}C chemical shifts of these samples are listed in Table 3.2. The PO_3-MPCs were not soluble in any common organic solvents and since ^1H-NMR of PO_3-MPCs in D_2O gave no signal, the solid-state ^{13}C NMR spectrum of pure MUP was shown instead. In alkanes a downfield shift of 2-5 ppm was usually observed, from a solution NMR shift of 29-30 ppm to solid-state NMR shifts of 31 ppm for disordered inner methylene groups and 33-34 ppm for the methylenes groups in an all-trans conformation.[63] In solution the

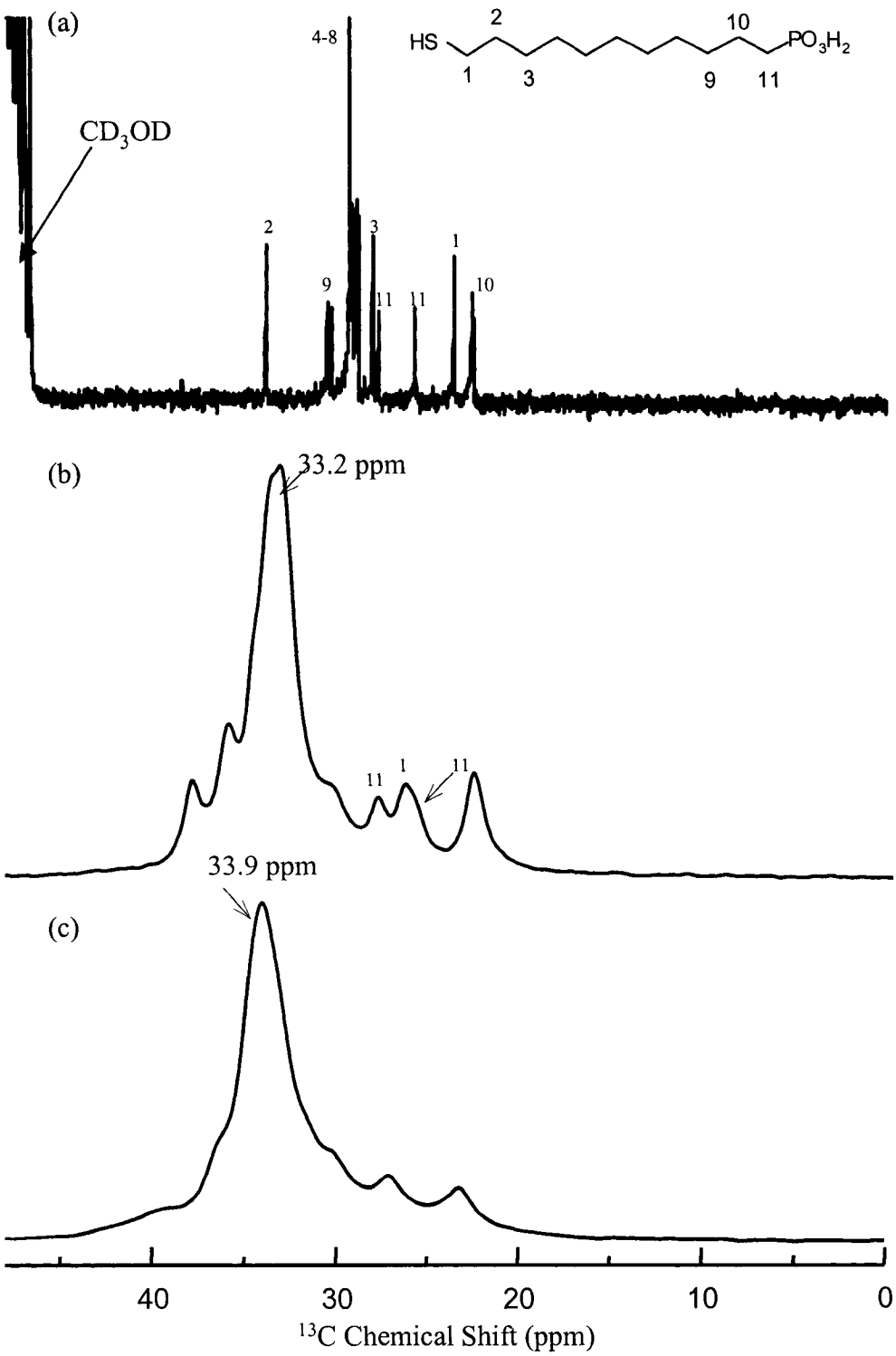

Figure 3.11 ^{13}C CP NMR spectra of 11-mercaptoundecanylphosphonic acid (a) in methanol-d_4 and (b) in solid state (c) on colloidal gold in the solid state. The PO_3-MPCs were not soluble in common organic solvents.

interior methylene peaks of the free surfactant (Figure 3.11a) had an average shift of 28-29 ppm whereas in solid-state the peaks shifted downfield to 33.1 ppm, an indication of high crystallinity in the solid. The solid-state spectrum of PO_3-MPCs showed an even

Table 3.2 ^{13}C Chemical shift of 11-mercaptoundecanylphosphonic acid in the free state and adsorbed onto gold.

MUP $HS(CH_2)_{11}PO_3H_2$	MUP MeOH-d_4 solution	MUP solid-state	PO_3-MPC solid-state
C1	23.6	26.4	-
C2	33.9	37.9	-
C3	28.1	30.2	30.3
C4-C8	29.3-28.3	33.1	34.0
C9	30.4 (d, J^2=16 Hz)	36.0	36.1
C10	22.6 (d, J^2 = 5 Hz)	22.7	23.2
C11	26.8 (d, J^2 = 138 Hz)	26.9 (d, J^2 = 143 Hz)	27.1

higher downfield shift, 34.0 ppm, which suggests a high conformational order with very few gauche defects[63] and an alkane-like monoclinic structure. Usually the trans peaks at ~ 33 ppm and ~ 34 ppm can be assigned to the orthorhombic and monoclinic alkane crystals, respectively.[64] The C1 at 26.4 ppm and C2 at 37.9 ppm in the bulk (Figure 3.11b), appeared to vanish completely in the PO_3-MPCs (Figure 3.11c). The large $^1J_{PC}$ coupling (i.e., ~ 140 Hz) observed for C11 in solution was also seen for the bulk surfactant in the solid-state. Only one peak of the C11 doublet was visible in the solid-state spectrum of PO_3-MPCs and the other peak was probably underneath the broad resonance of the interior CH_2.

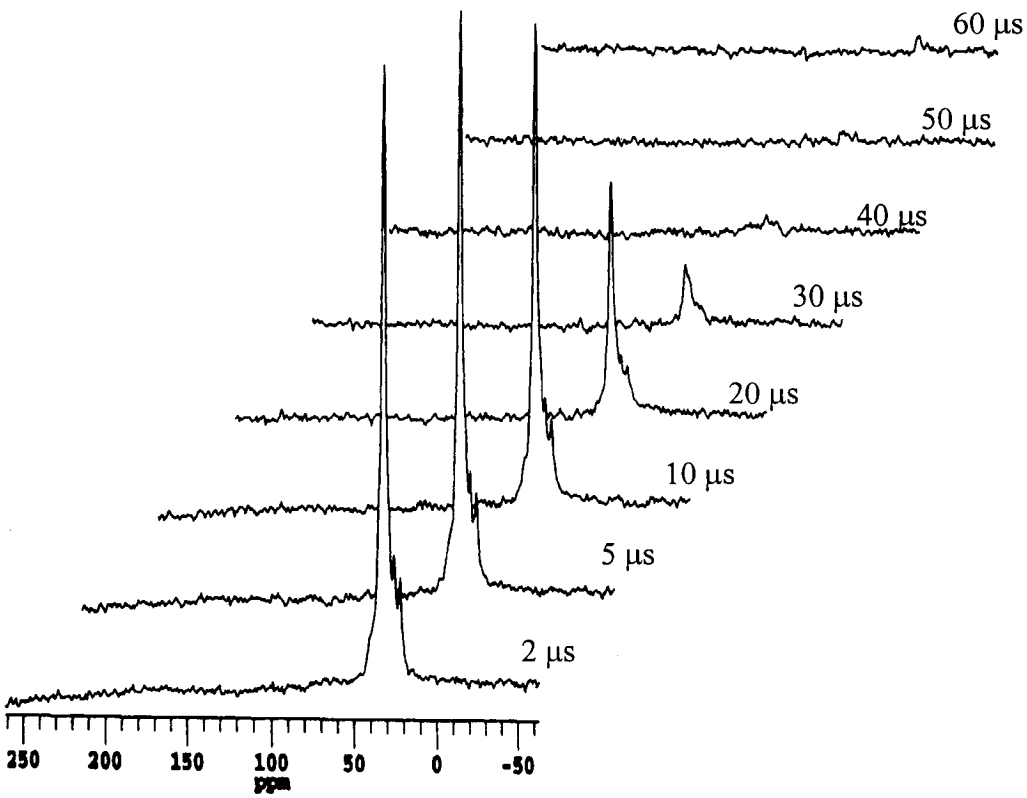

Figure 3.12 Dipolar dephasing spectra of PO_3-MPCs at selected dephasing times. The interior peaks and C10 decayed away completely at 40 μs.

The dense packing of the alkyl chains of PO_3-MPCs is further reflected in the reduced molecular mobility. The alkyl chains of the gold nanoparticles, HOC_{16}-MPCs, which have terminal OH groups, showed conformational order and restricted mobility when studied by relaxation and dipolar dephasing NMR experiments.[5] Dipolar dephasing spectra of PO_3-MPCs are shown in Figure 3.12 along with the dipolar dephasing times (T_{dd}, μs). In rigid solids, a Gaussian decay of methylene carbons is normally in the range of 10-30 μs (T_G) whereas non protonated carbons (e.g., C=O) exhibit an exponential (Lorentzian) decay usually between 75-200 μs (T_L).[38] In Figure 3.12, the peaks all vanished after 40 μs and even the C10 and C11 peaks at the chain ends were gone. The T_G for the interior methylene carbons at 34 ppm and the C10 of PO_3-MPCs were found to be 14 μs and 16 μs, respectively. Compared to the T_{dd} of HOC_{16}-MPCs which shows T_G = 17 μs for C4-C15 and T_L = 102 μs for C16, the dipolar dephasing times of PO_3-MPCs showed high rigidity of the chains, both interior and ends, possibly due to the presence of strong hydrogen bonding interactions.

The T_1 values for MUP ranged from 18-34 s depending on the position in the chain. At the PO_3H_2 end, the T_1 values were the longest, with T_1 (C10) = 33 s and T_1 (C11) = 34 s. The interior methylenes and the C2 group showed T_1 values of 19 and 18 s respectively. The T_1 values decrease towards the PO_3H_2 group, reflecting the restriction of motion caused by the bulkier group and hydrogen bonding. The T_1 values of the interior methylene carbons for PO_3-MPCs were found from a fit to a biexponential decay with a short decay time of 2.4 s (35 %) and a longer decay time of 190 s (65 %). Both decays decreased with increasing temperature, T_{short} = 1.1 s and T_{long} = 40.8 s at 60 °C, indicating that the chain motion of the PO_3-MPCs falls in the slow exchange limit ($\omega_o\tau_o$ >> 1). The long T_1 values of the PO_3-MPCs demonstrated that the PO_3H_2 group induced a restricted mobility associated with the dense chain packing compared to the bulk acid.

The ^{31}P CPMAS NMR spectra were shown in Figure 3.13 for MUP, PO_3Na-MPCs (i.e., PO_3-MPCs sample before dialysis) and PO_3-MPCs where the PO_3^{2-} groups are protonated. The 11-mercaptoundecanylphosphonic acid showed a ^{31}P chemical shift at 31.1 ppm (Figure 3.13a) similar to what was observed in the CD_3OD solution. The three-peak pattern observed in Figure 3.13b of PO_3Na-MPCs spectrum was also observed for sodium alkylphosphonate.[19] The upfield region of the ^{31}P signal, 24-29 ppm, was

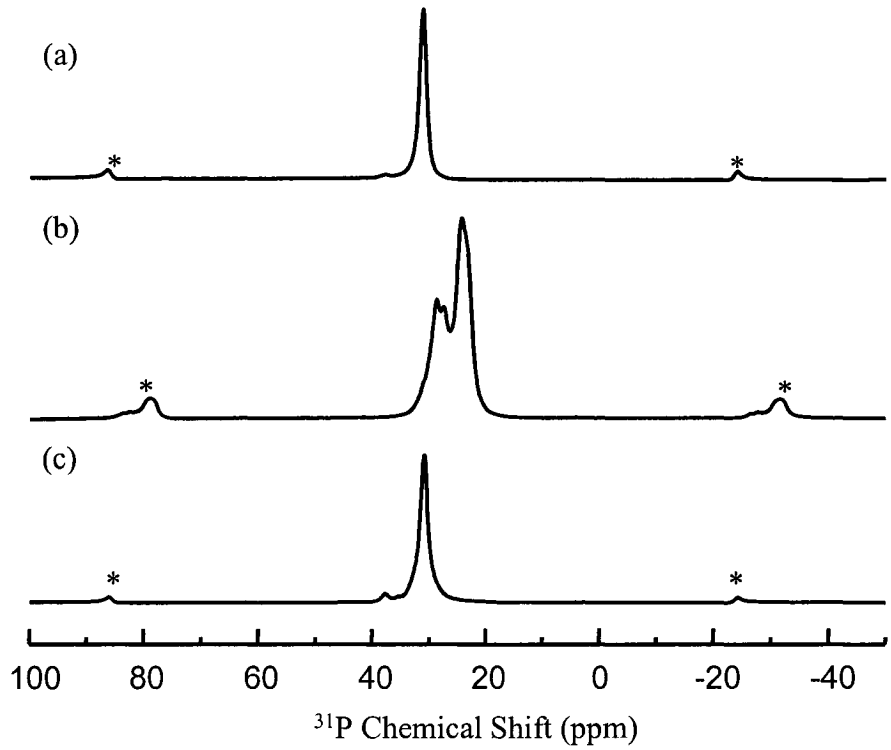

Figure 3.13 Solid-state ^{31}P CPMAS NMR spectra of (a) 11-mercapto-undecylphosphonic acid, (b) PO_3Na-MPCs and (c) PO_3-MPCs. The spectra were acquired at room temperature, with 1000 scans and a line broadening of 30. The ^{31}P spinning side bands are denoted by the asterisk.

associated with Na ions. The peak at 27.5 and 24.1 ppm corresponded to mono and disodium coordination, respectively and the chemical shift at 28.5 ppm is believe to be due to a weak association between sodium ion and phosphonic acid.[19] These signals due to the presence of Na salt vanished when the sample was dialyzed in milli-Q water. The dried dialyzed PO_3-MPCs gave a new ^{31}P chemical shift at 30.9 ppm, (Figure 3.13c) very close to that of the pure phosphonic acid and with no trace of peaks in the 24-29 ppm region.

3.3.9 ^{31}P chemical shift in solid state

Phosphonic acids are considered to form polymeric hydrogen bonded structures mostly due to the intermolecular hydrogen bonding of the type P-O-H $\cdots$ O=P. For example, in solid state, cyclohexylphosphonic acid[65] and 1-(benzyloxycarbonylamino)-ethylphosphonic acid[66] formed one-dimensional chains whereas a double-layer structure for benzenephosphonic acid[67] was observed. X-ray data showed that two different H-bonded solid-state forms of *tert*-butylphosphonic acid can be obtained when crystallized from different solvents.[30] A hexameric hydrogen-bonded cluster was obtained from $CDCl_3$ and a one-dimensional H-bonded polymer was produced from more polar solvents THF or acetonitrile. Short chain phosphonic acids, C5 and C7 were studied in water with respect to the concentration and temperature.[26] In the free water state, the X-ray data showed one-dimensional lammelar lattice for the n-phosphonic acids.

The ^{31}P chemical shift of 11-mercaptoundecanylphosphonic acid in solid state was ~ 31 ppm which coincides with the ^{31}P chemical shift in solution. The synthesis of MUP shows that the last two steps were performed in polar solvents, methanol and water which would favor the formation of H-bonded polymeric structure. The phosphorus chemical shift in the solid state of n-hexylphosphonic acid was found to be 37 ppm,[24] which coincides with the ^{31}P chemical shift of the MUP in chloroform. It was found out that the n-hexylphosphonic acid was recrystallized from hexane and heptane,[68] which would therefore favor the hydrogen-bonded cluster. In addition, the variable temperature studies, discussed in the following section, showed that 37 ppm shift was also observed in solid state for MUP and PO_3-MPCs after being heated.

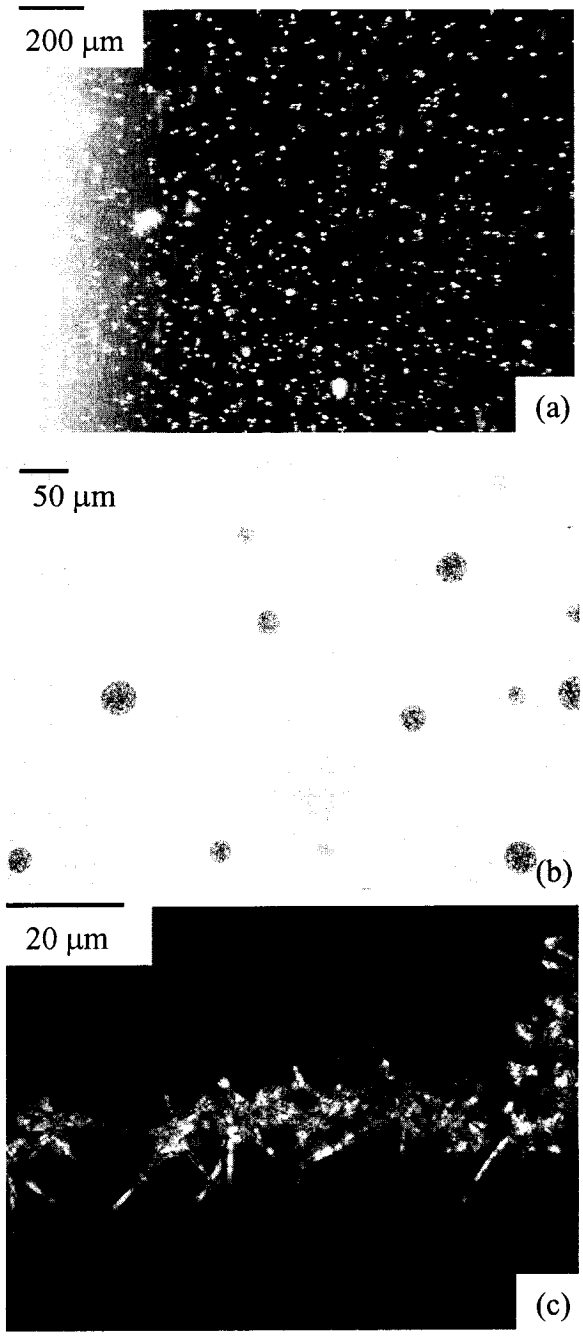

Figure 3.14 Optical microscope images of (a) MUP in $CDCl_3$, 30 mg/ml (with cross polarizers) and after drying (b) and MUP dried from $CDOD_3$ (with cross polarizers).

The images of the bulk MUP, obtained with the optical microscope are shown in Figure 3.14. The MUP in chloroform-d (30 mg/ml), Figure 3.14a, shows micelle-like aggregates seen as white dots under cross polarizers. After drying the solvent in the air, the aggregates self assembled into larger circular clusters, Figure 3.14b. Under the polarized light, these crystallites appeared as white circles. As soon as the drop of methanol containing the MUP was placed on the microscope slide, the solvent evaporated. Observing the slide under the polarizing optical microscope, Figure 3.14c, the needle-like crystallization morphology was observed. N-phosphonic acids that were recrystallized from water formed clusters of flat needles.[68]

3.3.10 Variable Temperature ^{13}C and ^{31}P

The variable temperature ^{13}C and ^{31}P NMR spectra of 11-mercaptoundecanyl-phosphonic acid were shown in Figure 3.15 and 3.16, respectively. The temperatures were selected with respect to the endotherm transition at 69 °C, observed in DSC, (Figure 3.7). At room temperature, the interior methylene carbons are mostly in a trans conformation as evidenced by the peak at 33 ppm in the ^{13}C NMR, and very few gauche defects are present. At the same time, the ^{31}P signal shows a resonance at 31.1 ppm. As the temperature is increased, a gradual thermal disordering is observed in ^{13}C NMR, indicating a growth in the peak at 31 ppm due to gauche defects, which coincided with the decrease of the ^{31}P signal at 31.1 ppm and an increase of a new peak at 37.8 ppm. Above the transition temperature (69 °C), the methylene chains were mostly disordered. In the ^{31}P NMR spectrum, the 31.1 ppm peak, identical to the ^{31}P shift of MUP in $CDOD_3$, has completely disappeared and the new peak at 37.8 ppm, same as the ^{31}P shift of MUP in $CDCl_3$, was observed. The downfield shift in the ^{31}P solid-state NMR spectra suggested that the PO_3H_2 group had undergone change in the environment as the alkane chains became disordered. As the hydrogen bonding was responsible for the stabilization of the clusters in chloroform seen by MS, ^{13}C-NMR and optical microscopy, the nature of the hydrogen bonding in the solid state is proposed to change from an extended chain structure to a micelle-like structure. Even though above the transition temperature the chains were all disordered, the good quality cross polarization spectra indicated that they

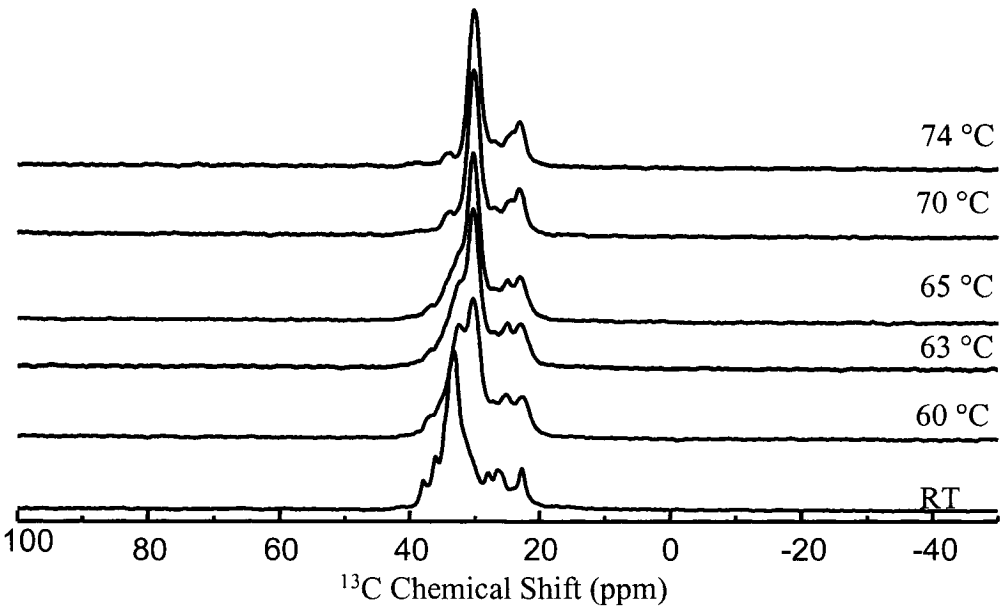

Figure 3.15 Variable temperature solid-state ^{13}C CP/MAS NMR spectra of 11-mercaptoundecanephosphonic acid. Line broadening of 30 was used.

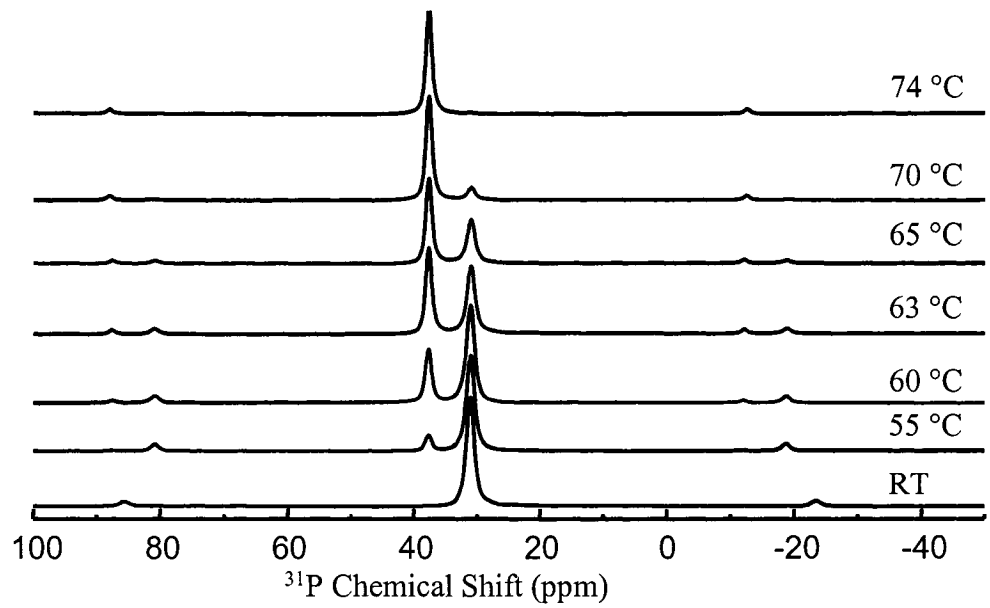

Figure 3.16 Variable temperature solid-state ^{31}P CP/MAS NMR spectra of 11-mercaptoundecanylphosphonic acid. Line broadening of 30 was used.

were not isotropically mobile. Closer to the melting point temperature (84 °C) of the surfactant, the cross polarization signal vanished due to high molecular mobility. When the sample was cooled down to room temperature, the spectra returned to the original state with a small increase in gauche defects as observed by DSC.

The variable temperature ^{13}C CPMAS spectra of PO_3-MPCs were shown in Figure 3.17. The thermal behavior of the sample showed an order/disorder transition temperature at ~ 105 °C, which agreed with the sharp endotherm found in the DSC spectrum, (Figure 3.7). As the sample was heated to 110 °C, a new peak appeared at 39.2 ppm which is close to that of an unbound dialkyldisulfides.[69] This suggests that upon heating some of the surfactant desorbed from the surface in the form of a disulfide. Upon examination of the sample in the rotor, a layer of white solid was deposited on the film of the black gold colloids. When the mixture was dissolved in CD_3OD, a triplet at 2.67 ppm confirmed the presence of disulfide. Heating the sample to 120 °C resulted in completely disordered mobile chains. When the sample was cooled down to room temperature, the chains stayed mostly disordered with partially ordered components, indicated by the broadening of the peak (Figure 3.17). Consequently, the irreversible chain order/disorder process occurred in the PO_3-MPCs consistent with what was previously observed for hydrogen bonded CO_2H terminal alkanethiolate gold nanoparticles (CO_2-MPCs) which decomposed upon heating.[16] The hysteresis observed in CO_2-MPCs was suggested to be due to a new hydrogen bonding configuration. This change in hydrogen bonding network had occurred in the PO_3-MPCs since heating the sample above the transition temperature showed a downfield shift from ~ 31 ppm to ~ 37 ppm in the ^{31}P spectrum. Contrary to the pure MUP where the spectrum returned to its original state upon cooling, the ^{31}P NMR spectra show that the chains remained in the disordered H-bonded conformation. The new hydrogen bond configuration in PO_3-MPCs could arise from breaking up the inter- and intra- particle hydrogen bonding where all the chains are in extended conformation and forming new hydrogen bonds due to the disordered chains between the thiols adsorbed on the surface and free disulfides. The structural disorder observed upon cooling can arise from the possibility that the free chains remained somehow tangled in the disordered chains on the surface.

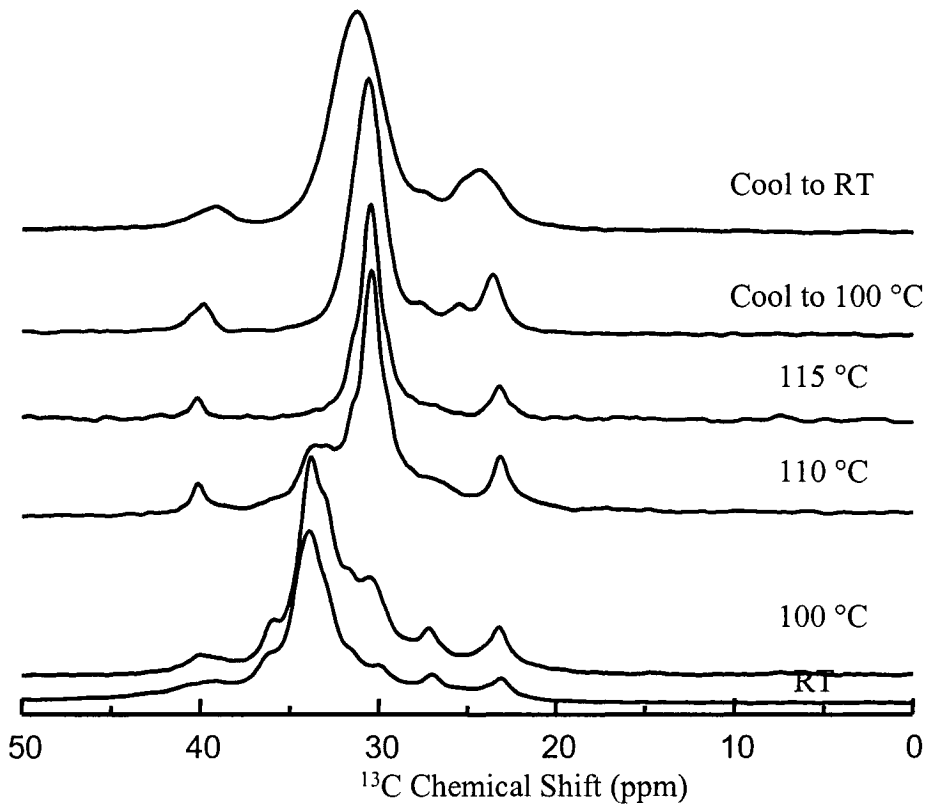

Figure 3.17 Variable temperature solid-state ^{13}C CP/MAS NMR spectra of PO_3-MPCs. Line broadening of 30 was used.

3.3.11 ^{31}P chemical shift anisotropy

In a static polycrystalline sample, the solid-state ^{31}P NMR spectra display the well known powder pattern due to the random distribution of orientations with respect to the external magnetic field. In ^{31}P NMR, the chemical shift anisotropy (CSA) pattern can be used to extract three principle components (i.e., δ_{11}, δ_{22}, δ_{33}) and provide further information about the ^{31}P local environment. For example, the CSA of phosphonic acids ($\Delta\sigma$ = 68-104) are much smaller than those of the esters ($\Delta\sigma$ = 145-195) mainly due to stronger hydrogen bonds.[23] The magnitude of the asymmetry parameter η can give an indication of the type of binding mode of the phosphonate group.[20] Figure 3.18 shows the static as well as the slow spinning spectra (1.5 kHz) of the unbound MUP, PO_3Na-MPCs, PO_3-MPCs and heated PO_3-MPCs. The peak intensities and the ^{31}P chemical shifts of the spinning side bands were fit using Herzfeld-Berger analysis.[18] The fitting of the experimental spectra gave the principle components of the chemical shift tensors of the compounds studied, and are summarized in Table 3.3.

Table 3.3 ^{31}P Chemical shift parameters of 11 mercaptoundecanylphosphonic acid and various PO_3-MPCs.

Compound	δ_{iso}[a](ppm)	η[b]	$\Delta\sigma$[c](ppm)	δ_{11}(ppm)	δ_{22}(ppm)	δ_{33}(ppm)
MUP	31.1	0.3	-71	62.3	47.3	-16.3
PO_3Na-MPC	23.1	0.7	-93.7	86.4	37.5	-31.8
PO_3-MPC	30.9	0.1	-58.7	51.1	49.4	-8.5
Heated PO_3-MPC	37.6	0.6	-52.7	65.0	45.3	2.5

[a] ^{31}P chemical shift, δ_{iso}, in solid-state. [b] Chemical shift asymmetry, $\eta = |\delta_{22} - \delta_{11}| / |\delta_{33} - \delta_{iso}|$. [c] Chemical shift anisotropy, $\Delta\sigma = \delta_{33} - \frac{1}{2}(\delta_{11} - \delta_{22})$.[19]

N-alkylposphonic acids have a small axially asymmetric ^{31}P shielding tensor (η = 0-0.3) due to rapid proton transfer between the P-O groups.[19] The three principal

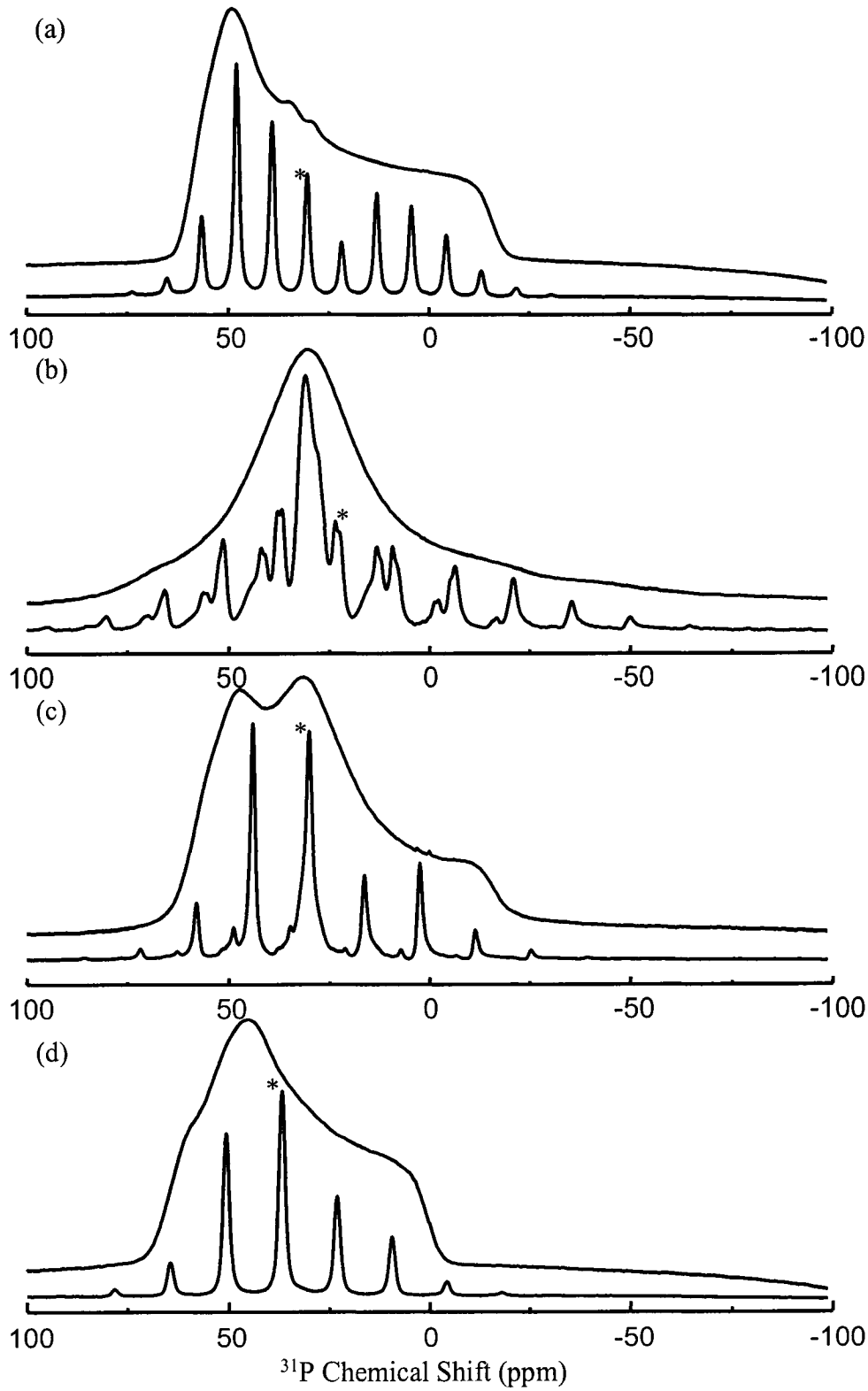

Figure 3.18 Static and slow spinning (1.0 - 1.5 kHz) ^{31}P CP solid-state NMR spectra of (a) 11-mercaptoundecanylphopshonic acid, (b) PO_3Na-MPCs in salt form, (c) dialyzed PO_3-MPCs and (d) PO_3-MPCs after being heated to 120 °C. The asterix denotes ^{31}P isotropic shift. A contact time of 1ms with a pulse width of 2.5 s were used.

elements and η of 11-mercaptoundecanylphosphonic acid (MUP) (δ_{11} = 62.3 ppm, δ_{22} = 47.3 ppm and δ_{33} = -16.3 ppm, η = 0.3) strongly agree with the ones reported for octadecylphosphonic acid (ODPA)[19] indicating that the PO_3H_2 group in MUP has a very similar environment to ODPA. The protonated phosphonate groups in PO_3-MPCs have low asymmetry parameter (η = 0.1) compared to PO_3Na-MPCs ((η = 0.7) where the phosphonate groups are associated with Na ions. The small asymmetry parameter of PO_3-MPCs indicates that the three oxygen atoms of phosphonate head groups are equivalent. In the case of PO_3Na-MPCs, the η value increased to 0.7. This increase can be due to the fact that sodium atoms create inequivalent oxygens which lead to an asymmetrical environment.[19,21] Furthermore, the increase in $\Delta\sigma$ (–58.7 ppm) of PO_3-MPCs compared to PO_3Na-MPC ($\Delta\sigma$ = –93.7 ppm) can be attributed to a strong formation of intra- and/or inter- particle hydrogen bonds.[23]

As can be seen from the static and slow spinning spectra of PO_3-MPCs (Figure 3.18c) and heated PO_3-MPCs (Figure 3.18d), the ^{31}P chemical shift asymmetry pattern for the two MPCs were quite different. Once again the η value increased from 0.1 to 0.6 when the PO_3-MPCs were heated and cooled down. The disordering of chains breaks the symmetric hydrogen bonded structure of the phosphonate head groups leading to a higher asymmetry parameter. The low value of $\Delta\sigma$ (-52.7 ppm) in heated PO_3-MPCs suggested that strong hydrogen bonds were still present. Like the ^{31}P chemical shift found at 37 ppm in both heated bulk and heated PO_3-MPCs, the CSA elements of these two compounds were rather similar. In addition, the three principal components of heated MUP agreed with the ones given for n-hexylphosphonic acid.[24] For the later compound, which was recrystallized from organic solvents, gave an isotropical shift at 37 ppm. This suggests that the phosphonate group in heated MUP is in the same H-bonded environment as the n-hexylphosphonic acid crystallized from organic solvent.

3.3.12 Encapsulating PO_3-MPC with PDADMAC

The negatively charged 3.1 nm diameter PO_3-modified gold nanoparticles were coated with poly(diallyldimethylammonium chloride), PDADMAC and characterized by TEM, UV-Vis absorption and ξ-potential measurements. Polyelectrolyte coating of metal nanoparticles is one method that alters the surface chemistry, with the polyelectrolyte

type determining the final surface characteristics of the particles. When the polyelectrolyte is adsorbed on different particle diameters, its conformation and its interaction with the particle is expected to be different. In the case of small, spherical particles, the high surface curvature can restrict polyelectrolyte adsorption because of the limit in polymer chain flexibility.[70] Small particles do not permit the adsorption of all the polyelectrolyte monomers owing to the confinement energy of the chain. As a result, extended tails are formed in solution. The smallest particles that were successfully coated by a polyelectrolytes were reported in Caruso's paper[36] were 7 nm diameter carboxylic acid-modified gold nanoparticles which were uniformly coated by two oppositely charged polyelectrolytes, PDADMAC and PSS. The 1.8 nm diameter SO_3-MPCs synthesized in chapter 2 showed clearly the small particle diameter limit when coated with PDADMAC. The extended tails of PDADMAC resulted in a multiple adsorption of SO_3-MPCs which was observed by almost a ten fold increase of the particle diameter in TEM pictures and a high red shift in the UV-Vis.

Negatively charged 3.1 nm diameter PO_3-modified gold nanoparticles had an initial ξ-potential value of -34.4 ± 0.6 mV and the surface plasmon absorption band (i.e., shoulder) was observed at 520 nm (Figure 3.5b). Particles that were coated with positively charged PDADMAC, the ξ-potential measurements indicated a value of 37 ± 2 mV, while the plasmon absorption band was found to red-shift to 525 nm (Figure 3.5d), which suggested PDADMAC adsorption. The TEM micrographs of the PDADMAC coated nanoparticles in Figure 3.4d, showed that the average particle size increased to $\sim$ $3.9 \text{ nm} \pm 0.9$ and the particles were well separated. No aggregation or large increase in the particle diameter was observed, indicating that the 3.1 nm PO_3-MPCs gave a sufficient surface for the adsorbed chains of PDAMAC without forming extended tails. The average polyelectrolyte layer thickness was found to be 0.5 nm in CO_2-MPCs when subsequently coated with layers of PDADMAC and PSS.[36] The coating of 3.1 nm diameter PO_3-MPCs with PDADMAC was shown to be successful. The low yield (5 mg) of coated PO_3-MPCs was suitable for the TEM and UV-Vis studies but for solid-state NMR studies, a higher yield is required.[71]

3.4 CONCLUSIONS

A phosphonic acid terminated 11C chain alkanethiol, 11-mercaptoundecanyl-phosphonic acid, MUP, was synthesized and reacted with a gold salt to form phosphonate functionalized monolayer protected gold clusters, PO_3-MPCs. TEM, UV-Vis indicated the successful synthesis of the PO_3-MPCs with the synthesis strategy used here. The changes in the environment of the hydrogen-bonded PO_3H_2 group were reflected by the ^{31}P chemical shift in solution and in solid-state NMR and by the CSA parameters. At high concentration, the bulk acid in $CDCl_3$ formed inverted micelle-like clusters giving a ^{31}P chemical shift at 37 ppm. In CD_3OD, the clusters were broken down into monomers showing a chemical shift at 31 ppm. At room temperature, in the ^{31}P solid-state, the peak at 31 ppm for the MUP suggests a possible extended H-bonded polymeric structure. A solid-solid phase transition in MUP was detected by DSC and the phase change was examined by optical microscopy and solid-state NMR. The optical microscopy showed a loss of birefringence above the transition indicating an amorphous state. The ^{13}C solid-state NMR showed the disordering of the methylene chains in the high temperature phase while the ^{31}P solid-state chemical shift at 37 ppm suggested changes in the hydrogen-bonding, possibly involving a break up of the polymeric structure into hydrogen-bonded clusters.

The variable temperature ^{13}C solid-state NMR along with FTIR and TGA showed that bound surfactant is highly ordered and more stable than in the free state. The high rigidity associated with the dense chain packing was reflected in the dynamic studies of PO_3-MPCs. As seen in carboxylate functionalized MPCs,[6] the nature of the hydrogen bonding in PO_3-MPCs induces a higher conformational order as compared to methyl terminated MPCs. Moreover, variable temperature NMR studies of PO_3-MPCs (C11) showed relatively high order/disorder transition temperature when compared to methyl- (C18) and hydroxy- (C16) terminated MPCs.[5] The irreversible chain melting of PO_3-MPCs was due to the change in hydrogen bond environment indicated by the new phosphorus chemical shift and partial decomposition which produced free disulfide.

The ξ-potential, TEM and UV-Vis measurements indicated that 3.1 nm negatively charged PO_3-MPCs were successfully coated with the first layer of positively charged

PDADMAC. To date, these are the smallest particles which have been successfully encapsulated by a polyelectrolyte.

3.5 REFERENCES

1. Templeton, A.C.; Chen, S.; Gross, S.M.; Murray, R.W. *Langmuir* **1999**, 15, 66.

2. Chen, S.; Murray, R. W. *Langmuir* **1999**, 15, 862.

3. Wuelfing, W.P.; Gross, S. M.; Miles, D. T.; Murray, R.W. *J. Am. Chem. Soc.* **1998**, 120, 12696.

4. Cliffel, D.E.; Zamborini, F.P.; Gross, S. M.; Murray, R.W. *Langmuir* **2000**, 16, 9699.

5. Badia, A.; Gao, W.; Singh, S.; Demers, L.; Cuccia, L.; Reven, L. *Langmuir* **1996**, 12, 1262.

6. Schmitt, H.; Badia, A.; Dickinson, L.; Reven, L.; Lennox, R. B. *Adv. Mater.* **1998**, 10, 475.

7. Choo, H.; Cutler, E.; Shon, Y.-S. *Langmuir* **2003**; 19, 8555.

8. Shon, Y.-S.; Mazzitelli, C.; Murray, R. W. *Langmuir* **2001**, 17, 7735.

9. Zhang, J.; Kirkham, J.; Robinson, C.; Wallwork, M. L.; Smith, D. A.; Marsh, A.; Wong, M. *Anal. Chem.* **2000**, 72, 1973.

10. Smith, D. A.; Wallwork, M. L.; Zhang, J.; Kirkham, J.; Robinson, C.; Marsh, A.; Wong, M. *J. Phys. Chem. B.* **2000**, 104, 8862.

11. Choi, G. Y.; Kang, J. F.; Ulman, A.; Zurawsky, W. *Langmuir* **1999**, 15, 8783.

12. Copie, V.; Faraci, W. S.; Walsh, C. T.; Griffin R. G. *Biochemistry* **1988**, 27, 4966.

13. Laber, B.; Gerbling, K.-P.; Harde, C. Neff, K.-H.; Nordhoff, E; Pohlenz, H.-D. *Biochemistry* **1994**, 33, 3413.

14. Bressy-Brondino, C.; Boutevin, B.; Hervaud, Y.; Gaboyard, M. *J. Appl. Polym. Sci.* **2001**, 83, 2277.

15. Pawsey, S.; Yach, K.; Reven, L. *Langmuir* **2002**, 18, 5205.

16. Pawsey, S.; McCormick, M.; De Paul, S.; Graf, R.; Lee, Y. S.; Reven, L.; Spiess, H. W. *J. Am. Chem. Soc.* **2003**, 125, 4174.

17. Herzfeld, J.; Griffin, R. G.; Haberkorn R. A. *Biochemistry* **1978**, 17, 2711.

18. Herzfeld, J.; Berger, A.E.*J. Chem. Phys.* **1980**, 73, 6021.

19. Gao, W.; Dickinson, L.; Morin, F. G.; Reven, L. *Chem. Mater.* **1997**, 9, 3113.

20. Massiot, D.; Drumel, S.; Janvier, P.; Bujoli-Doeuff, M.; Bujoli, B. *Chem. Mater.* **1997**, 9, 6.

21. Harris, R. K.; Merwin, L.H.; Hägele, G. *Naturforsch.* **1989**, 44b, 1407.

22. Klose, G.; Trahms, L.; Möps, A. *Chem. Phys. Letters* **1985**, 122, 545.

23. Klose, G.; Möps, A.; Grossmann, G.; Trahms, L. *Chem. Phys. Letters* **1990**, 175, 472.

24. Ohms, G.; Krüger, K.; Rabis, A.; Kaiser, V. *Phosphorus, Sulfur, and Silicon* **1996**, 115, 75.

25. Hammond, S. R.; Zhou, W.-J.; Gin, D. L.; Avlyanov, J. K. *Liq. Cryst.* **2002**, 29, 1151.

26. Klose, G.; Petrov, A. G.; Volke, F.; Meyer, H. W.; Förster, G.; Retting, W. *Mol. Cryst. Liq. Cryst.* **1982**, 88, 109.

27. Gaboyard, M.; Hervaud, Y.; Boutevin, B. *Phosphorus, Sulfur, and Silicon* **2002**, 177, 877.

28. Mahmoudkhani, A.; Langer, V. *J. Mol. Struct.* **2002**, 609, 97.

29. Genov, D. G.; Tebby, J. C.; *J. Org. Chem.* **1996**, 61, 2454.

30. Mehring, M.; Schürmann, M.; Ludwig, R. *Chem. Eur. J.* **2003**, 9, 838.

31. Mitsch, C. C.; Freedman, L. D.; Moreland, C. G. *J. Magn. Resonance* **1971**, 5, 140.

32. Badia, A.; Singh, S.; Demers, L.; Cuccia, L.; Brown, R.; Lennox, R. B. *Chem. Eur. J.* **1996**, 2, 205.

33. Lee, T. R.; Carey, R. I.; Biebuyck, H. A.; Whitesides, G. M. *Langmuir* **1994**, 10, 741.

34. Putvinski, T. M.; Schilling, M. L.; Katz, H. E.; Chidsey, C. E. D., Mujsce, A. M.; Emerson, A. B. *Langmuir* **1990**, 6, 1567.

35. Vallant, T.; Brunner, H.; Mayer, U.; Hoffmann, H. *Langmuir* **1998**, 14, 5826.

36. Mayya, K. S.; Schoeler, B.; Caruso, F. *Adv. Funct. Mater.* **2003**, 13, 183.

37. Torchia, D. A. *J. Magn. Reson.* **1978**, 30, 613.

38. Alemany, L. B.; Grant, D. M.; Alger, T. D.; Pugmire, R. J. *J. Am. Chem. Soc.* **1983**, 105, 6697.

39. Skulason, H.; Frisbie, C. D. *J. Am. Chem. Soc.* **2000**, 122, 9750.

40. Neff, G. A.; Page, C. J.; Meintjes, E.; Tsuda, T.; Pilgrim, W.-C.; Roberts, N.; Warren, W. W., Jr. *Langmuir* **1996**, 12, 238.

41. Lee, H.; Kepley, L. J.; Hong, H. G.; Akhter, S.; Mallouk, T. E. *J. Phys. Chem.* **1988**, 92, 2597.

42. Sahoo, Y.; Pizem, H.; Fried, T.; Golodnitsky, D.; Burstein, L.; Sukenik, C. N.; Markovich, G. *Langmuir* **2001**, 17, 7907.

43. Cheng, X.; Gao, Q.; Smith, R. D.; Simanek, E. E.; Mammen, M.; Whitesides, G. M.; *J. Org. Chem.* **1996**, 61, 2204.

44. Yamaguchi, K. *J. Mass Spectrom.* **2003**, 38, 473.

45. Huang, T.; Murray, R. W. *J. Phys. Chem. B.* **2001**, 105, 12498.

46. Simard, J.; Briggs, C.; Boal, A. K.; Rotello, V. M. *Chem. Commun.* **2000**, 19, 1943.

47. Shimizu, T.; Teranishi, T.; Hasegawa, S.; Miyake, M. *J. Phys. Chem. B.* **2003**, 107, 2719.

48. Teranishi, T.; Hasegawa, S.; Shimizu, T.; Miyake, M. *Adv. Mater.* **2001**, 13, 1699.

49. Naka, K.; Itoh, H.; Chujo, Y. *Langmuir* **2003**, 19, 5496.

50. Maye, M. M.; Zhong, C. J. *J. Mater. Chem.* **2000**, 10, 1895.

51. Jiang, D.D.; Michael. Q. Y.; McKinney, M. A.; Wilkie, C. A., *Polym. Degrad. Stab.* **1999**, 63, 423.

52. Selvakannan, PR.; Mandal, S.; Phadtare, S.; Pasricha, R.; Sastry, M. *Langmuir* **2003**, 19, 3545.

53. Porter, R. S.; Johnson, J. F. *Ordered Fluids and Liquid Crystals*. **1967**, 1-12.

54. D'Andrea, S. C.; Fadeev, A. Y. *Langmuir* **2003**, 19, 7904.

55. Gao, W.; Dickinson, L.; Grozinger, C.; Morin, F. G.; Reven, L. *Langmuir* **1996**, 12, 6429.

56. Danilich, M.J.; Burton, D.J.; Marchant, R.E. *Vib. Spectrosc.* **1995**, 9, 229.

57. Daasch, L. W.; Smith, D. C. *Anal. Chem.* **1951**, 23, 853.

58. Albouy, D.; Brun, A.; Munoz, A.; Etemad-Moghadam, G. *J. Org. Chem.* **1998**, 63, 7223.

59. Friedman, O. M.; Seligman, A. M. *J. Am. Chem. Soc.* **1951**, 73, 5292.

60. Genov, D. G.; Kresinski, R. A.; Tebby, J. C. *J. Org. Chem.* **1998**, 63, 2574.

61. Maeda, H.; Ozeki, A.; Ikeda, A.; Okabayashi, H., Matsushita, K. *J. Colloid. Interface. Sci.* **1979**, 76, 532.

62. Koga, K.; Kanazawa, Y. *Chem. Phys. Lipids* **1984**, 36, 153.

63. Clauss, J.; Schmidt-Rohr, K.; Adam, A; Boeffel, C.; Spiess, H.W. *Macromolecules* **1992**, 25, 5208.

64. Kitamaru, R.; Horii, F.; Murayama, K. *Macromolecules* **1986**, 19, 636.

65. Merz, K.; Knüfer, A. *Acta Cryst.* **2002**, C38, o187.

66. Chadha, R. K. *Acta Cryst.* **1995**, C51, 2340.

67. Weakley, T. J. R. *Acta. Cryst.* **1976**, B32, 2889.

68. Kosolapoff, G. *J. Am. Chem. Soc.* **1945**, 67, 1180.

69. Badia, A.; Demers, L.; Dickinson, L.; Morin, F. G.; Lennox, R. B.; Reven, L. *J. Am. Chem. Soc.* **1997**, 119, 11104.

70. Chodanowski, P.; Stoll, S. *J. Chem. Phys.* **2001**, 115, 4951.

71. Hulme, S. E. *LbL polyelectrolyte coating of COOH-derivatized gold nanoparticles.* Summer Project, **2003**.

Chapter 4

Overview, Conclusions, and Future Work

4.1 OVERVIEW AND CONCLUSIONS

This research involved the first dynamic solid-state NMR studies of functionalised protected gold clusters generated either from sodium, 10-mercaptodecanesulfonate (SO_3-MPCs) or from 11-mercaptoundecanylphosphonic acid (PO_3-MPCs). This thesis concluded that order-disorder transitions occurred in functionalized MPCs and that having the end methyl group replaced by a polar ionic group plays an important role in their physical and chemical properties as well as in the chain packing geometry.

Various particle sizes were synthesized by simply controlling the experimental conditions such as gold-to-thiol ratio, gold salt concentration and the type of stabilizing ligand. The medium chain length SO_3-MPCs (i.e, 10C) and PO_3-MPCs (i.e., 11C) showed high stability in alkaline water solution as well as in the dry form. In addition, the water-soluble SO_3-MPCs showed pH stability even at extremely low pH.

Solid-state NMR spectroscopy was shown to provide detailed structural and dynamic information about the nanoparticles. Complementary techniques like differential scanning calorimetry and infrared studies gave additional information on solid-solid transitions and the degree of chain order. The DSC curves showed clearly that the amphiphilic molecules, $HS(CH_2)_{10}SO_3Na$, MDS and $HS(CH_2)_{11}PO_3H_2$, MUP, undergo solid-solid transitions which is reflected in solid-state NMR as an order-disorder transition arising from an increased population of gauche chain conformers. The order-disorder transition in SO_3-MPCs occurred at a lower temperature than the order-disorder transition in the bulk acid, MDS, whereas in PO_3-MPCs, this transition was observed to be much higher than in MUP. These variable temperatures solid-state NMR experiments gave an indication of the thermal stability of the adsorbed chains on the nanoparticles.

The medium length chains of SO_3-MPCs were highly ordered at room temperature and relatively rigid when compared to long chains of methyl alkanethiolate MPCs. However, a larger effect was seen in the introduction of phosphonate group on the

surface of the gold nanoparticles where the more extensive hydrogen bonding interactions between the phosphonic acid groups led to a reduce chain mobility and a higher thermal stability of the chain order as compared to long chain OH functionalized MPCs.

The phosphonate group allowed studies of the dynamics and the hydrogen bonding behavior at the end chains. Solid-state ^{31}P NMR indicated that changes in crystal packing, mainly affected by the hydrogen bonding are reflected by the ^{31}P chemical shift and the chemical shift anisotropy. Two solid forms of MUP were found when characterized by solid-state NMR, optical spectroscopy and DSC. One could easily alternate between the two hydrogen-bonded structures by simply changing the temperature. In addition, it is probable that one can obtain the two existed hydrogen-bonded forms of the bulk MUP by using polar versus non-polar solvent crystallization.

4.2 FUTURE WORK

To confirm the last point and show that one can achieve the same H-bonded structure using both of the two experimental techniques, one would have to recrystallize the MUP bulk surfactant in a non-polar solvent such as heptane or chloroform and compare the ^{31}P solid-state NMR shift and the CSA patterns to the heated MUP bulk surfactant. The hydrogen-bonding interactions among the phosphonate groups, in the bulk and/or in the PO_3-MPCs can be investigated by additional solid-state NMR techniques such as 2D ^{1}H-^{31}P heteronuclear correlation experiments. These results, when added to the information from DSC and optical spectroscopy, can provide a more complete picture of the hydrogen-bonding interactions of MUP in the bulk state and as monolayers on gold nanoparticles. In addition, the X-ray diffraction patterns would be useful to determine the crystallinity and crystallite size of the bulk phosphonic acid for the two H-bonded structures. Furthermore, variable temperature infrared spectroscopy studies would give complementary information on the changes in hydrogen bonding interactions of the phosphate groups.

It was shown that polyelectrolyte coating of negatively charged gold nanoparticles was highly dependent on the radius size of the nanoparticles. In the case of 1.8 nm-diameter SO_3-MPCs, the positively charged polyelectrolyte chains bridged across

multiple particles, forming clusters with diameters larger than 10 nm. On the other hand, the polyelectrolyte could wrap fully around the 3.1 nm-diameter PO_3-MPCs without forming extended tails. However, one cannot conclude that the successful coating of the polyelectrolyte of larger ones (i.e., PO_3-MPCs) is only due to the core size. The different end group of the functionalized nanoparticles (i.e., SO_3Na versus PO_3H_2) could also affect to some extend the interaction of the polyelectrolyte. Future work would therefore require the coating of the various core size nanoparticles of the same functional end group. In addition, the synthesis of enough coated particles would be needed for solid-state NMR studies and for coating the particles with additional layers. Dynamic NMR measurments and other solid-state NMR techniques would then be used to monitor the particle-particle interactions between the phosphonate groups and the polyelectrolyte chains as well as the effect of the very high surface curvature on the structure of the polyelectrolyte multilayers.

Appendix

A1 SIZE DISTRUBTION OF SO_3-MPCs

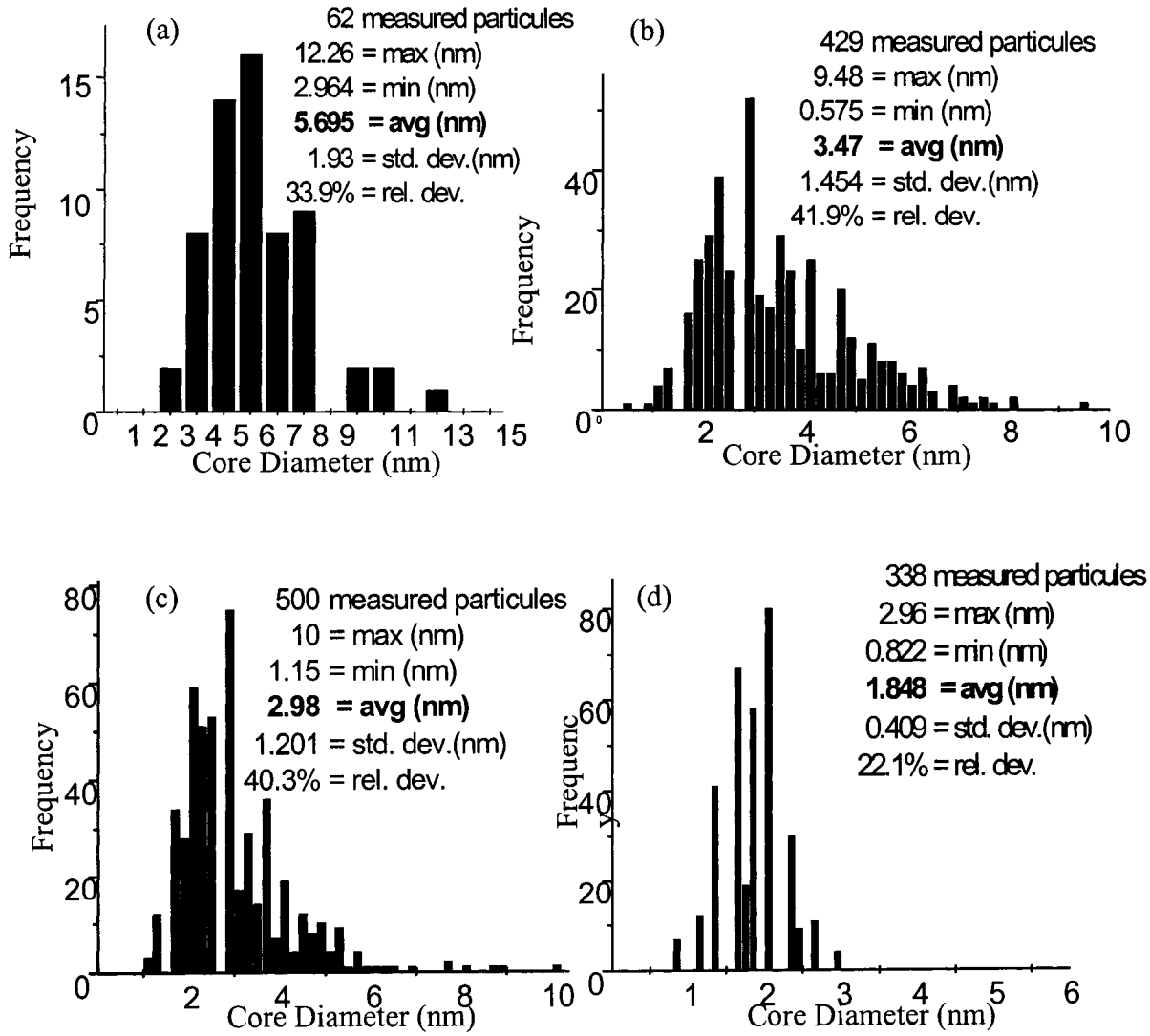

Figure A1 Size histograms of SO_3-MPCs prepared by varying two experimental conditions: MDS:Au ratio and [Au]. (a) 1:3, 15.7 mM. (b) 2:1, 15.7 mM. (c) 3:1, 15.7 mM. (d) 3:1, 3.8 mM.

A2 SIZE DISTRUBTION OF PO_3-MPCs

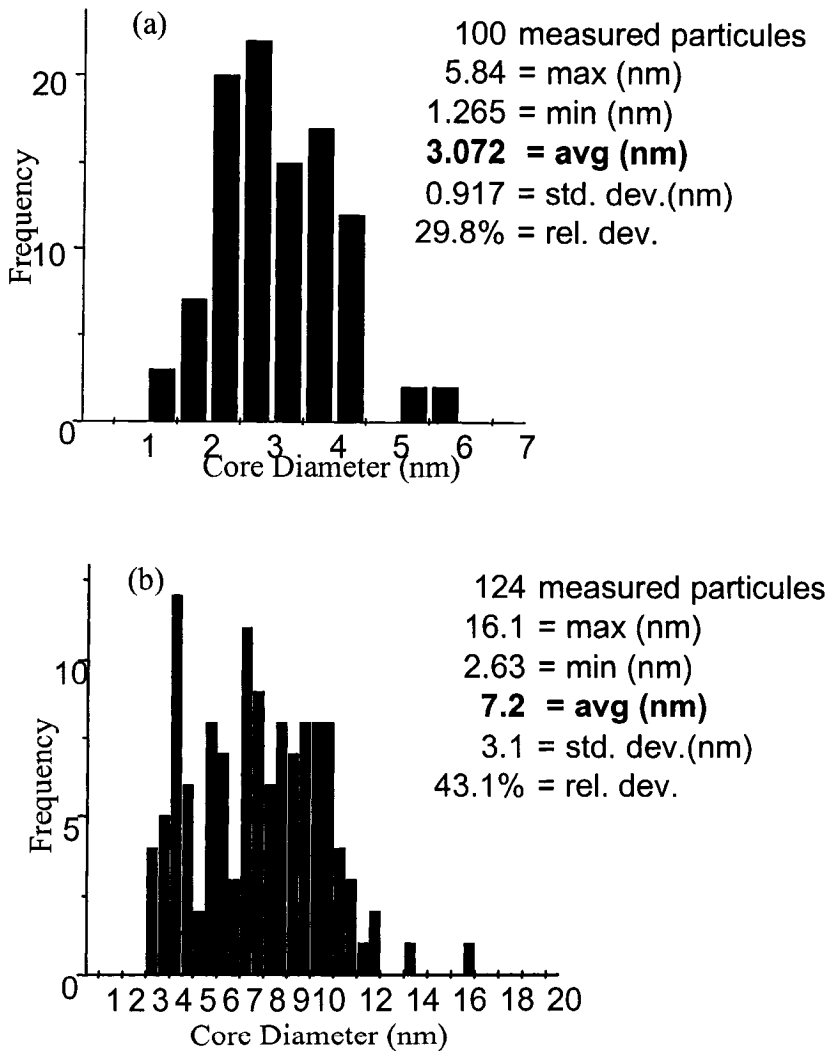

Figure A2 Size histograms of (a) PO_3-MPCs and after being heated to 120 °C (b).

A3 SYNTHETHIC ROUTES FOR SURFACTANTS

A3.1 Reaction scheme for sodium, 10-mercaptodecanesulfonate

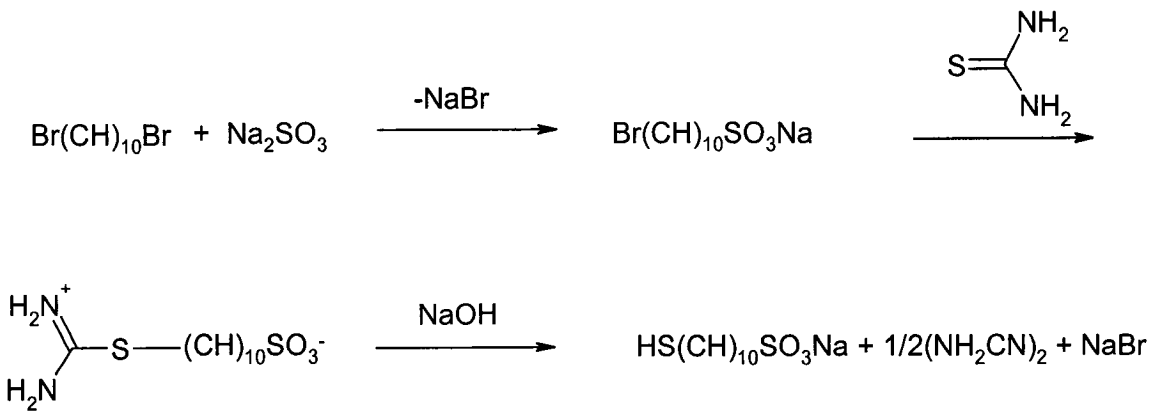

A3.2 Reaction scheme for 11-mercaptoundecanylphosphonic acid